UNIVERSITY OF LINCOLN

A systematic approach to cooperative driving systems based on optimal control allocation

by

Dong Zhang

A thesis submitted in partial fulfillment for the degree of Doctor of Philosophy

in the
College of Science
School of Engineering

04.24.2019

Declaration of Authorship

I, DONG ZHANG, declare that this thesis titled, 'A systematic approach to cooperative driving systems based on optimal control allocation' and the work presented in it are my own. I confirm that:

- This work was done wholly or mainly while in candidature for a research degree at this University.
- Where any part of this thesis has previously been submitted for a degree or any other qualification at this University or any other institution, this has been clearly stated.
- Where I have consulted the published work of others, this is always clearly attributed.
- Where I have quoted from the work of others, the source is always given. With the exception of such quotations, this thesis is entirely my own work.
- I have acknowledged all main sources of help.
- Where the thesis is based on work done by myself jointly with others, I have made clear exactly what was done by others and what I have contributed myself.

Signed: _____

Date: _____

"It is not always possible to be the best, but it is always possible to improve your own performance."

Jackie Stewart

UNIVERSITY OF LINCOLN

Abstract

College of Science
School of Engineering

Doctor of Philosophy

by Dong Zhang

This dissertation proposes a systematic approach to vehicle dynamic control, where interaction between the human driver and on-board automated driving systems is considered a fundamental part of the overall control design. The hierarchical control system is to address motion control in three regions. First is normal driving, where the vehicle stays within the linear region of the tyre. Second is limit driving, where the vehicle stays within the nonlinear region of the tyre. Third is over-limit driving, where the driver demands go beyond the tyre force limits. The third case is addressed by a proposed control moderator (CM). The aim is to consider all three cases within a consistent hierarchical chassis control framework. The upper-level of the hierarchical control structure relates to both optimal vehicle control under normal and limit driving, and saturating driver demands for over-limit driving, these corresponding to a fully autonomous controller and driver assistance controller respectively.

Model Predictive Control (MPC) is used as the core control technique for path following under normal driving conditions, and a Moderated Particle Reference (MPR) control strategy is proposed for the road departure mitigation during limit and over-limit driving. The MPR model is validated to ensure predictable and stable operation near the friction limits, maintaining controllability for curvature and speed tracking, which effectively limits demands on the vehicle while preserving the control interaction of the driver.

In the next level of the hierarchical control structure, a novel control allocation (CA) approach based on pseudo-inverse method is proposed, while a general linearly constrained quadratic programming (CQP) approach is considered as a benchmark. From extended simulation experiments, it is found that the proposed Pseudo-Inverse CA (PICA) method can achieve a close match to CQP performance in normal driving conditions. This applies for multiple control targets (including path tracking, energy-efficient, etc.) and PICA is found to achieve improved performance in limit and over-limit driving, again addressing multiple control targets (including road departure mitigation, energy-efficient, etc.). Furthermore, the PICA method shows its inherent advantages of achieving the same control performance with much less computational cost and is guaranteed to provide a feasible control target for the actuators to track during the highly dynamic driving scenarios. In addition, it can effectively solve the constrained optimal control problem with additional mechanical and electronic actuator constraints. Thus, the proposed PICA method, which uses Control Re-Allocation (making multiple calls to the pseudo-inverse operator) can be considered a feasible and novel alternative approach to control allocation, with advantages over the standard CQP method.

Finally, in the lower-level of the hierarchical control structure, the desired tyre control variables are obtained through an analytical inverse tyre model and a sliding mode controller (SMC) is employed for the actuators to track the control target. The proposed

hierarchical control system is validated with both driving simulator studies and from testing a real vehicle, considering a wide range of driving scenarios, from low-speed path tracking to safety-critical vehicle dynamic control. It therefore opens up a systematic approach to extended vehicle control applications, from fully autonomous driving to driver assistance systems and control objects from passenger cars to vehicles with higher centre of gravity (CoG) like SUVs, trucks and etc. ...

Acknowledgements

That is a beautiful autumn at 2015, when I came to the UK with my beloved wife. That was my first time to go aboard, everything was that much strange and fresh to us. Even though facing with an unfamiliar environment and food especially, my PhD mentor calm me down with a greeting which still remain fresh in my mind, "everything you need to to do right now is just to adapt your new life in UK ". After that, I began to breezily get used to the new environment and lifestyle in a totally different country. First and foremost, I want to thanks my supervisor Timothy Gordon, for your extremely patient and exhaustive guidance throughout my entire PhD study. Your enthusiasm and attitude towards research and life both inspire me deeply for the rest of my life. It is you who let me know that getting involved in the academic research is full of challenge but "Love is a better teacher than duty"; It is you who instruct me "Make things useful before make it complicated." when I am get stuck in some tough research problem; It is you who put the saying "Learning is an endless process" deeply in my mind. Example is always better than precept. I sincerely thank God bring you into my life and set a great example to me.

By taking this opportunity, I very much like to thank my parents formally. I am the only child for my family, studying aboard and being far away from home (8120km) is a really tough decision. I can't make up my mind without their understanding and encourage. It is their selfless support that makes me complete my PhD study smoothly and confidently. I am always very proud to be your child.

Also, I would like to express my sincere gratitude to all the staff in University of Lincoln who have greatly broadened my horizon and enriched my knowledge in my study. Dr. Yu Zhang, my second supervisor, thank you for your guidance both in my study and life. Prof. Ronald Bickerton, Dr. Jun Yao, Dr. Jun Chen thank you for the inspiring conversation and lectures. And a special thanks to Mr. Zhiqiang Huo, who is also a Chinese PhD student in School of Engineering. Although our research area is quite different, the joyful talks and even the hard time spent together will always be unforgettable. I would also want to express my appreciation to our admin team, especially Jen Smith and Alistair Soon, great thanks for your kind help for my adminstration work. Special thanks to Denise Bateman, you are the first one who makes me feel warm and fit myself into the new life in School. Your selfless and kind help to me will always be memorized.

Last but not least, I would like to thanks the teachers and students in China who engage into my research tests: Prof. Changfu Zong from Jilin University, who keeps teaching me from my graduated study; Dr. Guoying Chen from Jilin University, who provides lots of guidance in my knowledge about hardware development; Prof. Gang Li, who

offer great convenience for my experiments in Liaoning University of Technology, and by this chance thanks the students in there who participate into my driver-in-the-loop test; Yang Liu, who is PhD student in Jilin University, thank you for your patiently assisting in my experiments and helping me to collect and organise test data. ...

Contents

List of Figures

List of Tables

Abbreviations

MPC	**M**odel **P**redictive **C**ontrol
ADAS	**A**dvanced **D**river **A**ssitance **S**ystem
LKAS	**L**ane **K**eeping **A**ssitance **S**ystem
SMC	**S**liding **M**ode **C**ontrol
RPS	**R**ollover **P**revention **S**ystem
PPR	**P**ath **P**article **R**eference
MPR	**M**oderated **P**article **R**eference
CQP	**C**onstrained **Q**uadratic **P**rogramming
SQP	**S**equential **Q**uadratic **P**rogramming
MHA	**M**odified **H**amiltomian **A**lgorithm
LQR	**L**inear **Q**uadratic **R**egulator
CA	**C**ontrol **A**llocation
VDC	**V**ehicle **D**ynamic **C**ontrol
ESC	**E**lectronic **S**tability **C**ontrol
DSC	**D**ynamic **S**tability **C**ontrol
DLC	**D**ouble **L**ane **C**hange
FTC	**F**ault **T**olerance **C**ontrol
HIL	**H**ardware **I**n **L**oop
SUV	**S**ports **U**tility **V**ehicle
AFS	**A**ctive **F**ront **S**teering
PICA	**P**seudo **I**nverse **C**ontrol **A**llocation
TTR	**T**ime **T**o **R**ollover
LTR	**L**ateral-load **T**ransfer **R**atio
DoF	**D**egree **o**f **F**reedom
CoG	**C**entre **o**f **G**ravity

FDBW	**F**ull **D**rive **B**y **W**ire
EV	**E**lectric **V**ehicle
AI	**A**rtificial **I**ntelligence
SLS	**S**equential **L**east **S**quares
WLS	**W**eighted **L**east **S**quares
CRA	**C**ontrol **R**eallocation **A**lgorithm

Subscripts and Superscripts

^{c}	current value (exact)
$^{\sharp}$	pseudo-inverse matrix
^{ref}	reference value
^{min}	minimum value
^{max}	maximum value
^{lim}	limiting value
^{DI}	command from Driver intepreter
^{RPS}	command from rollover prevention system
^{d}	desired value
$_{**}/_{ij}$	wheel location
$^{\sharp}$	pseudo-inverse operator

Nomenclature

X	vehicle mass center longitudinal force in vehicle coordinate	[N]
X^g	vehicle mass center longitudinal force in global coordinate	[N]
Y	vehicle mass center lateral force in vehicle coordinate	[N]
Y^g	vehicle mass center lateral force in global coordinate	[N]
x	vehicle longitudinal displacement in global coordinate	[m]
y	vehicle lateral displacement in global coordinate	[m]
F_x	longitudinal tire force	[N]
F_y	lateral tire force	[N]
F_z	wheel vertical load	[N]
M_z	yaw moment	[Nm]
m	overall vehicle body mass	[kg]
g	gravitational constant	[m/sec^2]
m_s	vehicle sprung mass	[kg]
m_u	vehicle unsprung mass	[kg]
h_s	height of sprung mass	[m]
v_x	longitudinal velocity	[m/s]
v_y	lateral velocity	[m/s]
r	yaw rate	[rad/s]
ψ	yaw angle	[rad]
ϕ	roll angle	[rad]
ρ	mass density of air	[kg/m^{-3}]
C_d	aero dynamic drag coefficient	–
A_f	frontal area of vehicle	[m^2]
l_1	distance from the mass centre to the front axle	[m]
l_2	distance from the mass centre to the rear axle	[m]

L	vehicle wheel base	[m]
b, B	vehicle track width	[m]
I_z	yaw moment inertia	[kgm^2]
I_w	wheel rotation inertia	[kgm^2]
a_x	longitudinal acceleration	[ms^{-2}]
a_y	lateral acceleration	[ms^{-2}]
β	vehicle body sideslip angle	[rad]
δ_h	steering angle at the handwheel	[rad]
δ	wheel steering angle	[rad]
κ	tire slip ratio	–
α	tire slip angle	[rad]
μ	road friction coefficient	–
T_ω	wheel torque	[Nm]
v_ω	wheel centre speed	[ms^{-1}]
ω	wheel rotational speed	[rad/s]
R	wheel radius	[m]
f_r	wheel rolling resistance	–
K_s	understeer gradient	–
C_α	cornering stiffness of the steering axle	[N/rad]
I_{xeq}	rotational inertia of sprung mass around X axis	[kgm^2]
e	distance from vehicle roll centre to mass centre	[m]
C_ϕ	roll damping coefficient	–
K_ϕ	effective roll stiffness	[Nm/rad]
λ	Lagrange multiplier	–
Q,R,W,W_i,γ	weight coefficient	–
ε	relaxation factor	–
T_0	sampling time of the controller	[s]
T_p	preview time	[s]
T_D	driver brain response delay	[s]
T_N	driver action delay	[s]
T_C	driver correction time	[s]
G_{ay}	vehicle steady-state steering gain	–
i_{SW}	steering ratio	–

$\mathbf{u}$	general vehicle tire control vector	–
$\mathbf{V}$	general vehicle mass center control vector	–
ϱ	actuator rate limits	[N/s]
H	Hamiltonian function	–
L^{-1}	Inverse Laplace transform	–
R_t	LTR threshold	–

To my father...

Chapter 1

Introduction

1.1 Motivation

Recently, several companies including Google, Volvo, Tesla and Daimler have been demonstrating fully self-driving vehicles that use computers rather than humans to do the driving. However, in recent years, there are about 88 reported accidents caused by the autonomous driving vehicles from 2014 to 2018 [4]. It is hardly likely in the next several decades to have systems sufficiently reliable that they fully shut the driver out, rather they will engage when the driver is no longer competent by some objective standard. For safety reasons, these driverless or autonomous vehicles have test engineers closely supervise their progress. While there have been plenty of headlines about these autonomous vehicles, handing over complete control of our cars to computers is just one end of a spectrum of automation options. We can expect to see further evolutionary development, with cars becoming progressively smarter, and therefore providing more assistance to the driver behind the steering wheel.

1.2 Current progress and challenge

There has been lots of great progress in the intelligent car research area which benefit from control and computer technology, nowadays facing explosive development. However, there are still some common challenges about the fast-growing technology which can be summarized as :

1) Monitoring the driver state– Driver monitoring system, sometimes known as the driver attention monitor, is a vehicle safety system which uses cameras with infra-red capability to monitor driver attentiveness in real time, and then alarm and assist the driver

avoid to risky situations. Specifically, the Driver Monitoring System typically consists of a camera located on the steering column which is capable of eye tracking; if the driver is not paying attention to the road ahead and a dangerous situation is detected, the system will warn the driver by flashing lights, or issuing warning sounds. If no action is taken, the vehicle may apply the brakes (a warning alarm will sound followed by a brief automatic application of the braking system). However, these current technologies are only focusing on the facial expression, eye tracking and physiological index rather the driver's driving behavior to monitor the driver state. Driving behavior is more close and crucial to the vehicle safety problem, hence monitoring the driver state via the driving behavior (steering, acceleration and braking) will be of increasing importance. There are some systems largely in use in current cars: Pilot Assist System from Volvo and Lane Keeping Support system from Nissans, can monitor if the vehicle is leaving the current lane without use of a turn signal to detect drowsy or careless drivers to prevent accidents; the systems can either alert the driver if a lane change is detected without the use of a turn signal or go a step past alerting the driver and take steps to control vehicle steering to stay in the current lane [5].

2) Preserving the safety envelope– it is not hard to understand that preserving the safety envelope is crucial to the vehicle safety. The safety envelope means that it seeks to guarantee the vehicle stays out of danger until the 'last-second' before an impending crash. However, it is not always clear how to estimate the current driving state and preserve a 'last-second safety' envelop, so this remains a great challenge.

3) Coordinating with the traffic and road environment– there are many research papers focusing on the traffic coordinating control development which is known as the intelligent transportation system. Most of the study in intelligent transportation system are focusing on the vehicle platoon control firstly, which began with the PATH project in the 1990s, in California [6][7]. Subsequently, other researches and applications have been carried out, including the GCDC in the Netherlands [8], SARTRE in Europe [9] and Energy-ITS in Japan [10]. However, the nondeterminacy of the traffic participants makes it hard to predict the manners of surrounding traffic; the precise identification of traffic and road environment still remains big challenge.

4) Technology development: Sensors, actuators, algorithms, communications– Although the sensing technologies are nowadays facing explosive development both in software and hardware, the sensors for vehicle requires higher precision and computing speed with lower price. The conflicting problems pose a great challenge to the intelligent vehicle practitioner.

5) Fault-tolerance and fail-safe– As the level of automation increase, as more and more sensors and actuators are being fitted into the vehicle, then the vehicle system failure

problem will be aggravated. The failure of any sensors or actuators can cause the vehicle to be pushed into a dangerous state. Hence the fault-tolerance and fail-safe qualities will become a growing challenge to the developing technology of intelligent vehicles.

1.2.1 Hierarchical vehicle control system

The hierarchical structure for vehicle control is largely accepted by the researchers [11][12]. Many companies and universities have recently developed the fully automated driving system based on the multi-sensor fusion and control integration technology, where the sensing information come from the Vehicle-to-Vehicle, Vehicle-to-Infrastructure communication and vehicle self-equipped environment sensors. Data fusion provides the vehicle with desired speed and path information, then for the lower-level chassis and drive systems to track. Furthermore, the path tracking control will then be fully integrated with minimum energy performance criteria, which has several meanings including preserving and recovering battery charge (not considered in this dissertation) and limiting the energy dissipated in the tyres via correct control allocation (to be introduced in section 5.2) as well as respecting stability margins; a fully hierarchical control optimization method will then drive the independent wheel actuators. A centralized and hierarchical structure for the whole vehicle control system [13], which consists of Sensor Layer, Identification and Estimation Layer, Objective Control Layer, Forces and Motion Distribution Layer and Executive Layer is shown in Figure 1.1. It includes the environmental information identification (in sensor layer), vehicle state and driver identification (in system identification and estimation layer), then (in the integrated control layer) the vehicle can realize different control objectives including the ideal and personalized vehicle dynamic control, energy conversion and regeneration, and stability control. In particular, the energy conversion and regeneration mentioned in this structure are considered in vehicle-level control objectives (objective control layer), the energy efficiency which will be discussed in chapter 5 is considered in the forces and motion distributer layer, focusing on the unnecessary dissipation of energy in the tyres. Then the control objectives will be achieved via the control allocation (in forces and motion distributer layer) and vehicle actuators and their controllers (in executive layer).

The merits of the hierarchical structure are:

1. Algorithms in every layer can be designed and verified independently.

2. Encapsulation, modularity will be achieved more easily in each layer.

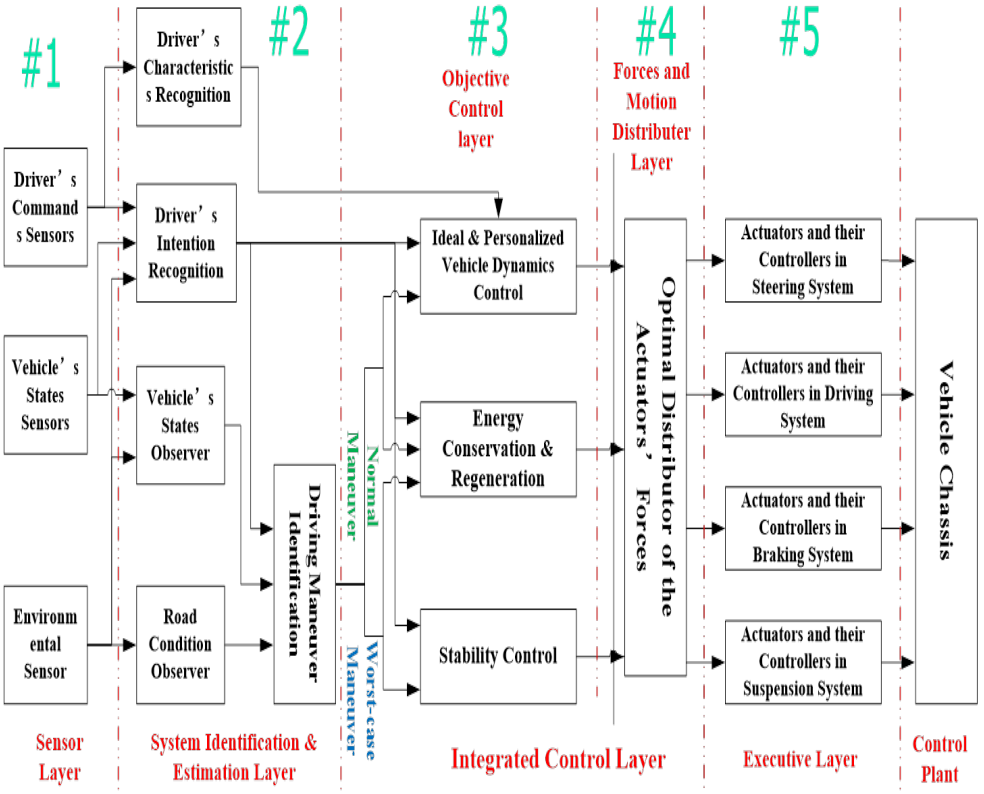

FIGURE 1.1: Hierarchical structure for the whole vehicle control systems

3. Different performance objectives can be assigned to different layers; hence the vehicle can achieve various performances all alone, such as active safety, handling stability, ride comfort, energy efficiency.

1.2.2 Self-driving technology

The self-driving technology has been largely accepted as the most critical innovative technology during the next several years for the car industry [14]. Recently, *SAE International* announces a new visual chart for use with its $J3016^{TM}$ "Levels of Driving Automation" (Figure 1.2) standard that defines the six levels of driving automation, from no automation to full automation. The new chart offers more "consumer-friendly" terms and definitions for the levels, which are frequently cited and referred to by industry and media. It is issued, in part, to speed the delivery of an initial regulatory framework and best practices to guide manufacturers and other entities in the safe design, development, testing, and deployment of highly automated vehicles (HAVs) [15].

Several companies including Google, GM/Cruise and Tesla have been demonstrating fully self-driving vehicles with different automation levels. Note that, any vehicle may have multiple SAE Levels that apply to it at various times. For example a Tesla Model

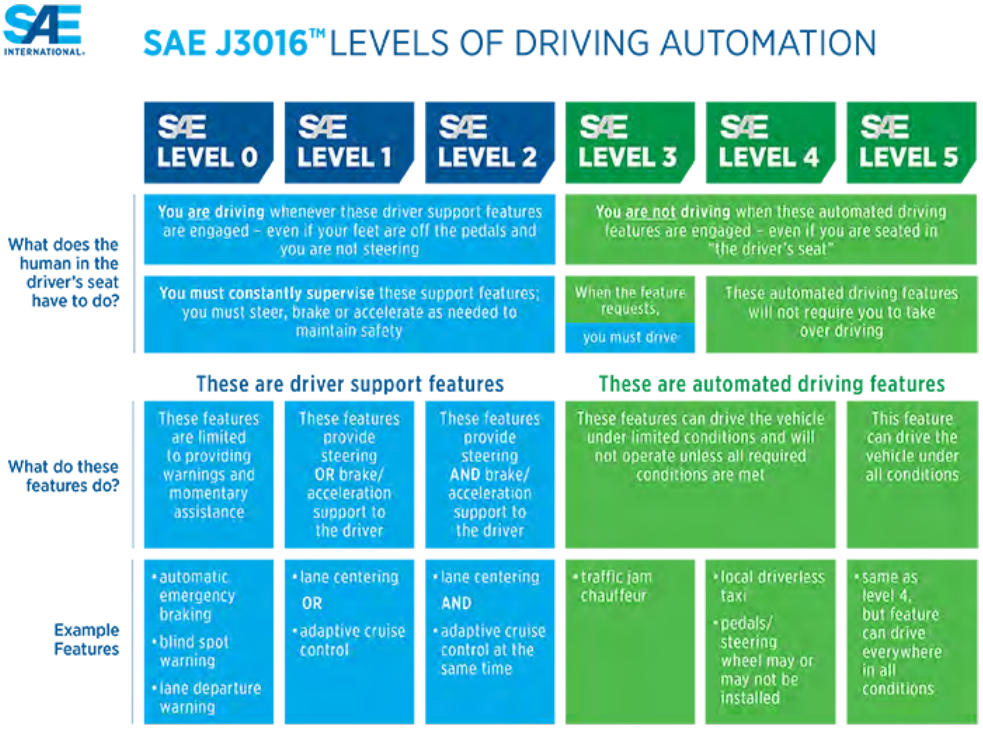

FIGURE 1.2: Levels of driving automation

S has an SAE Level 2 capability– Autopilot. If the user does not turn on Autopilot, then the Tesla has mainly ADAS components that are part of the SAE Level 1 definition. Tesla is currently producing its own vehicles (playing both the automation developer and vehicle manufacturing role) with SAE Level 2 Autopilot on both Level 1 and 2 hardware with an announced future capability that enables driverless operation. Tesla's Autopilot capability varies between a Level 1 and 2 hardware, but they are already advertising that an upgrade to Level 3 hardware will be required to reach full driverless capability ; Waymo (Google) has a target of SAE Level 4 for their automation controller, and their advertising claims that they are building a driver not a vehicle; GM/Cruise also has a target of SAE Level 4 for their vehicles, with no human backup support in the vehicle [16].

However, in recent years, there have been several reported accidents caused by the autonomous driving vehicles. In July, 2015, Google revealed that one of its self-driving cars had been involved in the first such crash to injure a human [15]. The incident involved one of Googles self-driving Lexus SUV vehicles being rear-ended in Mountain View, CA, during testing. The worlds first apparent death in a semi-autonomous car took place in early 2016 [17]. Less widely covered than subsequent instances, it occurred in China, just three months after Teslas autopilot feature was introduced to the Chinese market. One of Googles self-driving Lexus SUV cars was involved in a non-fatal crash with a bus on Silicon Valleys El Camino Real road at February 2016. This was the

18th accident involving a Google autonomous vehicle, but is significant because it was the first time that the Google vehicle is apparently at fault. An autonomous car killed 49-year-old Arizona resident Elaine Herzberg in what is believed to be the first fatal U.S. crash involving a pedestrian and self-driving vehicle in March 2018 [18].

These reported crashes cause the public's concern and force us to re-examine the very fast development of self-driving technology. The current technology road map for self-driving technology can be divided into two separate ways:

1) most of the main car companies would like to achieve the fully autonomous driving technology step-by-step from L1 to L5, during this developing progress, and during the development various kinds of ADAS will be gradually implemented into the cars.

2) some large technology companies like Google and Apple will start the research and development directly from the L4 to L5, with their great advantages in sensing and computer technology.

It's hard to say right now which approach will be more successful. But in either case, with the fast development of control technology and computer technology like Artificial Intelligence (AI), it can be anticipated that the self-driving and related vehicle automation technologies will soon enter the lives of the general public.

1.2.3 Advanced driver assistance system

It is easy to underestimate how good we humans actually are at driving. According to US traffic statistics [19], out of roughly three trillion vehicle miles travelled, there were a total of 5.6 million police-reported traffic accidents, 30,800 of them involving a fatality. This equates to roughly one crash per 500,000 miles and one fatal crash per 100 million miles. In this situation, with the rapid development of sensor technology (radar, lidar, camera, etc. as shown in Figure 1.3), the research focus on the driver assistance system is more practical and reasonable.

Advanced driver-assistance systems are systems developed to automate, adapt and enhance vehicle systems for safety and better driving. The automated system which is provided by ADAS to the vehicle is proven to reduce road fatalities, by minimizing the human error [20]. The current functions of ADAS include autonomous lighting, adaptive cruise control and collision avoidance, pedestrian crash avoidance mitigation (PCAM), incorporate satnav/traffic warnings, lane departure warning system, automatic lane centering, blind spots detecting, etc. Some kinds of functions and its corresponding sensors are shown in Figure 1.3. However, the adoption rate of the ADAS is far lower than expected as shown in Figure 1.4 [2]. It was expected that the adoption rate would face

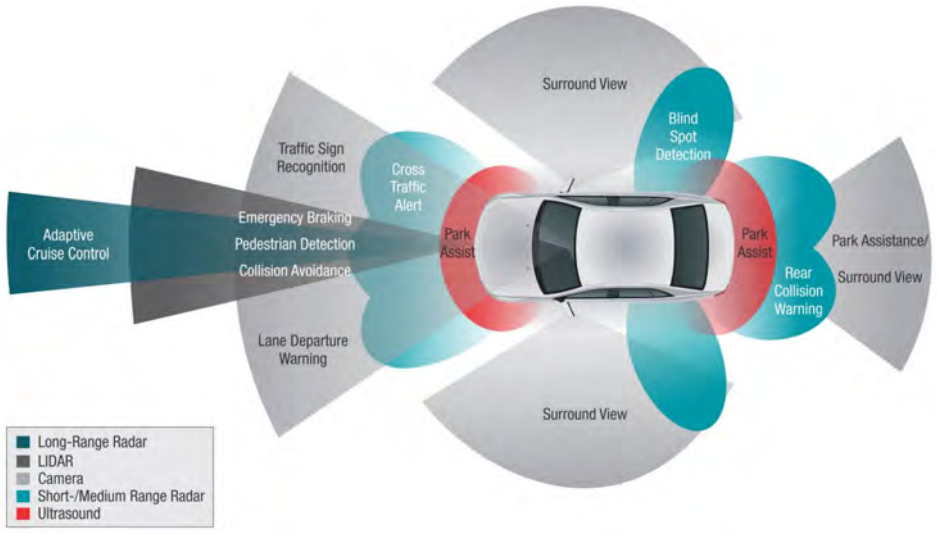

FIGURE 1.3: Overview of current ADAS sensors and functions [1]

a rapid increasing from 2017, however we have not introduced as many technologies as expected. The establishment of relative standards and regulations for the car industry may play some role to increase the adoption rate, however, developing more intelligent and driver-adaptive ADAS within an acceptable price range would be the key impetus for the popularity of ADAS.

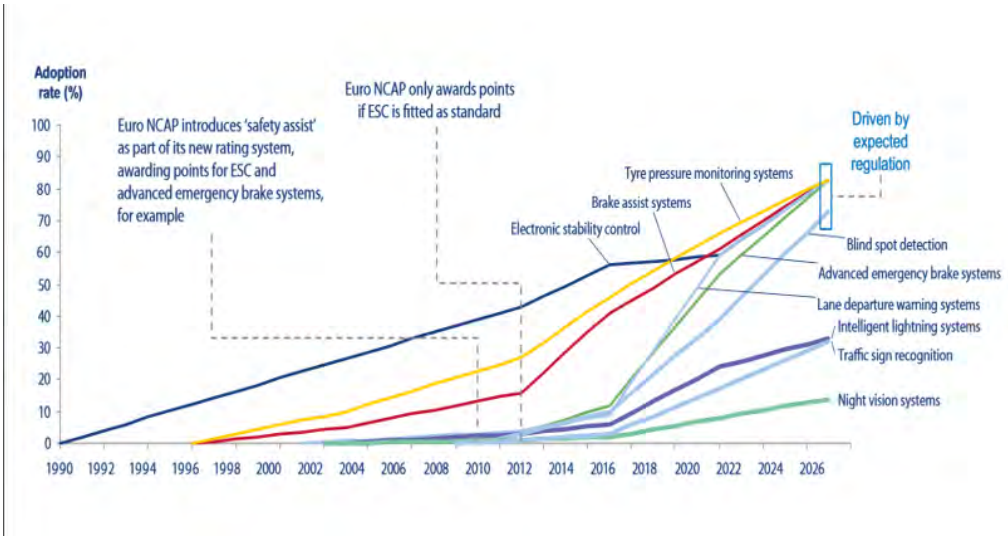

FIGURE 1.4: Adoption rate of ADAS technologies in Europe [2]

1.2.4 Fully actuated electric vehicle

Electric vehicles (EVs) offer benefits through energy security, energy efficiency, low emissions and precision in their control, hence the great interest in this technology from

industry, academia, government and regulators. With electrification comes increasing opportunities for on-board intelligent control measures to improve vehicle safety, comfort, energy conservation and environmental protection. The past several years has witnessed a great progress on advanced electric vehicle technology which can achieve the status of a fast-growing disruptive technology through their inherent flexibility and modularity. The current technology includes in-wheel motors (IWMs) and supporting power electronics to enable all-wheel drive. Traction drive plus (regenerative) braking can form a single system, fully controlled by electronic/ electrical means. The addition of a suspension mechanism and steering actuator then provides a set of corner modules leading to a Full Drive-by-Wire (FDBW) vehicle platform which is commonly assumed as the ideal platform for the vehicle dynamic control and the next-generation vehicles [13][3].

The latest generation of electric vehicles (EV's) offers great potential benefits in terms of energy security, fuel economy, low emission etc. and has generated great interest among the industry, academia, government and regulators. And the use of electrical technology coupled with 'electronic intelligence' for improving vehicle safety, comfort, energy conservation and environmental protection may be considered as key factors to break the 'bottle necks' of EV's marketization. With the rapid development of in-wheel motors (IWMs) and supporting power electronics, a novel form of EV for which all four wheels can be independently controlled by the integrated chassis control system is also widely considered as a suitable architecture for next-generation EV's [21][13][3]. This kind of four-wheel-distributed traction, braking and steering system is able to enhance the performance of integrated vehicle dynamics and motion control by fully coordinating the resultant forces of the four tyres, where the relevant path planning and tracking controls are integrated with the optimal energy consumption minimizing control.

The ideal fully drive-by-wire (FDBW) EV therefore comprises: (1) a vehicle motion controller with an electronic interface to the driver; (2) a power management system with batteries and power electronics; (3) typically four identical corner modules each with two active degrees of freedom-steer and drive/brake-plus one passive degree of freedom for the suspension (which could optionally become actively controlled in the future).

In addition, this architecture supports autonomous or semi-autonomous operation via three types of enhancement of the motion control system:

First is the use of additional sensors, sensor fusion and advanced control algorithms (1), this based on the current trends in improved information processing. Since the driver need not be the ultimate fail-safe, the four-wheel independent driving system (4WIDS) provides a desired platform for the EV to achieve safe operation, fault-tolerance and

reliability. For example, in the case of a serious fault at one of the four wheels, the EV may still be controlled intelligently with the other three wheels, at least sufficient to navigate to a safe area.

Second is the power management system (2). The EV with the use of power management system is expected to be capable of a better energy saving performance than the normal EV since: a) the structure of IWMs has an innate advantage to achieve full energy regeneration in braking; b) the braking/driving force control allocation method for 4WIDS can be integrated with the optimal minimizing energy consumption control.

Third is the typical structure of four identical corner modules (3), this helps the vehicle obtain higher flexibility and maneuverability with additional active degrees of freedom, so that the vehicle can achieve more modes of motion, in other words, the vehicle can move towards any direction with the control of four wheel steering angle. In addition, the modular structure has significant economic benefits for mass production.

Integration via self-driving technology based on environment sensing, path planning and path tracking has become increasingly feasible, and has become a very 'hot topic' for both academia and the automotive industry. The next-generation EVs should be configured with self-driving capability built-in, including sensing and communication interfaces to support the fast growing technology of intelligent transportation system. This is the vision for future vehicle technologies that inspires the research presented in this dissertation.

1.3 Research Hypotheses

The focus of this research is to design a systematic controller for cooperative driving systems. The focus is on the hierarchical control architecture discussed above. A particular focus is on driver interpretation and the effects of constraints. Hence, the research in this dissertation is founded on the following hypotheses:

1) The systematic method for moderating driver or system demands is feasible so that an integrated chassis and driveline control system can operate in a predictable manner.

2) The moderated particle reference (MPR) model can ensure predictable and stable operation near the friction limits, maintaining driver's controllability for curvature and speed tracking.

3) Control moderation (via MPR) can be extended to address rollover prevention (R-MPR). This can address issues such as the trade-off between path following and rollover prevention, and also the need for a seamless transition between keeping the driver in

the control loop and allowing an electronic safety system to make a fully autonomous intervention.

4) A novel control allocation (CA) approach can replace the common technique of constrained quadratic programming. Such an approach may have several advantages for real-time control within the cooperative driving system.

1.4 Main Research Contributions

This dissertation proposes an original and systematic method for moderating driver or system demands so that an integrated chassis and driveline control system can operate in a predictable manner. The moderated particle reference (MPR) model has been validated to ensure predictable and stable operation near the friction limits, maintaining controllability for curvature and speed tracking; and R-MPR is developed to satisfy the issues relating to both un-tripped and tripped rollover. This includes the trade-off between path following and rollover prevention, and also need for a seamless transition between keeping the driver in the control loop and allowing an electronic safety system to make a fully autonomous intervention.

To ensure the proposed control method can be fully implemented into the real-time controller, this dissertation proposes a novel CA approach based on the pseudo-inverse matrix. This PICA method shows great potential and it is shown to obtain desired CA performance and improve on existing methods both inside and near the limits of friction. The hardware and driver in the loop driving simulator test results are used to test and validate the approaches.

1.5 Related Publications

1. The implementation of PPR/MPR control strategy with hardware and human driver in the control loop test and the influences of the human driver steering behavior on vehicle motion performance with PPR/MPR presented in chapter 3 and 6 are based on the following papers:

Zhang, D., Gordon T., Gao, Y. and Zong, C., "Intelligent Electronic Steering Program Based on Road Departure Mitigation Control", Proceedings of the 2016 IEEE International Conference on Systems, Man, and Cybernetics (*SMC 2016*)

Zhang, D., Gordon T., Zong, C. and Zhang, R., "Development and Validation of the Moderated Particle Reference Strategy with Driver in the Loop", Proceedings of 14th

International Symposium on Advanced Vehicle Control *AVEC'18*, Beijing, China July 2018.

Zhang, D., Zhang, R., Gordon, T., "A Novel Approach of Combined Control Allocation and Moderation for Road Departure Mitigation" submitted to *IEEE Transactions on Vehicular Technology*

2. The R-MPR control strategy presented in chapter 4 are based on the following papers:

Zhang, D., Gordon, T., Gao, Y., Zong, C. and Lidberg, M,"A Novel Control Mediation Approach to Active Rollover Prevention", Proceedings of 13th International Symposium on Advanced Vehicle Control *AVEC'16*, Munich, Germany September 2016.

Zhang, D., Gordon T., Zhang, R., Yuan, H. and Zong, C.,"A Unified Approach to Rollover Prevention Based on Control Allocation", Proceedings of the 25th International Symposium on Dynamics of Vehicle on Road and Tracks (*IAVSD 2017*)

Zhang, D., Gordon, T., Zong C., "Integrated Chassis Controller for Combined Approach of Vehicle Rollover Prevention and Road Departure Mitigation" submitted to *Vehicle System Dynamics*

3. The pseudo-inverse based control allocation method and its comparison with sequential quadratic programming approach presented in chapter 5 are based on the following papers:

Zhang, D., Gordon T., Zong, C. and Zhang, R., "Development and Validation of the Moderated Particle Reference Strategy with Driver in the Loop", Proceedings of 14th International Symposium on Advanced Vehicle Control *AVEC'18*, Beijing, China July 2018.

Zhang, D., Gordon, T., Liu, Y., Zong C., "Approach of Constrained Control Allocation Method based on Pseudo-Inverse Matrix for Real Vehicle Application" submitted to *IEEE/ASME Transactions on Mechatronics*

1.6 Dissertation Outline

This dissertation is organized in seven chapters. Chapter 1 has given a short overview of the current intelligent vehicle control approach and its challenge, as well as the areas where the present research contributes to the literature. Chapter 2 introduces the research background of the relevant technology progress. A hierarchical vehicle dynamics control system with three control layers including the current approaches in every layer is introduced for vehicles with "over-actuated" chassis control systems. Chapter 3

introduces a systematic method for moderating driver or system demands so that an integrated chassis and driveline control system can operate in a predictable manner within available friction constraints. Demands from a driver interpreter are fed into the proposed moderator, based on the dynamics of a friction-limited particle, the result being a moderated particle reference (MPR). Chapter 4 presents a novel technique for transforming driver commands into chassis control signals in the context of rollover prevention when a vehicle with a high mass center is driven at high speed on a curved road. The proposed R-MPR is to establish best-case methods for autonomous and driver-adaptive interventions based on different road conditions. Chapter 5 proposes a new approach for the constrained CA based on the pseudo-inverse matrix. It is validated that the proposed PICA method can obtain desired CA performance and improve on existing methods both inside and near the limits of friction, and shows great advantages to be well applied in the real-time vehicle control applications. In chapter 6, the proposed systematic control approach is tested via the hardware and driver in the loop experiments to test whether the new methods can be effectively implemented in real-time control applications while preserving the control interaction of the driver. Finally, the summary and conclusion are given in chapter 7, and some potential future works based on the proposed systematic control approach are indicated.

Chapter 2

Research Background

Active chassis and driveline control for ground vehicles has made remarkable progress in recent years. Such systems make use of brake, steering and driveline actuators (including active differentials) and provide individual control functions such as antilock brakes, traction control and vehicle stability control. Much work has previously been done in this area during recent years, e.g. [22][23][24]. For vehicle dynamic control (VDC) systems, typical control states are longitudinal velocity, lateral velocity, and yaw rate, while the actuator set could include individual wheel drive/brake and steering, comprising a redundantly actuated system. Considerable research has focused on integrated vehicle dynamics control systems [25][26][27][28][29]. For example, He et al. coordinated active front steering (AFS) and dynamic stability control (DSC) subsystems based on the fact that AFS and DSC can both influence the lateral vehicle dynamics and have control objectives and effective regions of their own [30]. Nagai proposed the integrated control system of the front steering angle compensation and the braking force distribution with the application of model-matching control technique based on optimal control theory [25].

There are many advantages of employing a centralized control system of hierarchical structure for the whole vehicle control system. Commonly the vehicle motion controller with a redundant set of actuators include three levels (Figure 2.1). First, a high-level motion controller commands a vector of vehicle mass-center forces and yaw moment in order to meet the overall motion control targets. Second, a control allocation algorithm generates different actuator control targets such that they together produce the desired global control efforts. Third, the low-level control algorithm will control the actuators to achieve the control objectives. In this dissertation, we also consider the vehicle motion control with a hierarchical control architecture that includes high-level controller, control allocation, and low-level controller, as summarized in Figure 2.1.

As upper-level controller, motion controller translates optimal vehicle performance into desired acceleration vectors. Then the required vehicle-level control efforts can be obtained via the vehicle reference model with the actual vehicle running parameters. This is important so that force allocation is guaranteed to be feasible. The desired lateral and longitudinal tire forces in this case for each tire can be optimally distributed by the CA algorithm with the consideration of tire friction limits and other constraints. An inverse tire model transforms the desired longitudinal/lateral forces of each tire to the corresponding tire slip ratio and slip angle. Then for the actuator control inputs, which are tire braking/acceleration torques and steering angles can be finally calculated through the analytical inverse tire model. The resulting vehicle states are then fed back to the high-level controller to close the loop.

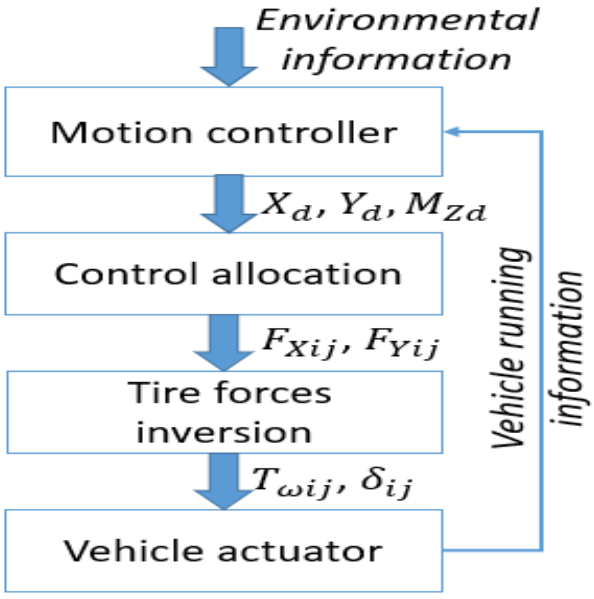

FIGURE 2.1: Hierarchical control structure (driver inputs can come in from the top as well as environmental information)

2.1 Vehicle dynamics and tire model

In VDC it is common to adopt the well-known 2-DOF linear bicycle model as a reference, to generate reference vehicle states based on driver inputs. The 2-DOF linear bicycle model typically assumes the vehicle moves on a high friction road and has lateral acceleration less than around 0.4g, in which region tire characteristics may be considered linear. However, when a vehicle moves on a low friction road or the lateral acceleration is relatively large, then the linear bicycle model is no longer suitable. Further, speed control is an integral part of the control methods introduced below so the 2-DOF linear bicycle model is not suitable. Hence, in this dissertation, we employ a standard 3-DOF

vehicle dynamic model including longitudinal, lateral and yaw motions of planar motion. The model also allows for nonlinear tire forces.

2.1.1 Vehicle dynamic model

The primary motions associated with handling and stability are the longitudinal, lateral and yaw motions of planar motion as shown in Figure 2.2.

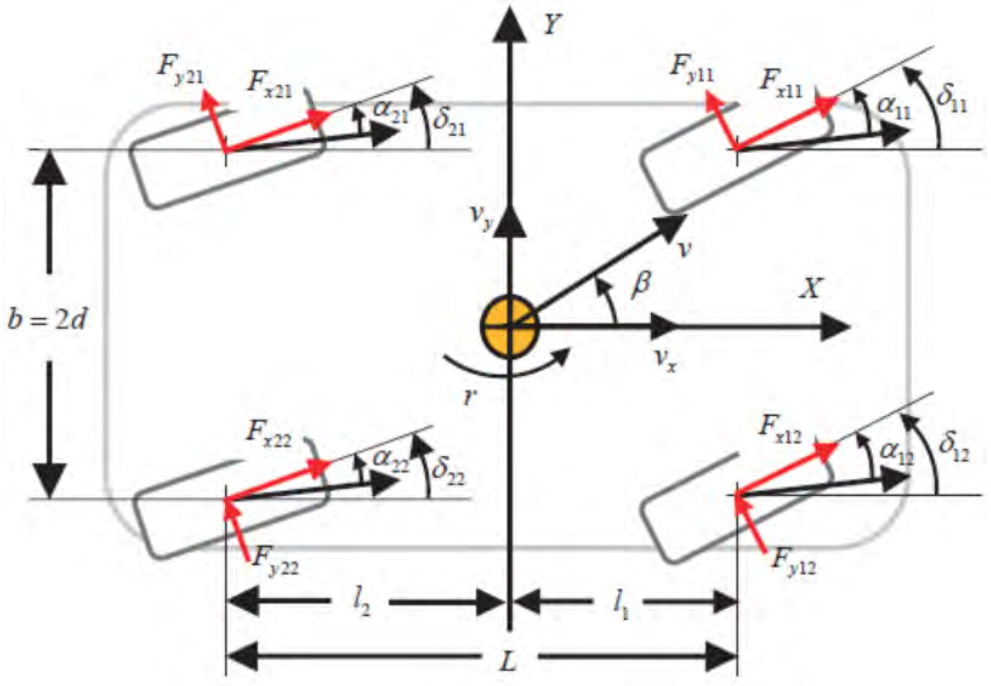

FIGURE 2.2: Vehicle dynamic model

The planar dynamics are derived from the standard Newton-Euler theory using motion variables in the vehicle fixed X-Y chassis (CoG) coordinate system. The high-level nonlinear feedback controller will specify in-plane forces and yaw moment:

$$\begin{aligned} X &= \sum F_{xij} = m(\dot{v_x} - v_y r) + \frac{\rho}{2} C_d A_f v_x^2 \\ Y &= \sum F_{yij} = m(\dot{v_y} + v_x r) \\ M_z &= \sum [(-1)^j d F_{xij} - (-1)^i l_i F_{yij}] = I_z \dot{r} \\ F_{Xij} &= F_{xij} \cos\delta_{ij} - F_{yij} \sin\delta_{ij} \\ F_{Yij} &= F_{xij} \sin\delta_{ij} + F_{yij} \cos\delta_{ij} \end{aligned} \tag{2.1}$$

The vertical load on each wheel F_{zij} is a function of both the vehicles static load distribution and dynamic weight transfer associated with longitudinal and lateral acceleration. The longitudinal acceleration influences the normal loading between front and rear wheels while the lateral acceleration affects the normal loading between left and

right wheels. Then, ignoring front-rear variations in roll center heights and suspension roll stiffness, the vertical load at each wheel is estimated as:

$$F_{zij} = \frac{mgl_{i'}}{2L} + (-1)^i \frac{ma_x h_s}{2L} + (-1)^j \frac{ma_y h_s l_{i'}}{2Lb} \tag{2.2}$$

where $i' \neq i, (i, i') \in 1, 2$.

2.1.2 Tire model

The nonlinear tire model characteristics are crucial to solving this problem in limiting road/tire conditions. In the low-level controller (introduced below in section 2.4), the tire model is employed for calculation of the tire sideslip angles (via tire model inversion). Hence, to facilitate the real-time implementation and precisely inverse the tire model, a simple tire model in [31] is employed in this dissertation to depict the relationship between the lateral force and sideslip angle in the tire stable and monotonic region by using the arctangent function to fit the experimental curve, given by [32]:

$$F_{yij} = -C_{\alpha ij} \sqrt{1 - (\frac{F_{xij}}{\mu F_{zij}})^2} \ \frac{\mu}{k} tan^{-1}(\frac{k}{\mu}\alpha_{ij}) \tag{2.3}$$

where,

$$k = \frac{C_{\alpha ij}\pi}{pF_{zij}}, p = 2 \tag{2.4}$$

where $C_{\alpha ij}$ is the tyre cornering stiffness of each wheel; μ is the tyre-road friction coefficient (assuming each wheel's tyre-road friction coefficient is same as μ) ; α_{ij} is the tyre sideslip angle. p is a curve-fitting constant, which can be further fitted in order to improve the tire model accuracy in relatively large sideslip angle region.

By fitting the parameter p in the tire model, a tire lateral force comparison between the tire model and CarSim test data are shown in Figure 2.3. As indicated in Figure 2.3, the calculated lateral forces under varying vertical loads are compared with CarSim test data, implying that the modified tyre model can describe tyre non-linearities with acceptable accuracy in the controlled region (in small slip angle area) [3]. The controlled region can be improved by fitting the parameter p, however in the meantime the accuracy will become worse.

Note that, the F_{xij} is used as an input to the tyre model, rather than slip ratio, so the wheel spin dynamics are excluded.

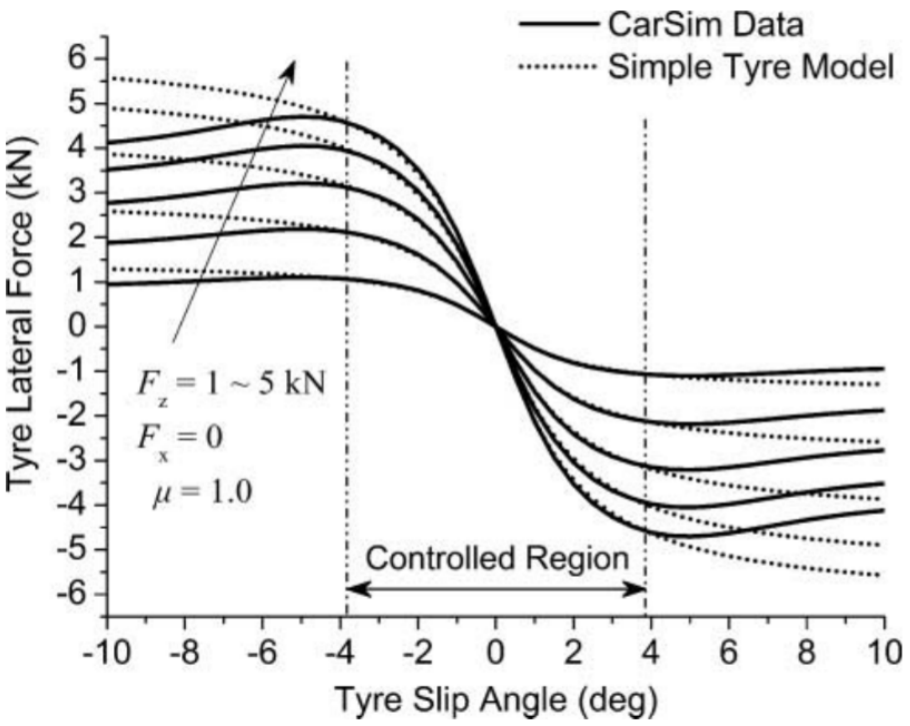

FIGURE 2.3: Tyre lateral force comparison: simple tyre model and CarSim test data

2.2 Upper-level controller

Generally the upper-level control layer (as shown in Figure 2.1) is obtaining the environmental and vehicle running information, and interpreting driver inputs, then calculating the resultant vehicle-level longitudinal and lateral forces and moments of the vehicle to make it realize the desired path and speed targets. Usually the upper-level controller follows a model which can be particle, bicycle model, etc., or it can be some geometric path and speed profile obtained from a mathematical formula (e.g. polynomial). Besides, other upper-level controllers can take the ideal and personalized vehicle dynamics control [33] and energy conservation control target [34]. However, for the active safety controller, the desired vehicle particle path performance is taken as the main control reference for the collision avoidance.

In this dissertation, we mainly propose two control strategies as the upper-level controller: Model Predictive controller and Path Particle Reference based controller. The MPC control is commonly used as the high-level controller for path tracking which has been proved to be efficient enough to solve the path tracking problem in normal conditions [35][36]. The PPR based control strategy is based on the optimal control of a friction-limited particle, the target being to minimize the maximum off-tracking from the commanded trajectory [37]. The PPR based reference can provide combined braking and turning accelerations of the vehicle mass center in limited situation for the optimal

road departure control [38]. Hence, these two upper-level control strategies are proposed to cover all the possible driving situations under various tire force conditions.

In addition to these, in 2002, T. J. Gordon proposed a driver model for self-driving vehicles based on the convergent vector field [39]. By establishing a reference vector field, non-linear feedback control and residual friction control were used to ensure that the vehicle's driving direction converges to the reference path, and pointed out the application prospect in advanced cruise control systems. Since then, the reference vector field method has been more widely studied and applied in the fields of path planning and tracking, obstacle avoidance and extremum seeking [40][41][42][43]. When it is used as the motion controller of the vehicle, the flow vector field can be constructed by the look-ahead point, the reference path and the current position to provide the desired forces and moment for the vehicle. It is more suitable for the vehicle dynamic controller which can decouple the total force and control the tires independently. The RVF based upper-level control strategy has shown great potential and been proved to be efficient enough for the real-time control, however, the optimal parameter fitting of the RVF takes lots of control efforts to obtain the optimal control effect, and it will have a great influence from the online vehicle running states which affect the comparison between proposed control allocation methods in following chapters.

2.2.1 Model predictive controller

An integrated controller based on MPC is introduced to realize the optimal path tracking. The integrated controller is comprised of MPC motion control layer and actuator control layer. To predict the motion of the vehicle in controller, a single-track 3-DOF model is used. As shown in Figure 2.4, the MPC motion control layer is used to calculate the desired force of the front and rear tires by minimizing an error function defined below. And the desired tire forces are obtained by controlling the drive torques and the steering angles of tires using the actuator control layer.

Consider the conversion relationship between the local coordinate system and the global coordinate system.

$$\begin{bmatrix} X^g \\ Y^g \end{bmatrix} = \begin{bmatrix} cos\psi & -sin\psi \\ sin\psi & cos\psi \end{bmatrix} \begin{bmatrix} X \\ Y \end{bmatrix} \tag{2.5}$$

where X and Y denotes the forces in vehicle coordinate, and the X^g and Y^g denotes the forces in global coordinate, and ψ denotes the yaw angle. Combining the two equations of Equation (2.1) (ignoring the effect of vehicle aerodynamics) and Equation (2.5), to obtain the linear time-varying model predictive control, it is necessary to linearize the

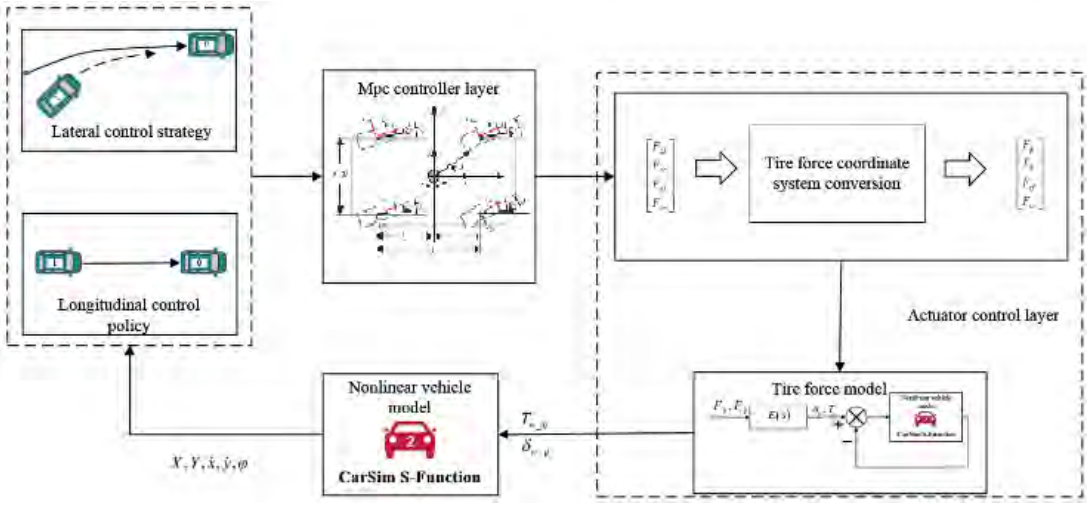

FIGURE 2.4: The schematic diagram of integrated controller

nonlinear dynamic model, so the system is described as:

$$\dot{P} = A(t)P(t) + BU(t) \tag{2.6}$$

where

$$A(t) = \begin{bmatrix} 0 & \dot{\psi} & 0 & v_y & 0 & 0 \\ -\dot{\psi} & 0 & 0 & -v_x & 0 & 0 \\ 0 & 0 & 0 & 1 & 0 & 0 \\ 0 & 0 & 0 & 0 & 0 & 0 \\ \cos\psi & \sin\psi & -v_x\sin\psi - v_y\cos\psi & 0 & 0 & 0 \\ \sin\psi & \cos\psi & v_x\cos\psi - v_y\sin\psi & 0 & 0 & 0 \end{bmatrix} \tag{2.7}$$

$$B = \begin{bmatrix} 1/m & 0 & 0 \\ 0 & 1/m & 0 \\ 0 & 0 & 0 \\ 0 & 0 & 1/I_z \\ 0 & 0 & 0 \\ 0 & 0 & 0 \end{bmatrix} \tag{2.8}$$

and $P(t) = [v_y, v_x, \psi, \dot{\psi}, y, x]^T$, where x denotes vehicle longitudinal displacement in global coordinate and y denotes vehicle lateral displacement in global coordinate, and control variables are selected as: $U(t) = [X, Y, M_z]^T$.

The first order interpolation method is used to discretise the equations of motion, and the discrete state space equation is obtained as:

$$\begin{aligned} P(k+1) &= [I+TA]P(k)+TBU(k) \\ &= A_t P(k)+B_t U(k) \end{aligned} \tag{2.9}$$

where T denotes the sample time, and I denotes the unit matrix.

The control objective in this analysis is to manage the position errors, especially the lateral position error and yaw angle error. The mathematical expression of the control objective can be written as equation 2.10.

$$\begin{aligned} J(k) = &\sum_{i=1}^{N_p} \parallel \eta(k+i \mid t) - \eta_{ref}(k+i \mid t) \parallel_Q^2 \\ &+ \sum_{i=1}^{N_e-1} \parallel \Delta U(k+i \mid t) \parallel_R^2 + \gamma\varepsilon^2 \end{aligned} \tag{2.10}$$

where R, Q and γ are weight coefficients, in this dissertation, to balance the weights of feedback variables and control variables [44], Q is tuned as: $Q = \begin{bmatrix} 1000 & 0 & 0 \\ 0 & 10000 & 0 \\ 0 & 0 & 10000 \end{bmatrix}$, R is tuned as $R = \begin{bmatrix} 0.005 & 0 & 0 \\ 0 & 0.005 & 0 \\ 0 & 0 & 0.005 \end{bmatrix}$, and γ is tuned as $\gamma = 1000$; and η denotes the reference obtained by trajectory as $[x, y, \psi]^T$. The first term of the formula represents expectation that the error between the predicted trajectory $\eta(k+i \mid t)$ and the expected trajectory $\eta_{ref}(k+i \mid t)$ should be smallest. The second term denotes that the change of control values $\Delta U(k+i \mid t)$ should be small as much as possible. And in the third term, ε denotes the relaxation factor, preventing the occurrence of no feasible solution by proper release of the hard constraint (transforming hard constraint into soft constraint).

Defining: $\xi(k \mid t) = \begin{bmatrix} P(k \mid t) \\ U(k-1 \mid t) \end{bmatrix}$, we can get that:

$$\begin{aligned} \xi(k+1 \mid t) &= \tilde{A}_t \xi(k \mid t) + \tilde{B}_t \Delta U(k \mid t) \\ \eta(k \mid t) &= \tilde{C}_t \xi(k \mid t) \end{aligned} \tag{2.11}$$

where $\tilde{A}_t = \begin{bmatrix} A_t & B_t \\ 0_{m\times n} & I_m \end{bmatrix}$, $\tilde{B}_t = \begin{bmatrix} B_t \\ I_m \end{bmatrix}$, n denotes the dimension of state variables and m denotes the dimension of the control variables. The systems predicted output

expression is:

$$Y(t) = P_t\xi(t) + K\Delta U(t) \tag{2.12}$$

where

$$\begin{aligned}
Y(t) &= \begin{bmatrix} \eta(t+1 \mid t) \\ \eta(t+2 \mid t) \\ \cdots \\ \eta(t+N_c \mid t) \\ \cdots \\ \eta(t+N_p \mid t) \end{bmatrix}, P_t = \begin{bmatrix} C_t\tilde{A}_t \\ C_t\tilde{A}_t{}^2 \\ \cdots \\ C_t\tilde{A}_t{}^{N_c} \\ \cdots \\ C_t\tilde{A}_t{}^{N_p} \end{bmatrix} \\
K &= \begin{bmatrix} C_t\tilde{B}_t & 0 & 0 & 0 \\ C_t\tilde{A}_t\tilde{B}_t & C_t\tilde{B}_t & \cdots & 0 \\ \cdots & \cdots & \cdots & \cdots \\ C_t\tilde{A}_t{}^{N_c-1}\tilde{B}_t & C_t\tilde{A}_t{}^{N_c-2}\tilde{B}_t & \cdots & C_t\tilde{B}_t \\ C_t\tilde{A}_t{}^{N_c}\tilde{B}_t & C_t\tilde{A}_t{}^{N_c-1}\tilde{B}_t & \cdots & C_t\tilde{A}_t\tilde{B}_t \\ \cdots & \cdots & \cdots & \cdots \\ C_t\tilde{A}_t{}^{N_p-1}\tilde{B}_t & C_t\tilde{A}_t{}^{N_p-2}\tilde{B}_t & \cdots & C_t\tilde{A}_t{}^{N_p-N_c}\tilde{B}_t \end{bmatrix} \\
\Delta U(t) &= \begin{bmatrix} \Delta U(t \mid t) \\ \Delta U(t+1 \mid t) \\ \cdots \\ \Delta U(t+N_c \mid t) \end{bmatrix}
\end{aligned} \tag{2.13}$$

For minimizing the objective function shown above by quadratic programming, it should be transformed into standard form [45][44]. With the equation 2.13, the solution U can be obtained, and the actual control output is shown as:

$$U(t+1) = U(t) + \Delta U(t+1) \tag{2.14}$$

The key parameters in MPC for the application in the simulation of later double-lane change (DLC) path tracking control is: the prediction horizon $N_p = 40$, the control horizon $N_c = 1$, the sampling time $T = 0.02s$.

2.2.2 Particle reference

The problem of disconnect between driver demands and vehicle response is well-known in the context of terminal *understeer* [46][47][37][48][49]. In this event, during cornering, the front lateral tire forces become saturated; if the driver increases the steering

wheel angle, there is no consequent increase in path curvature; thus the driver experiences a dead-band in term of vehicle lateral control. Recent approaches to understeer mitigation have considered path curvature as the primary control target, and this is partially controlled via reduced vehicle speed [46][47][37]. Note that the particle ignores yaw motion but integrates both path and speed control. In particular, the Parabolic Path Reference (PPR) [50][37][38] is based on the optimal control of a friction-limited particle, the target being to minimize the maximum off-tracking from the commanded trajectory. For any given recovery from the terminal understeer strategy, the maximum off-tracking occurs when the velocity is tangential to the reference trajectory. It is found that minimization of the maximum off-tracking is achieved by directing the force in a globally fixed direction, perpendicular to the path tangent at the anticipated point of the maximum off-tracking. The optimal recovery from the terminal understeer to the reference trajectory is identified as a parabolic motion. This way of representing the dynamics of the vehicle under terminal understeer condition also provides greater insight into the fundamentals of the recovery from terminal understeer. The PPR reference combines braking and turning accelerations of the vehicle mass center in such a way that a reduction in speed is coordinated with increasing path curvature. It emerges that the acceleration vector is fixed in the inertial reference frame as shown in Figure 2.5. In this figure the geometry is exaggerated; the particle enters a curve with entry point at $t = 0$; the point of maximum off-tracking (lateral path deviation) occurs at $t = T$. The constant optimal global force vector is shown as F, and the resulting path is analogous to that of a projectile motion under gravity; this minimizes the maximum off-tracking provided the dominant vehicle acceleration constraint is a circular boundary in the $G-G$ diagram of the vehicle.

The PPR strategy is designed to minimize the maximum distance of off-tracking in the above condition. We should note that PPR strategy above is "event-based" rather than continuous: the initial speed v_0 and step-steer angle are used to define the reference.

The driver interpreter (DI) includes both longitudinal and lateral control. For the former, a target a_x^d is derived from driver pedal actions, while for lateral control the bicycle model is initially used:

$$\begin{bmatrix} \dot{\beta}^{DI} \\ \dot{r}^{DI} \end{bmatrix} = \begin{bmatrix} -\frac{2(C_{\alpha f}+C_{\alpha r})}{mv_x} & -\frac{2(l_1C_{\alpha f}-l_2C_{\alpha r})}{mv_x^2} - 1 \\ -\frac{2(l_1C_{\alpha f}-l_2C_{\alpha r})}{I_z} & -\frac{2(l_1^2C_{\alpha f}+l_2^2C_{\alpha r})}{I_z v_x} \end{bmatrix} \begin{bmatrix} \beta^{DI} \\ r^{DI} \end{bmatrix} + \begin{bmatrix} \frac{2C_{\alpha f}}{mv_x} \\ \frac{2C_{\alpha f}l_1}{I_z} \end{bmatrix} \frac{\delta_h}{i_w} \quad (2.15)$$

In parallel, a desired path curvature, K^{DI}, is obtained from the steady-state cornering condition, for steering-wheel angle δ_h and wheelbase L, the neutral steer condition will be assumed, giving:

$$K^{DI} = \frac{\delta_h}{i_w L} \quad (2.16)$$

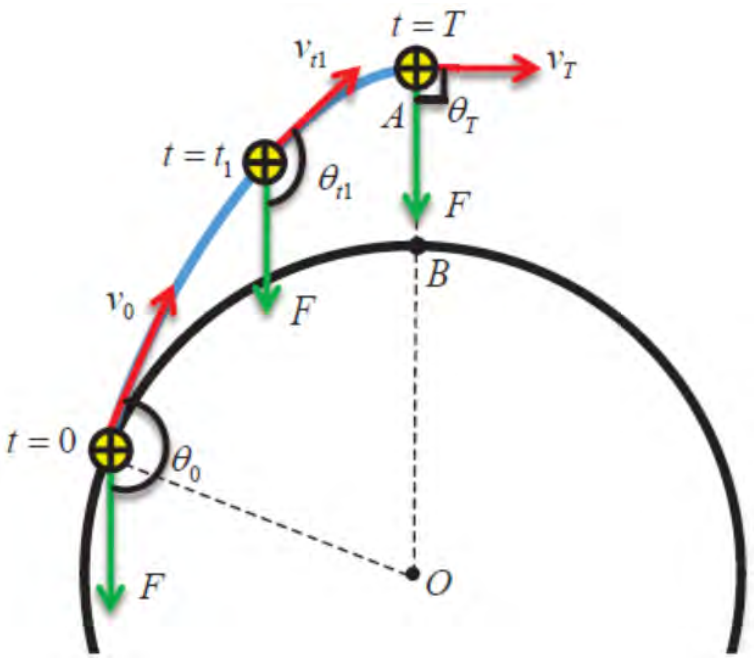

FIGURE 2.5: Kinematics of Parabolic Path Reference

Then a synthetic acceleration vector is then defined:

$$(a_x^{DI}, a_y^{DI}) = (a_x^d, v_x^2 K^{DI}) \tag{2.17}$$

Provided the magnitude remains within friction limits:

$$a^{DI} = \sqrt{(a_x^{DI})^2 + (a_y^{DI})^2} \leq \mu g \tag{2.18}$$

the bicycle reference is adopted. Otherwise some form of moderation of driver demands is required.

Note that for PPR, the authors explicitly assumed $a_x^{DI} = 0$ i.e. the driver does not directly command a change in speed. Then Equations 2.17 and 2.18 imply the friction condition takes the form $v_x \leq v_{lim}$, where

$$v_{lim} = \sqrt{\frac{\mu g}{K^{DI}}} \tag{2.19}$$

With the particle representation of vehicle motion expressed in the inertial reference frame as:

$$ma_x = -F \sin\theta \tag{2.20}$$

$$ma_y = F \cos\theta \tag{2.21}$$

The set of admissible controls, in terms of the magnitude and global direction of the synthetic force vector, is given by:

$$U = \{F \in [0, \mu mg], \theta \in [0, 2\pi]\} \tag{2.22}$$

The optimizing control input $(F^*(t), \theta^*(t))$ at time t:

$$F^*(t) = \mu g, \theta^*(t) = \theta \tag{2.23}$$

where

$$\cos\theta = \frac{v_{lim}^2}{v_0^2} \tag{2.24}$$

2.2.3 Sliding mode controller

As the vehicle is a nonlinear system, sliding mode control (SMC) is adopted as a suitable and simple vehicle motion controller design technique, based on the 3 DOF vehicle model. The SMC can be considered as a separate approach from MPC for the generation of vehicle center forces and yaw moment targets, particulary in this dissertation, SMC is mainly employed to generate yaw moment for the particle reference control strategy (introduced in chapter 3 and 4). The system state vector is chosen as $[v_x, v_y, r]^T = [x_1, x_2, x_3]^T$, and the vehicle motion equation can be written

$$\dot{x} = \begin{bmatrix} x_2 x_3 - \frac{\rho}{2m} C_d A_f v_x^2 \\ -x_1 x_3 \\ 0 \end{bmatrix} + \begin{bmatrix} 1/m & 0 & 0 \\ 0 & 1/m & 0 \\ 0 & 0 & 1/I_z \end{bmatrix} \begin{bmatrix} X_d \\ Y_d \\ M_{zd} \end{bmatrix} \tag{2.25}$$

The system output is $y = [x_1, x_2, x_3]^T$ and the control vector $u = [X_d, Y_d, M_{zd}]^T$ is to be chosen to track the output targets. It is apparent that the mass matrix $diag[m, m, I_z]$ is invertible and the system has a vector relative degree $[1, 1, 1]^T$ so there are no zero dynamics involved in the system. SMC is well-known to ensure system robustness against un-modeled dynamics such as body roll, disturbances such as wind gust, and parametric uncertainties such as variations in vehicle mass caused by load change [51]. In the SMC design, the choice of switching function is critical, because the desired dynamic performances are reflected by a proper sliding surface. For the longitudinal, lateral speed and yaw rate tracking problem, the sliding surface is selected as:

$$\begin{aligned} s_1 &= x_1 - x_1^{ref} \\ s_2 &= x_2 - x_2^{ref} \\ s_3 &= x_3 - x_3^{ref} + \lambda \int_t^{t0} (x_3 - x_3^{ref}) d\tau \end{aligned} \tag{2.26}$$

The attractive equations are:

$$\begin{aligned}
\dot{s_1} &= \frac{X_d}{m} - \frac{\rho}{2m} C_d A_f v_x^2 + x_2 x_3 - \dot{x_1}^{ref} = -\eta_1 sign(s_1) \\
\dot{s_2} &= \frac{Y_d}{m} - x_1 x_3 - \dot{x_2}^{ref} = -\eta_2 sign(s_2) \\
\dot{s_3} &= \frac{M_{zd}}{I_z} - \dot{x_3}^{ref} + \lambda(x_3 - x_3^{ref}) = -\eta_3 sign(s_3)
\end{aligned} \tag{2.27}$$

Defining $V_i = 1/2 s_i^2$, it is easy to derive the inequality: $\dot{V_i} = s_i \dot{s_i} = -s_i \eta_i sign(s_i) \leq -\eta_i |s_i|$, thus by choosing η_i large enough the sliding motion can be guaranteed and the sliding surfaces are attractive. To eliminate chattering effects from discontinuous switching, $sign(s_i)$ can be replaced by a continuous saturation function operating in a thin boundary layer [3] [52]:

$$\begin{aligned}
\dot{s_1} &= \frac{X_d}{m} - \frac{\rho}{2m} C_d A_f v_x^2 + x_2 x_3 - \dot{x_1}^{ref} = -\eta_1 sat(\frac{s_1}{\phi_1}) \\
\dot{s_2} &= \frac{Y_d}{m} - x_1 x_3 - \dot{x_2}^{ref} = -\eta_2 sat(\frac{s_2}{\phi_2}) \\
\dot{s_3} &= \frac{M_{zd}}{I_z} - \dot{x_3}^{ref} + \lambda(x_3 - x_3^{ref}) = -\eta_3 sat(\frac{s_3}{\phi_3})
\end{aligned} \tag{2.28}$$

where ϕ_i is the boundary layer thickness, hence, the control law is obtained:

$$\begin{aligned}
X_d &= m[\dot{x_1}^{ref} - \eta_1 sat(\frac{s_1}{\phi_1}) - x_2 x_3] + \frac{\rho}{2} C_d A_f v_x^2 \\
Y_d &= m[\dot{x_2}^{ref} - \eta_2 sat(\frac{s_2}{\phi_2}) + x_1 x_3] \\
M_{zd} &= I_z[\dot{x_3}^{ref} - \eta_3 sat(\frac{s_3}{\phi_3}) - \lambda(x_3 - x_3^{ref})]
\end{aligned} \tag{2.29}$$

2.3 Control allocation

This layer (as shown in Figure 2.1) is for converting the control objective (resultant forces and moments of the vehicle) obtained from the objective control layer into a constrained optimization control problem; in the meantime the optimized objective function can be chosen according to different goals. Then the further steps are solving the optimization problem and sending the distributed forces and motions to each actuator (e.g. longitudinal tire forces and steering angles of four wheels).

The concept of control allocation (CA) firstly appeared in the airplane flight controls and marine applications with the idea of a single controller for each rotational degree of freedom [53][54]. Recently, there has been increasing interest in automotive applications that the CA is widely used to deal with the actuator control constraints and faults problems with the increasing capability of realtime onboard controller [55][56][57][58][59][60].

Besides, CA which determines how to distribute the required vehicle-level acceleration to the vehicle actuators, is adopted as a suitably flexible and powerful control technique to address the challenge, since it fits neatly into a general hierarchical control architecture.

CA can be generally classified into unconstrained control allocation methods and constrained control allocation methods according to whether taking the actuator limitations into consideration. For unconstrained CA, the common way to deal with such over-actuated system is to use generalized inverses [61][62], especially the Moore-Penrose inverse method [63]. Under the normal driving situation, it is assumed that the control target can be achieved easily, hence the unconstrained CA method can obtain many solutions and a reasonable choice is to pick that with the lowest energy consumption (least-norm) [64]. However, the vehicle load transfer will result in different tire force capacities during the vehicle running process. Hence, the tire forces obtained by control allocation must take it into consideration in the possibility of actuator saturation, for which, the unconstrained CA methods seems unreliable and imprecise for the application of vehicle control. Therefore, large amount of researchers focus more on the constrained CA method.

CA determines how to distribute the required vehicle-level control efforts (virtual control inputs) $V(t) = [X_d, Y_d, M_{zd}]$ to the vehicle actuators; this is formulated as a constrained optimization problem as follows. Denote the virtual control input vector $V(t) \in R^k$ the output of the control allocator is the actual control vector, $u(t) \in R^n$, where $n > k$. Given $V(t)$, $u(t)$ is sought such that $g(u(t)) = V(t)$. In the control allocation, the linear case is almost exclusively studied [53], where the actual and virtual controls are related by a control effectiveness matrix B.

Generally, there are two different approaches to allocation adopted in the literature: allocation to individual tire forces [65][66] and allocation to individual tire slip ratio and tire slip angle [65] [67] [68]. From the above vehicle dynamic model as shown in Figure 2.2 and Equation (2.1), it is obvious that the relationship between generalized forces/-moments and tire longitudinal/lateral forces are linear, while the relationship between generalized forces/moments and tire slip ratio, tire slip angle is nonlinear because of the nonlinear tire characteristics. It can be predicted that if we directly use the nonlinear actuation relationship in the control allocation, the computational cost cannot easily satisfy the high-speed vehicle real-time control. Hence, here the control allocation problem is divided into two layers as shown in the figure 2.1: in the first layer, the longitudinal and lateral force components at the tires are chosen as the actual control variables to avoid complicated nonlinear computation, then in the second layer, based on the inverse tire model, the actual tire force control parameters, tire slip ratio and tire side slip angle,

can be obtained finally. Here the longitudinal and lateral force components at the tire are chosen as the actual control variables.

At each sampling instant t_k, $V_k = [X_d, Y_d, M_{zd}]^T$ is computed by the high-level controller, as above. Assuming each wheel can be independently controlled,

$$u_k = [F_{x11}, F_{x12}, F_{x21}, F_{x22}, F_{y11}, F_{y12}, F_{y21}, F_{y22},]^T \tag{2.30}$$

where the u_k is the control input to be determined at this stage. The goal of control allocation is to manipulate u_k so that the linear mapping $V_k = B \cdot u_k$ can be attained. The control effectiveness matrix B can be obtained from Equation (2.1) as the derivatives of the generalized forces/moment with respect to individual tire forces:

$$B = \begin{bmatrix} a_{11} & a_{12} & a_{21} & a_{22} & -b_{11} & -b_{12} & -b_{21} & -b_{22} \\ b_{11} & b_{12} & b_{21} & b_{22} & a_{11} & a_{12} & a_{21} & a_{22} \\ c_{11} & c_{12} & c_{21} & c_{22} & d_{11} & d_{12} & d_{21} & d_{22} \end{bmatrix} \tag{2.31}$$

with:

$$\begin{aligned} a_{ij} = \cos\delta_{ij}; c_{ij} = (-1)^j d\cos\delta_{ij} + (-1)^{i+1} l_i \sin\delta_{ij} \\ b_{ij} = \sin\delta_{ij}; d_{ij} = (-1)^{j+1} d\sin\delta_{ij} + (-1)^{i+1} l_i \cos\delta_{ij} \end{aligned} \tag{2.32}$$

The core technical methods solving constrained CA can be summarized as: Constrained Quadratic programming(CQP) and Pseudo-Inverse based CA.

2.3.1 Sequential Quadratic Programming (Constrained Quadratic Programming)

A common technique is the constrained quadratic programming (CQP),which is viable but not fully reliable near the friction limits because of the inaccuracy of the inverse tire model. Besides, due to the high computational load, CQP can not provide the most optimal control allocation solution in real-time controller. However, the CQP approach can be considered as a benchmark here.

Control allocation is formulated as an optimization problem in which the allocation error $\| Bu - V \|_2$ is minimized, subject to actuator constraints. In the case of VDC with control reference included, it is expected that $Bu = V$ can be achieved. However, in the presence of actuator constraints and actuator redundancy, optimization is still required. In the presence of bound-type actuator constraints, a linearly constrained quadratic

programming problem may be formulated, taking the form:

$$\begin{aligned} J_1 &= \arg\min \parallel W_1(Bu - V) \parallel_2, \underline{u} \leq u \leq \overline{u} \\ J_2 &= \arg\min \parallel W_2(u - u_c) \parallel_2, u \in \Omega \\ J_3 &= \arg\min \parallel W_3 u \parallel_2, u \in \Omega \end{aligned} \tag{2.33}$$

where u denotes the target value of tire forces and u_c denotes the current value of tire forces. $\underline{u}$ and $\overline{u}$ denotes the upper and lower limits of tire force value, Ω denotes the tire force friction constraint. In equation 2.33, the J_1 represents minimizing the control allocation error, subject to actuator constraints, while J_2 penalizes deviations from the current control set u_c, mainly so that the controller demand will be smooth; J_3 presents the minimization of the tire force utilization, to improve the control allocation efficiency. The J_2 and J_3 will be further discussed below in section 5.2.

This type of problem may be solved via Sequential Least-Squares (SLS), and needs three steps to solve. First, the weighted allocation error $\parallel W_1(Bu - V) \parallel_2$ is minimized. If feasible solutions are found, then the best solution is obtained by minimizing $\parallel W_2(u - u_c) \parallel_2$ and $\parallel W_3 u \parallel_2$. A faster alternative, used here, is obtained by approximating the SLS formulation as a Weighted Least-Squares (WLS) problem:

$$\begin{aligned} J = \arg\min(&\parallel W_1(Bu - V) \parallel_2^2 \\ &+ \gamma \parallel W_2(u - u_c) \parallel_2^2 + \lambda \parallel W_3 u \parallel_2^2) \end{aligned} \tag{2.34}$$

With correct determination of road surface friction μ then feasible solutions normally exist, and the tire model inversion will also be available. In that case we solve the linear equation via an active set method [69]. When using CQP in the tire force allocator layer, the lateral and longitudinal force of the tires need to meet the limits of the friction circle. However, it is challenging and time consuming to use it as a nonlinear constrained optimizing problem. As shown in Figure 2.6, researchers normally adopt the linear polygon constraint method to simplify the nonlinear friction circle constraint [3], and the specific octagon constraint is shown as:

To be mentioned, the polygon constraint is an approximation method which can not fully describe the whole tire friction limits, which in other words cannot take full use of the tire forces. However, the ideal tradeoff between computational cost and linearization of friction circle are still open to be discovered.

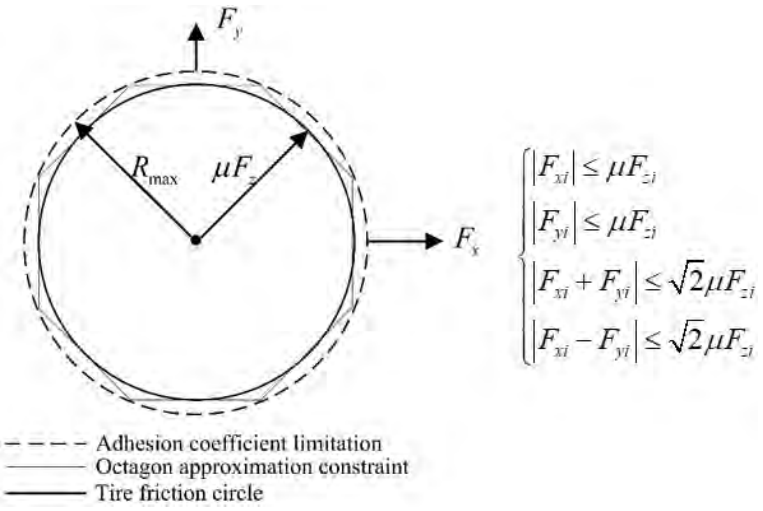

FIGURE 2.6: The schematic of linear octagon constraint [3]

2.3.2 Pseudo-inverse matrix

As stated above, control allocation is commonly formulated as an optimization problem in which the allocation error $\| Bu - V \|_2$ is minimized. However the normal CA method was found difficult to execute in the real-time [70], due to the high computational load, especially from the Sequential Quadratic Programming (SQP) of the CA algorithm. Hence, a Pseudo Inverse Matrix approach was employed to implement the CA problem, this being likely to have reduced computational cost. The first step of the Pseudo-Inverse based constrained CA is to solve optimal CA problem utilizing the mathematic characteristics of Pseudo-Inverse matrix ignoring the limitations:

$$u = B^{\sharp} V \tag{2.35}$$

where the $\sharp$ denotes the pseudo inverse operator.

For computing the pseudo inverse, the Singular Value Decompensation (SVD) is employed [71][72]. Formally, the singular-value decomposition of an $m \times n$ real or complex matrix $\mathbf{M}$ is a factorization of the form:

$$\mathbf{M} = \mathbf{U}\mathbf{\Sigma}\mathbf{V}^{*}, \tag{2.36}$$

where $\mathbf{U}$ is an $m \times m$ real or complex unitary matrix, $\mathbf{\Sigma}$ is an $m \times n$ rectangular diagonal matrix with non-negative real numbers on the diagonal, and $\mathbf{V}$ is an $n \times n$ real or complex unitary matrix. The diagonal entries σ_i of $\mathbf{\Sigma}$ are known as the singular values of $\mathbf{M}$. The columns of $\mathbf{U}$ and the columns of $\mathbf{V}$ are called the left-singular vectors and right-singular vectors of $\mathbf{M}$, respectively. $\mathbf{V}^{*}$ is the Hermitian conjugate and in the current

application where $\mathbf{M}$ is real, $\mathbf{V}^* = \mathbf{V}^\mathbf{T}$ and $\mathbf{U}$ and $\mathbf{V}$ are orthogonal matrices with $\mathbf{U}\mathbf{U}^\mathbf{T} = \mathbf{U}^\mathbf{T}\mathbf{U} = \mathbf{I_m}$ and $\mathbf{V}\mathbf{V}^\mathbf{T} = \mathbf{V}^\mathbf{T}\mathbf{V} = \mathbf{I_n}$, where $\mathbf{I}$ is the unit matrix.

The SVD can be used for computing the pseudoinverse of a matrix. Indeed, the pseudoinverse of the matrix $\mathbf{M}$ with SVD is:

$$\mathbf{M}^\sharp = \mathbf{V}\mathbf{\Sigma}^\sharp\mathbf{U}^*, \tag{2.37}$$

where $\mathbf{\Sigma}^\sharp$ is the pseudoinverse of $\mathbf{\Sigma}$, which is formed by replacing every non-zero diagonal entry by its reciprocal and transposing the resulting matrix.

If the solution of equation 2.35 of u satisfies the friction constraints, then no further steps are needed, otherwise, the over-saturated elements of the control vector will be recomputed by solving a reconstructed pseudo-inverse matrix, which is called redistributed pseudo-inverse method [73] or control reallocation algorithm (CRA) [70].

Some other researchers also introduce the method of building a Hamiltonian function, as shown in equation 2.38 [74] [64]:

$$H = \frac{1}{2}u^T W u + \lambda(Bu - V) \tag{2.38}$$

where λ is a vector of Lagrange multipliers. The control objective is set to minimize the control inputs of $\parallel u \parallel$ and the control error of $\parallel Bu - V \parallel$.

Introducing the partial derivatives of H on u and λ for the Hamilton function and make it equal to 0, finally it can obtained that:

$$u = W^{-1}B^T(BW^{-1}B^T)^{-1}V \tag{2.39}$$

It can be found that the $W^{-1}B^T(BW^{-1}B^T)^{-1}$ is recognised as the generalized inverse, setting the $W = I$, which denotes that treating the minimization of the control inputs of u and the control error of $\parallel Bu - V \parallel$ equally, then the expression 2.39 reduces to the special case of Moore-Penrose pseudo-inverse, which applies when the bracketed square matrix is invertible:

$$B^\sharp = B^T(BB^T)^{-1} \tag{2.40}$$

Finally, we can find that, with the method of building the Hamiltonian function, the results are exactly same with the Moore-Penrose pseudo-inverse and completely reflects its mathematic characteristics [75]. Hence, this method can be classified into the Pseudo-Inverse based CA method.

In addition to these, recently a simpler approach known as the MHA (modified Hamiltonian algorithm) for control allocation in limit handling is published by Gao [76] [77] which is derived from the quadratic linear optimal control (QLOC) method. This method fully respects nonlinear tire characteristics, and has been proved to be efficient enough to be executed in real-time, and appears general enough to be applied to a wide variety of vehicle manoeuvres. However, it is only validated to be efficient on the friction limit conditions so far, due to the limit of the tire model inversion process in MHA (The tire model inversion process employed in MHA is only based on the tire force data on friction limit).

2.4 Low-level controller

Below the Control Allocation layer (as shown in Figure 2.1) are the low-level controllers. To make the problem tractable in real-time, two layers are used. From the longitudinal and lateral force components at the tires, a simplified inverse tire model determines the chassis control inputs (slip ratio and slip angles). As shown in Figure 2.3, it can be expected that this method can work well except at the region with large sideslip angle, where the model inversion is less precise. Then the actuator controller converts these targets to actuator control signals, i.e. braking torques and steering actuator controls.

2.4.1 Tire model inversion

Given tire forces (F_{xij}, F_{yij}) and other sensor information, the desired tire slip variables $(\kappa_{ij}, \alpha_{ij})$ can be calculated through an analytical inverse tire model which may be efficiently implemented via a look-up table (which can be obtained from CarSim); this is not discussed further here, except to mention that model inversion requires feasibility with respect to tire force constraints, and hence the relevance of using a moderator. However, the interaction between the tire slip variables $(\kappa_{ij}, \alpha_{ij})$ is not considered for the tire force data obtained from the CarSim. The influence on this interaction will be further discussed in the chapter 3. Hence, a combined tire model inversion method based on the Equation 2.3 can be obtained as:

$$\alpha_{ij} = tan(\frac{F_{yij}}{-\chi})\frac{\mu}{k} \tag{2.41}$$

where,

$$\chi = C_{\alpha ij}\sqrt{1-(\frac{F_{xij}}{\mu F_{zij}})^2}\ \frac{\mu}{k}; k = \frac{C_{\alpha ij\pi}}{pF_{zij}}, p = 2 \tag{2.42}$$

Parameter p is a curve-fitting constant which can be further fitted to improve the accuracy of tire model inversion.

For low-level actuation, the steering system dynamics are neglected; hence the increment of steering angle $\Delta\delta_{ij}$ is equated to the desired slip angle increment $\Delta\alpha_{ij}^{d}$, as $\Delta\delta_{ij} = \Delta\alpha_{ij}^{d}$. On the other hand, for low-level regulation of wheel torque, wheel spin dynamics are significant, hence a sliding mode controller is commonly used, which is to track desired tire slip ratio κ_{ijd} using the in-wheel motor control torque T_{wij}.

2.4.2 Wheel dynamic model

The wheel dynamic are modeled as:

$$I_{\omega}\dot{\omega}_{ij} = T_{wij} - F_{xij}R - F_{zij}f_rR \tag{2.43}$$

Tire slip angle of each wheel can be calculated as,

$$\alpha_{ij} = \delta_{ij} - \arctan(\frac{v_y - (-1)^i l_i r}{v_x + (-1)^j rd}) \tag{2.44}$$

The component of the velocity of the wheel center that is parallel to the vertical wheel plane v_{wij} is given as:

$$v_{wij} = (v_x + (-1)^j rd)\cos\delta_{ij} + (v_y - (-1)^i l_i r)\sin\delta_{ij} \tag{2.45}$$

Tire slip ratio κ_{ij} of $(ij)^{th}$ wheel is defined as:

$$\begin{aligned} \kappa_{ij} &= \frac{\omega_{ij}R - v_{wij}}{\omega_{ij}R}, \omega_{ij}R \geq v_{wij}, Traction \\ \kappa_{ij} &= \frac{\omega_{ij}R - v_{wij}}{v_{wij}}, \omega_{ij}R < v_{wij}, Braking \end{aligned} \tag{2.46}$$

2.4.3 Actuator regulation

Taking the braking condition as an example, differentiating $\kappa = \frac{\omega R - v_w}{v_w}$ with respect to time, and using Equation 2.44, we can obtain

$$\dot{\kappa} = \frac{R}{I_w v_w}T_w - \frac{R^2}{I_w v_w}(F_x + F_z f_r) - (1+\kappa)\frac{\dot{v}_w}{v_w} \tag{2.47}$$

A sliding variable s_κ is chosen as the error between the actual slip ratio and the desired one,

$$s_\kappa = \kappa - \kappa_d \tag{2.48}$$

The approximation of the control law $\widehat{T}_w$ to achieve $\dot{s}_\kappa = 0$ is

$$\widehat{T}_w = \frac{I_w v_w}{R}\dot{\kappa}_d + \frac{I_w(1+\kappa)}{R}\dot{v}_w + \widehat{F}_x R + \widehat{F}_z f_r R \tag{2.49}$$

$\widehat{T}_w$ can be interpreted as the best estimation of the equivalent control. The control law should account for uncertainty in the estimation of longitudinal forces and rolling resistance, in order to guarantee the sliding condition:

$$\frac{1}{2}\frac{d}{dt}s_\kappa^2 = s_\kappa \dot{s}_\kappa \leq -\eta_k \mid s_\kappa \mid, \eta_k > 0 \tag{2.50}$$

To achieve this we select the control law $T_w = \widehat{T}_w - k_b sign(s_\kappa)$, choosing k_b in the form $k_b = \frac{I_w v_w}{R}(f_e + \eta_\kappa)$, where f_e is upper bound for the estimation error of tire longitudinal forces and rolling resistance. To suppress chattering, and analogous to the high-level controller, the braking torque control law takes the final form:

$$T_w = \frac{I_w v_w}{R}\dot{\kappa}_d + \frac{I_w(1+\kappa)}{R}\dot{v}_w + \widehat{F}_x R + \widehat{F}_z f_r R - k_b sat(\frac{s_\kappa}{\phi_w}) \tag{2.51}$$

2.5 Summary

A hierarchical vehicle dynamics control system with three control layers, including the current approaches in every layer are introduced for vehicles with over-actuated chassis control systems, i.e., having more than three independent actuator modes. For the upper-level controller, the MPC control strategy is employed as an optimal path tracking controller under normal driving conditions and a PPR based control strategy is proposed as an optimal understeer mitigation controller under limited and over-limited driving conditions. Sliding mode control is also adopted for the high-level vehicle motion controller, to provide the generalized forces/moment, then distributed to longitudinal and lateral forces of each wheel by control allocation. In the following chapters, the moderated particle reference control strategy will be proposed based on the previously published PPR method. In the control allocation layer, two particular CA methods, constrained quadratic programming and pseudo-inverse, are introduced in detail. Based on the current progress of the two CA methods, in the following chapter, a novel CA method based on the pseudo-inverse matrix is proposed. The results demonstrate that the CA method is viable for the real vehicle controller and shows significant advantages in comparison with the current CA approach. Finally, tire slip ratio is controlled by a lower-level sliding mode controller to track the desired slip ratio, manipulating the in-wheel motor torque and steering angle of each wheel.

Chapter 3

Moderated Particle Reference

In this chapter we consider the vehicle with an agile active chassis to avoid particular effects from any specific actuator constraints; more precisely, we assume the vehicle is equipped with four in-wheel electric motors and a steer-by-wire system, which can independently control each individual wheel. The in-wheel motors provide drive and brake torque, so each wheel control unit has the maximum degree of control possible (though without vertical load control). Thus we consider a four wheel independent drive/brake/steer (4WIDBS) electric vehicle as the example application.

A continuous version of PPR, based on instantaneous states, was proposed in [78], and this is developed further here. The concept of moderated particle reference (MPR) model has been proposed to ensure predictable and stable operation near the friction limits, maintaining controllability for curvature and speed tracking [78]. The MPR strategy effectively limits demands on the vehicle while preserving the control interaction of the driver, which is in contrast to simpler yaw rate based controllers, like ESC. The moderator also ensures that reference demands are feasible and hence tire model inversion and control allocation can be precisely implemented. The driver model and driving simulator tests demonstrate the proposed MPR strategy can be effectively implemented in real-time control applications while preserving the control interaction of the driver.

3.1 Background

Vehicle desired states derived from a drivers steering input can be interpreted in terms of path curvature and also speed, especially when the limits of friction are approached. Yamakado et al. attempted to address the problem of understeer by a combination of speed reduction and yaw control [46]. The proposed control reduces the vehicle speed

during the turn-in phase of the maneuver, the braking being set as proportional to lateral jerk. While it is reported that this control reduces the effects of understeer, no formal control scheme or control objective is defined. In an earlier study [47] the focus was again on modulating the direction of the acceleration vector of the mass center, here with a more explicit focus on using the combined cornering and braking forces to increase path curvature. Klomp et al. [37] formulated the problem of combined speed and directional control to minimize off-tracking when the curve entry speed is too high, or equivalently the tire-road friction is too low. The parabolic particle reference (PPR) strategy has been demonstrated as a suitable way to reduce off-tracking from a reference path [37][38].

3.2 Formulation and representation of MPR

Based on the above PPR (event-based, road geometry known), it is intended to extract a local version that induces a similar combination of braking and cornering forces in response to a step-steer input. The *moderated particle reference* (MPR) strategy is proposed, as both a simplification and a generalization of PPR. It is a simplification in that sensing of the road geometry and the motion of the vehicle relative to the road is to be excluded; it is also a generalization, in that longitudinal demands will be considered as an integral part of the driver interpreter. Initially, however, we assume $a_x^{DI} = 0$ in which case MPR is required to reduce demands when $a_y^{DI} > \mu g$ in a way that is consistent with PPR.

Figure 3.1 shows the kinematics of the PPR-controlled vehicle when $a_y^{DI} > \mu g$; the solid curve represents the actual path of the vehicle mass center and the larger dashed circle is the path derived from the driver interpreter at the initial time instant.

From the PPR theory [38] [37], the x-component of the reference acceleration (moderator output) a_x^{ref} can be obtained as,

$$a_x^{ref} = -\mu g \cdot \sqrt{1 - \frac{v_{lim}^4}{v_0^4}} \tag{3.1}$$

Further, it follows that

$$a_y^{ref} a_y^{DI} = (\mu g)^2 \tag{3.2}$$

During a sudden input from the driver, there will be a delay in building lateral acceleration, due to the transient vehicle dynamics; hence, triggering the moderator may be similarly delayed in order to fully utilize the available friction. To implement this, we adopt the trigger condition $a_y(t) a_y^{DI} > \mu g$ where $a_y(t)$ is the actual lateral acceleration;

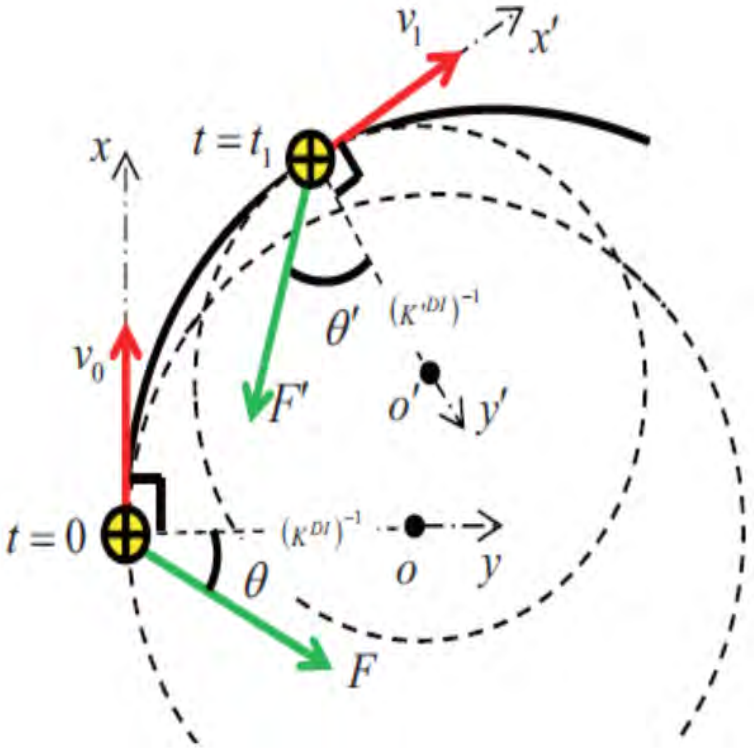

FIGURE 3.1: Kinematics of Moderated Particle Reference

the moderator lateral acceleration is however still to be based on the demanded lateral acceleration,

$$a_y^{ref} = \frac{(\mu g)^2}{a_y^{DI}} \tag{3.3}$$

3.2.1 MPR representation in the G-G diagram

The relationship between demanded and moderated mass-center accelerations can be revealed in a geometric and highly intuitive way - see Figure 3.2. When the driver demand (A) is beyond friction limits, the reference is obtained from the tangent point on the friction circle (A'). The figure also shows the geometric interpretation of angle θ in Figure 3.1; for example, theoretically, when $a_y^{DI} \to \infty, \theta \to \pi/2$ and full braking results. To confirm this geometric interpretation of the PPR/MPR mapping, we note that a_y^{DI} and a_y^{ref} satisfy the theorem of the adjacent sides in right-angled triangles,

$$\overline{OB} \cdot \overline{OA} = \overline{OA'}^2 \tag{3.4}$$

i.e. $a_y^{DI} a_y^{ref} = (\mu g)^2$, in agreement with Equation 3.2. Similarly, angle θ in Figure 3.2 is seen to satisfy:

$$\cos\theta = \frac{\mu g}{a_y^{DI}} = \frac{\mu g}{K^{DI} v^2} \tag{3.5}$$

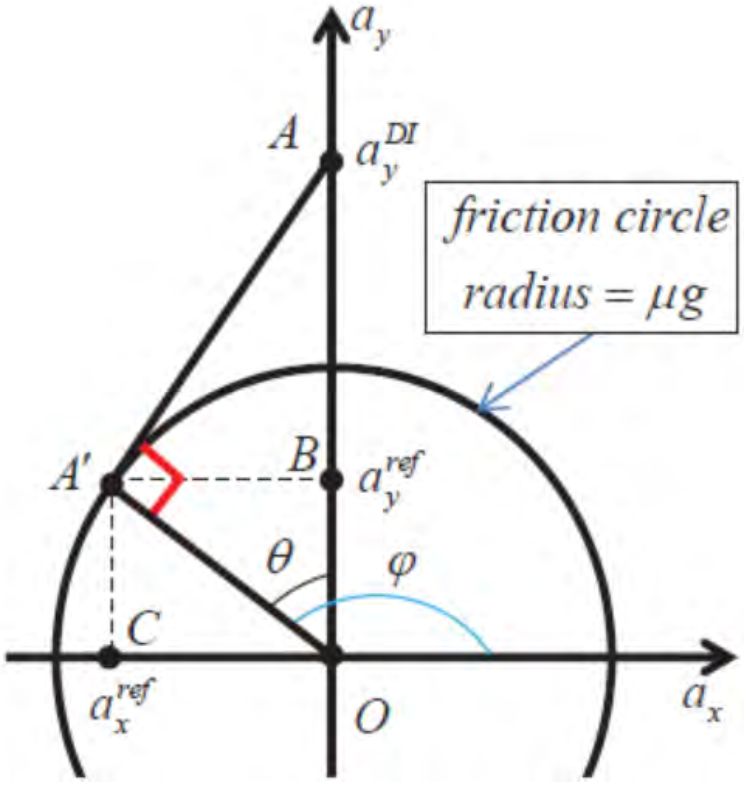

FIGURE 3.2: Friction circle interpretation of the Parabolic Particle Reference (PPR)

3.2.2 Extended mapping of synthetic acceleration in G-G diagram

The above assumes $a_x^{DI} = 0$, consistent with the PPR reference [50]. Now we remove this condition. In order to formulate the mapping back to the friction circle, we take the first quadrant (combined steering and traction) and second quadrant (combined steering and braking) of the $G - G$ diagram as an example. While there is no unique way to achieve this, the intention is to reduce longitudinal and/or lateral acceleration demands in a systematic way.

In this figure, point C represents the mapping method derived from the PPR, as the point A in Figure 3.2. Considering point F as a starting point, continuing with this aforementioned mapping idea, the mapping way become: horizontal mapping to the Y-axis, and then tangential mapping to the circle at point F'. Based on the previous experiments [78], it is found that the horizontal mapping to the Y-axis in the first step is a suitable choice if the lateral dynamic is priority for achieving the best road departure mitigation performance. To be specific, with the horizontal mapping method, steady state forward speed is the lowest, and steady state yaw rate is the highest; with the mapping angle to the Y-axis increasing, steady state forward speeds increase, and steady state yaw rates decrease; turning radius also increases. The mapping is symmetric

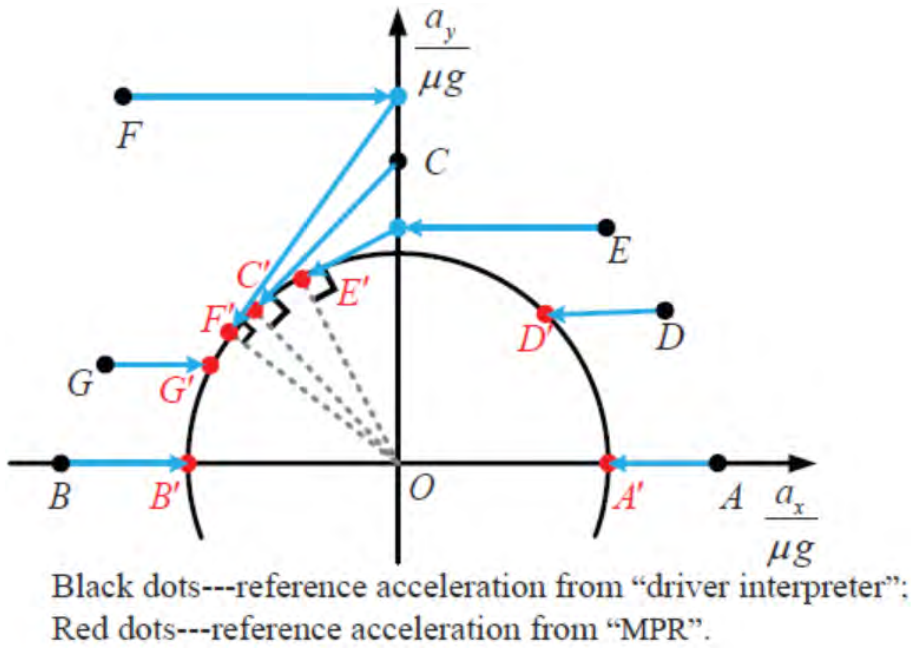

FIGURE 3.3: MPR mapping from driver interpreter to control reference-normalized G-G diagram

in the lower half-plane, while not symmetric about left and right plane (braking/acceleration). When the driver interpreted acceleration demand (a_x^{DI}, a_y^{DI}) is located in the area including point D or G, the MPR accelerations are expressed as:

$$\begin{aligned} a_y^{ref} &= a_y^{DI}; \\ a_x^{ref} &= sign(a_x^{DI}) \cdot \sqrt{(\mu g)^2 - (a_y^{ref})^2} \end{aligned} \tag{3.6}$$

And if the input demand is located in the area including point E or F, then the MPR-moderated output is defined by:

$$\begin{aligned} a_y^{ref} &= \frac{(\mu g)^2}{a_y^{DI}}; \\ a_x^{ref} &= -\sqrt{(\mu g)^2 - (a_y^{ref})^2} \end{aligned} \tag{3.7}$$

We will however revert to using (x, y) notation for reference signals in vehicle coordinates. Since wheel steering angle and braking/traction force of each wheel can be fully independently controlled, we expect the vehicle can achieve a desirable performance by manipulating torque and steering angle of each wheel, hence tracking the desired values generated from control allocation. Here, the vehicle sideslip target is assuming set to zero: $\beta^{ref} = 0$. Then the reference vehicle dynamic states are given by:

$$
\begin{aligned}
v_x^{ref} &= v_x + \int a_x^{ref} dt \\
r^{ref} &= \frac{a_y^{ref}}{v_x^{ref}}
\end{aligned}
\tag{3.8}
$$

Note that, the r^{ref} denotes the reference yaw rate in this driving situation, which will be used for the calculation of desired yaw moment as described in Equation 2.29 in section 2.2.3. This reference will also be employed in the next chapter for the validation of R-PPR/R-MPR.

3.3 Simulation results and analysis

As mentioned, we consider the control of a four wheel independent drive/brake/steer (4WIDBS) electric vehicle with a hierarchical control architecture that includes moderation and allocation, as summarized in Figure 2.1 in chapter 2. Including driver interpreter and control moderator, MPR translates driver demands into a desired acceleration vector. Then the required vehicle-level control efforts can be obtained via the vehicle reference model with the actual vehicle running parameters. This is important so that force allocation is guaranteed to be feasible. The desired lateral and longitudinal tire forces in this case for each tire can be optimally distributed by the control allocation (CA) algorithm with the consideration of tire friction limits and other constraints. As stated above, an inverse tire model transforms the desired longitudinal/lateral forces of each tire to the corresponding tire slip ratio and slip angle. Then for the actuator control inputs, which are tire braking/acceleration torques and steering angles can be finally calculated through the analytical inverse tire model. The resulting vehicle states are then fed back to the high-level controller to close the loop.

Previous simulation results have suggested reasonable vehicle performance of MPR strategy with responses of step steer with constant reference longitudinal acceleration and slowly increasing steer maneuver [78]. To further validate the vehicle-driver interaction performance with proposed control implementation, a driver model is introduced firstly in this chapter, and then the high-fidelity full-scale driving simulator and human drivers are also employed to investigate how drivers interact with MPR-based control in chapter 6.

3.3.1 Driver model

The driver model includes both speed and steering control, and outputs three command signals: acceleration (drive command), braking (brake command), and steering (steering wheel angle in rad). The acceleration and braking commands are in nominal unit ms^{-2} of vehicle acceleration, corresponding to the total drive or brake torque. Note that, by considering the vehicle capability more than driving flexibility, the combined control of longitudinal and lateral dynamic is neglected by assuming that the driver's task is only to track the given speed and path [79]. The design target of driver model is not to fully reflect the human driver behavior, but instead to operate and test the proposed control algorithm.

3.3.1.1 Speed control

The speed controller is set to track a reference speed with a simple feedback PID controller, and then the drive and brake command signals are converted from command acceleration to equivalent drive/brake torques. The tracking error between the current vehicle speed and reference speed is considered as the inputs of PID controller as shown in Figure 3.4. PID gains are set based on the desired accuracy and of speed tracking performance, for an off-line simulation, the parameter can be optimally tuned via the MATLAB PID function. The additional parameters including upper and lower saturation limits need to be tuned via considering the coupled problem between a reasonable reference speed and path tracking performance.

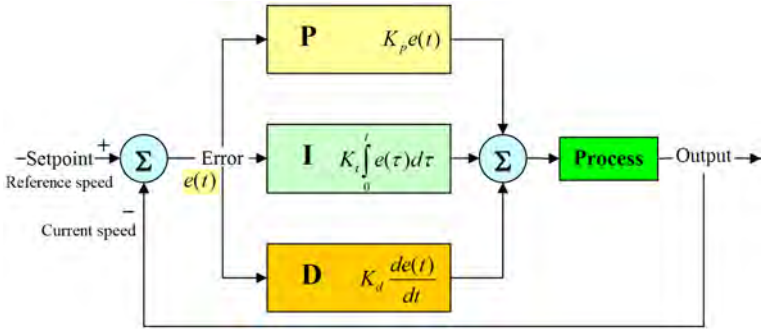

FIGURE 3.4: PID control diagram

3.3.1.2 Steering control

Here we use an optimal preview acceleration (OPA) driver model proposed in [80].

As shown in the schematic representation (Figure 3.5), the driver model predicts the vehicle's future position at the preview point by assuming that the vehicle proceeds with

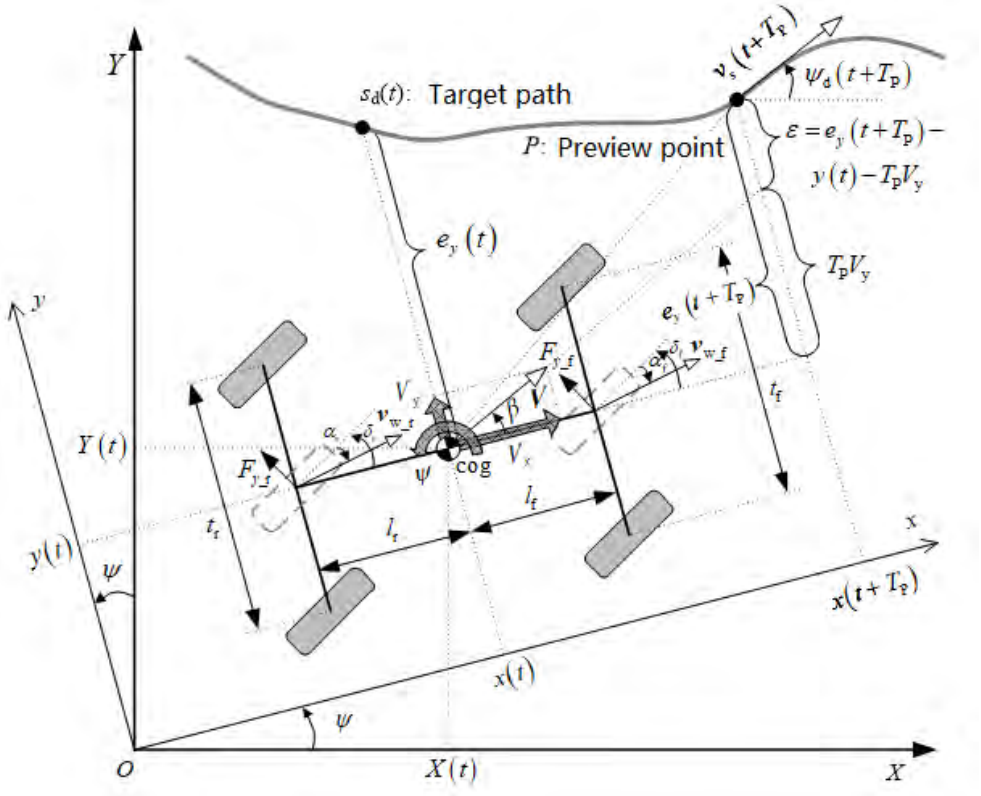

FIGURE 3.5: Schematic of OPA driver model

the current velocity at the current heading angle. Thus, the predicted lateral error ε is obtained by:

$$\varepsilon = e_y(t + T_p) - y(t) - T_p V_y(t) \tag{3.9}$$

where T_p is the preview time, $e_y(t + T_p)$ is the desired path after T_p, y is the lateral offset of vehicle mass center and V_y is the lateral velocity.

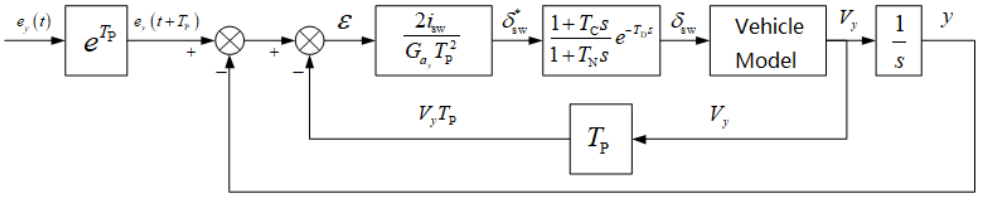

FIGURE 3.6: OPA driver model

Figure 3.6 shows the block diagram of this single-point preview model. Based on the driver model's anticipation of the vehicle response information that is the same linear response of the traditional bicycle model, a steering input that would generate the optimal lateral acceleration $a_y^{opt} = 2\varepsilon/T_p^2$ which is to minimise the lateral error [3]. The optimal steering wheel angle δ_{SW}^{opt} is given by Equation 3.10, where the G_{ay} denotes the

steady-state steering gain, defined by Equation 3.11:

$$\delta_{SW}^{opt} = \frac{2i_{SW}\varepsilon}{G_{ay}T_p^2} \tag{3.10}$$

$$G_{ay} \equiv \frac{\dot{r}}{\delta_f} \cdot v_x = \frac{v_x^2/L}{1 + K_s v_x^2} \tag{3.11}$$

where the i_{SW} denotes the steering ratio, and K_s is defined as the understeer gradient, by $K_s = \frac{m}{L^2}(\frac{l_1}{C_{\alpha r}} - \frac{l_2}{C_{\alpha f}})$.

Considering the physical limits of driver, the applied steering wheel angle δ_{SW} follows from a first-order lead-lag element with a pure time-delay, given by:

$$\delta_{SW} = (1 + T_C s)\frac{e^{-T_D s}}{1 + T_N s}\delta_{SW}^{opt} \tag{3.12}$$

where T_D is the driver brain response delay, T_N is the driver action delay; T_C is the driver correction time, with $T_C < T_D$. The term $1+T_C s$ denotes the driver's anticipation of the vehicle response information.

The OPA driver model can predict the driver's manoeuvre with reasonable accuracy as verified in [80] [81].

3.3.2 Simulation validation

As the MPR is designed to mitigate the understeer while preserving the control interaction of the driver, it can be expected that combining MPR with driver model should approximate to the PPR performance in understeer mitigation and respond to the driver model inputs. Note that, previous simulation tests [37] [38] and real-vehicle experimental tests [82] showed that four-wheel braking vehicle with PPR control strategy can achieve a much better performance in understeer mitigation than a conventional form of electronic stability controller (ESC). As an extended version of PPR, the MPR is validated via the overspeed cornering condition in comparison with PPR in this chapter. Using vehicle dynamic simulation software CarSim, combined with the above proposed hierarchical control structure which implemented in Matlab/Simulink, close-loop test (overspeed cornering condition) are simulated for the validation of the proposed control method. Particularly, the CA method based on pseudo-inverse matrix which will be described in section 5.1.1 is employed in this simulation. Note that with the CA method of CQP (introduced in section 2.3.1), the simulation results would be similar since the CA requirement are met. The vehicle parameters used in CarSim are listed in Appendix A.

In this simulation, the driving scenario consist of a straight-line tangent connected to a constant-radius curved road, and the overspeed cornering test are carried out at the initial speed of 140km/h under road condition of $\mu = 1.0$ and $R = 100m$. The MPR control strategy is implemented with the step-steer inputs and driver model inputs separately. The magnitude of the step-steer is set as 27.8° from $\delta_h = K^{DI} i_w L$ based on the Equation 2.16 in section 2.2.2. It can be expected that, the MPR test with step-steer inputs will not take account of the changing viewpoint of the driver, while MPR test with driver model can show interactive effect between vehicle running performance and driver inputs.

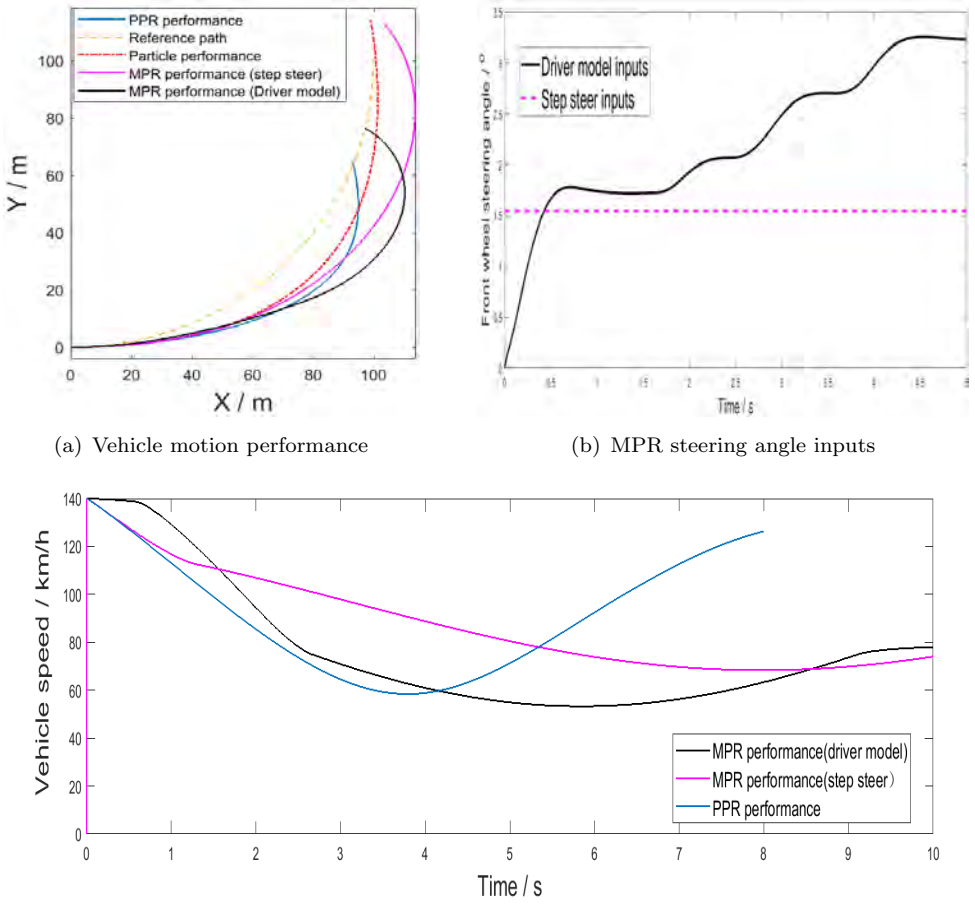

(a) Vehicle motion performance

(b) MPR steering angle inputs

(c) Vehicle velocity comparison

FIGURE 3.7: Vehicle motion performance with MPR

As shown in the Figure 3.7, the comparison of PPR performance and MPR performances with step steer and driver model inputs validate the feasibility of proposed control structure. The path performance of MPR is close to PPR at the beginning of simulation, but becomes worse in the latter half. The maximum path deviation of PPR performance is about $14.1m$ with a stable velocity of $59km/h$; the maximum path deviation of MPR performance with step steer inputs is about $16.3m$ with a stable velocity of $68km/h$; the

maximum path deviation of MPR performance with driver model inputs is about $22.1m$ with a stable velocity of $53km/h$. Specifically, the path off-tracking performance of PPR is the best, because it controls the vehicle motion based on an optimal particle motion to achieve the minimum path off-tracking distance, which is in agreement with the PPR strategy of globally minimizing the lateral path deviation of vehicle motion [50][38].

PPR is a fully autonomous controller based on optimal understeer mitigation control, however MPR is a sub-optimal control strategy where the optimization process is based only on the driver inputs. As shown in Figure 3.7, the MPR with step-steer inputs can achieve a better path deviation performance than with driver model inputs, which is due to a faster response of steering angle inputs of step-steer. According to the design concept of MPR, larger vehicle deceleration will result from faster steering angle response. To be specific, during the $0-1$ second time period of simulation, MPR with the driver model does not make the vehicle slow down quickly because of the smaller steering angle inputs, which demonstrate that the faster/larger steering angle inputs lead to faster/larger vehicle deceleration. This phenomenon is in good consistency with the mapping method of MPR which is described in section 3.2.2. Then during the $1-2$ second time period, the steering angle of driver model become larger, which results in a sharper speed reduction. During the $2-5$ second time period, the driver model roughly follows a ramp input, but the speed reduction is not corresponding with the increasing of steering angle inputs, because a^{DI} reaches the friction circle at the lower speeds. The stable velocity of MPR with driver model inputs is lower than with step steer inputs, which is also due to the faster longitudinal deceleration response of step steer inputs. Hence, the first second of the MPR control system is more critical. The real human driver's steering reactions and driving performance will be further presented in Chapter 6.

Note that, the reason PPR can perform much better in vehicle motion performance is because the proposed driver model is not designed to achieve a global minimum path off-tracking distance. The vehicle motion performance is only relevant up to the point of maximum off-tracking. Apart from the ideal particle, no simulation recovers to the ideal path at a tangent. In reality the driver will adopt a different strategy to recover the target path.

Note that, the particle performance (red dash dotted line) is slightly better than the PPR performance (blue full line) as expected, due to the inclusion of yaw dynamics via the vehicle dynamic model. Although ignoring the coupled problem with longitudinal and lateral forces in vehicle model, the additional yaw degree of freedom has a large influence for the CA process. Particularly, in this case, the desired vehicle yaw moment obtained from SMC (introduced in section 2.2.3) will become an additional CA target which will

effect the tracking of desired vehicle mass-center longitudinal and lateral forces, then as a consequence it will influence the stability performance as shown in Figure 3.8.

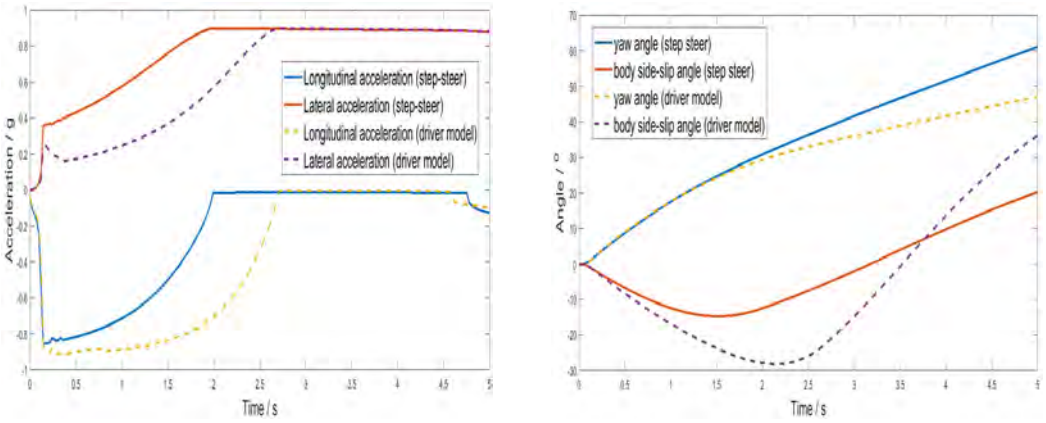

(a) Vehicle acceleration performance (b) Vehicle stability performance

FIGURE 3.8: Vehicle dynamic performance with MPR

From the velocity comparison in Figure 3.7, the MPR strategy reduces the longitudinal velocity in a systematic way maintaining driver in the control loop, and between M-PR control strategy with step-steer input and driver model demonstrate that the driver steering inputs indeed effect the mass-center longitudinal and lateral accelerations in Figure 3.8. The vehicle stability performance seem to be quite close, with a relatively larger side-slip angle coming from the driver model. In addition, although with PPR strategy the vehicle tends to achieve a minimum path off-tracking performance while ignoring and overriding the driver inputs, with MPR the vehicle can maintain maneuverability and flexibility from the driver. Note that a very simple path follower driver model has been used in this. Driving response to emergency condition and learning of the driver to adapt to MPR is not yet tested.

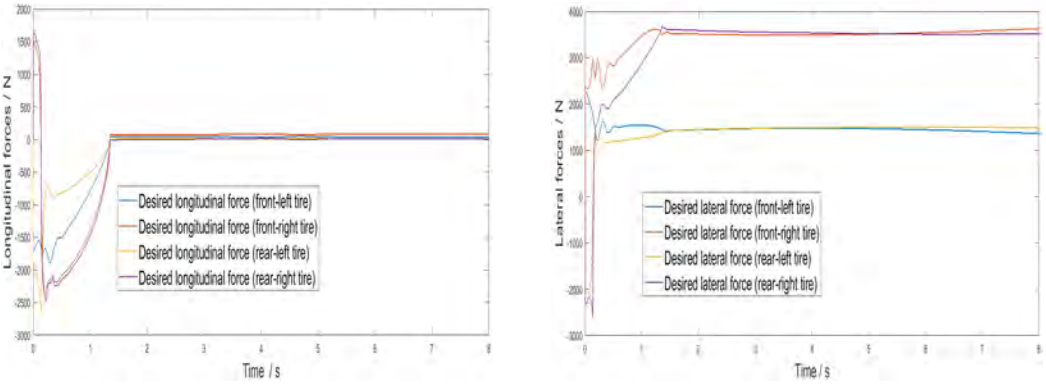

(a) Desired longitudinal tire forces from CA (b) Desired lateral tire forces from CA

FIGURE 3.9: Vehicle actuator performance with MPR

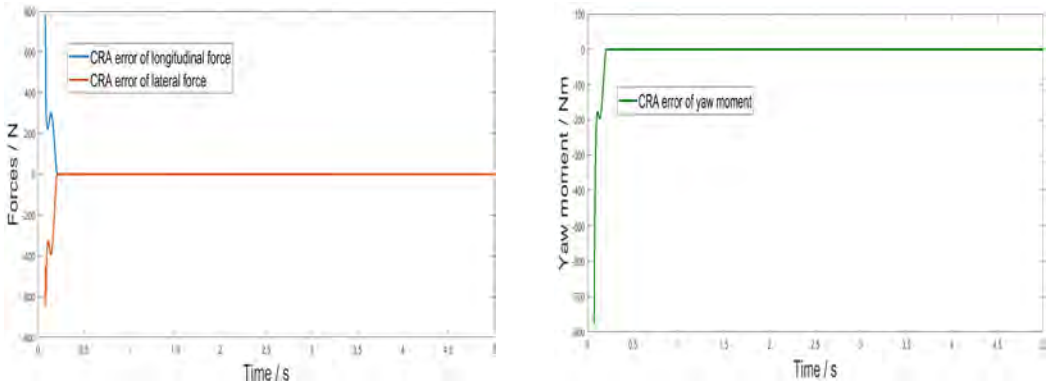

(a) CA error of vehicle-level forces (b) CA error of vehicle yaw moment

FIGURE 3.10: CA performance with MPR

Note that, the control allocation algorithm of section 5.1.1 was used to generate these results. It is found from Figure 3.12 that this CA method can guarantee a desired CA performance (approximate to zero CA errors $\| Bu - V \|_2$). Hence, through these results obtained by far, it demonstrate that the proposed CA method can well track the desired vehicle mass center target forces, and can satisfyingly be implemented in this limit control situations.

3.3.3 Actuator control

Note that, as the hierarchical control structure shown in Figure 2.1 in Chapter 2, the vehicle actuators control variables (individual tire steering angles δ_{ij} and wheel torques T_{wij}) should be the final results of the control inputs to the vehicle actuators (CarSim model in the simulations). Hence, the low-level controller should also be implemented into the hierarchical controller.

In section 2.4, the low level controller was described using sliding mode control. This standard approach was found to give errors in the case where the tyre model is not accurate. For the tracking of desired longitudinal force, assuming the rotational dynamic equilibrium in this driving situation, we employ a simple wheel model obtained from Equation 2.43 as: $T_{wij} = F_{xij}R$, and then input the obtained wheel torques to the CarSim model (including tire model). The tracking results can be found in Figure 3.11, which demonstrate that, even with this simple wheel model, the obtained wheel torque can well track the desired longitudinal forces with acceptable tracking errors.

Then for the calculation of desired sideslip angle, an analytical inverse tire model which is implemented via a look-up table obtained from CarSim is employed firstly. Note that the interaction between the tire slip variables $(\kappa_{ij}, \alpha_{ij})$ is not considered for this look-up table obtained from the CarSim. The final results of wheel steering angles,

which are calculated through the Equation 2.44 based on the results of tire sideslip angles α_{ij} obtained from the analytical inverse tire model, are considered as the inputs of CarSim model (including tire model). The tracking performance of desired lateral forces is shown in Figure 3.11. Note that, in this close-loop control simulation, the actual performance of vehicle lateral tire forces (vehicle running state) will influence the calculation of desired lateral tire forces (via control allocation). It can be found that, without considering the interaction between the tire slip variables $(\kappa_{ij}, \alpha_{ij})$, the tracking performance is totally unacceptable. Because in this combined longitudinal and lateral tire forces interacting situation, the longitudinal tire forces (tire slip angle) is making a significant effect on the relationship between the lateral tire forces and its corresponding tire sideslip angles. Hence, it is unreliable to directly implement the tire model inversion via a simplified look-up table.

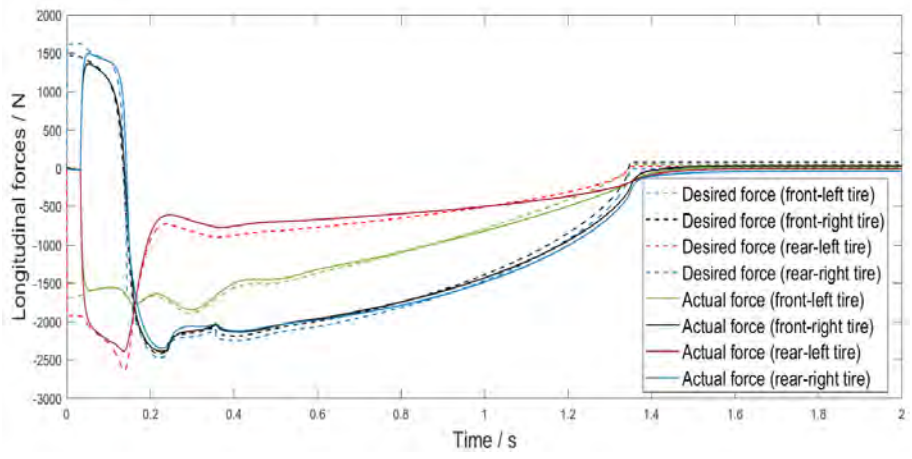

(a) Longitudinal tire forces tracking performance

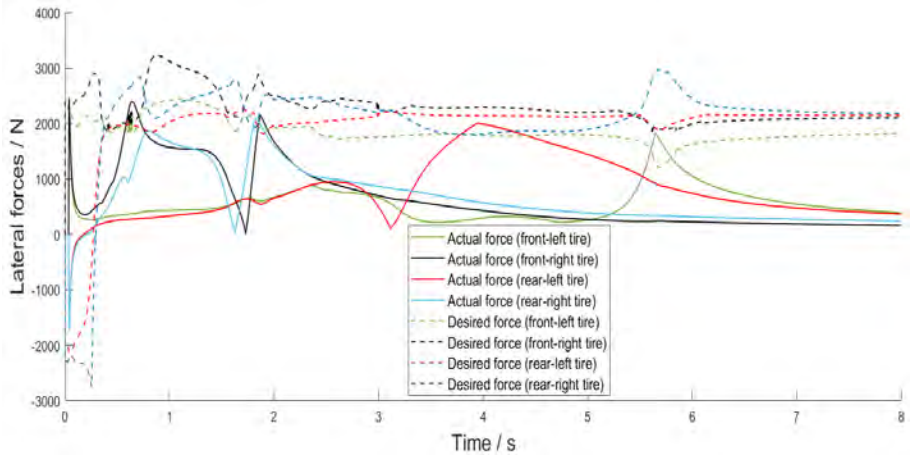

(b) Lateral tire forces tracking performance

FIGURE 3.11: Vehicle actuator tracking performance via 3-D look-up table

Then we employ the combined tire model inversion as Equation 2.40 in section 2.4 for the calculation of wheel steering angles. The obtained steering angles and tracking result

are shown in Figure 3.12. It is found that, with the combined tire model inversion, the obtained wheel steering angles as the control inputs of CarSim model (including tire model) can well track the desired lateral tire forces. Hence, for the latter simulation tests via CarSim, this proposed low-level controller can be reliably implemented into the hierarchical control structure.

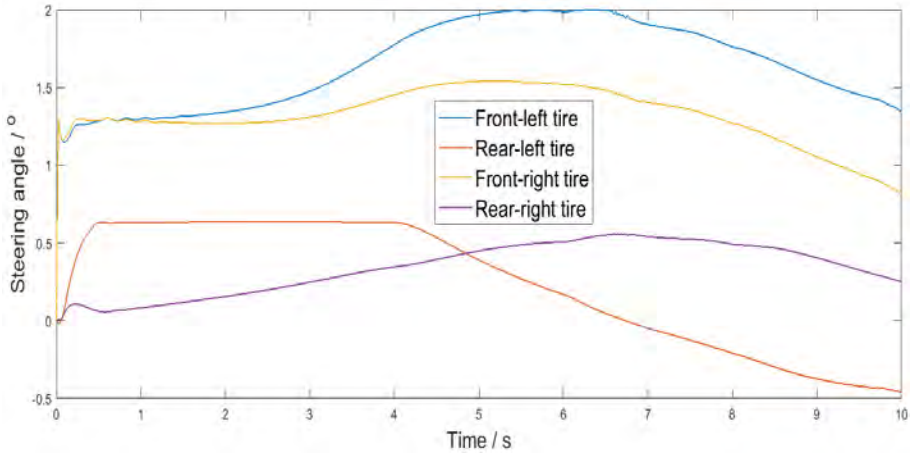

(a) Inputs of wheel steering angles

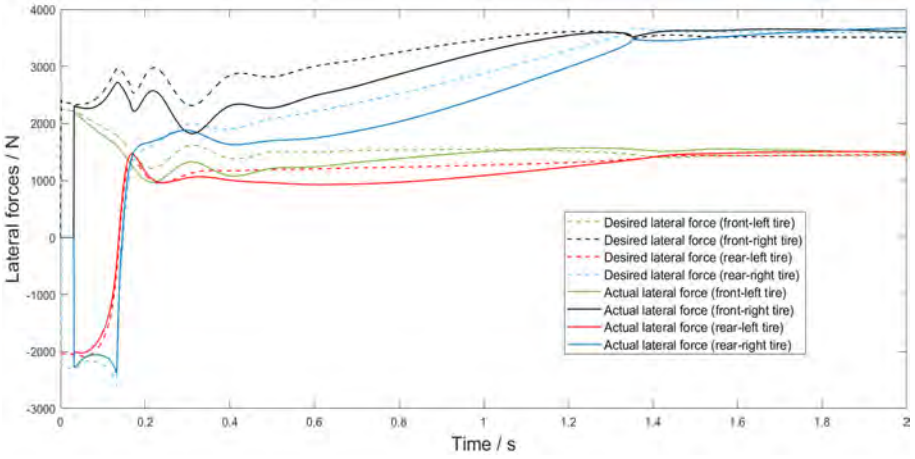

(b) Lateral tire forces tracking performance

FIGURE 3.12: Lateral force tracking performance via combined tire model inversion

The longitudinal and lateral tire forces results obtained from the CA and the CA performance demonstrate the effectiveness of CA process, the distribution of tire force are reasonable and achievable for the low-level controller to track. The low-level controller proposed can also satisfy its control target with acceptable tracking errors in comparisons with other published low-level controllers. Overall, from the simulation results, the proposed methods effectively close the hierarchical control loop and realize the proposed particle reference based control strategy.

3.4 Summary

This chapter has proposed a systematic method for moderating driver or system demands so that an integrated chassis and driveline control system can operate in a predictable manner within available friction constraints. A chassis/driveline control system is considered, based on control allocation and a particle reference model. The methodology is applied to a highly actuated vehicle: individual four-wheel steering and independent driveline/braking torque, however, based on imposing actuator constraints and uncontrolled axle sets, the conclusions appear general, provided the over-actuated condition is met. Demands from a driver interpreter are fed into the new moderator, based on the dynamics of a friction-limited particle, the result being a moderated particle reference (MPR). MPR is derived from a previously published Parabolic Particle Reference (P-PR), based on optimal control theory. The moderated particle reference (MPR) model has been proposed to ensure predictable and stable operation near the friction limits, maintaining controllability for curvature and speed tracking.

Evaluation of the overall system is accomplished by simulation testing with a driver model under vehicle over-speed cornering conditions. The results demonstrate that the vehicle with MPR can achieve some of the performance benefits obtained by the fully autonomous controller with PPR for road departure mitigation. The MPR strategy effectively limits demands on the vehicle while preserving the control interaction of the driver, which is in contrast to the simple yaw rate based controller, like electronic stability control (ESC). The comparison between the ESC and particle reference based control strategy will be discussed in next chapter, it will be found that the particle reference based control strategy (even with rollover limits in next chapter) can perform much better than the ESC. The moderator also ensures that reference demands are feasible, and from the results obtained, it is expected that tire model inversion and control allocation (CA) can be precisely implemented. To show these results from the high-level controller, it was necessary to include CA in the lower levels for simulation. These methods will be considered in detail in Chapter 5. In the next chapter, the rollover aspect of MPR will be analyzed.

Chapter 4

Moderated Particle Reference including rollover limits

This chapter proposes a combined approach to active rollover prevention and road departure mitigation, incorporating estimation of the vehicle running parameter and driver's intended path. The understeer mitigation performance with rollover constraint and driver inputs are to be taken into consideration and driver intent prediction is applied via a mediator (to combine with the autonomous function). In the previous chapter we used PPR to map demands into the feasible control space of the vehicle (G-G diagram), for high mass centre vehicles the lateral acceleration is further constrained by the rollover limit, in this case the mapping should be modified to exclude such cases but in a way that continues to keep the driver in the control loop. Hence, this control approach considers rollover prevention as a constraint rather than the final control objective; rather, an intended path is inferred and the control objective is to minimize the lateral deviation from that path. As with PPR, speed is progressively reduced as part of the control strategy, based on the PPR optimal speed profile. The overall control objective is to find out a suitable control reference for rollover prevention and road departure mitigation, in addition with the moderated approach based on the optimal performance while preserving the responsiveness of the vehicle to driver commands, even when friction limits are exceeded (according to a linear bicycle reference). The rollover problem including tripped rollover and un-tripped rollover are analysed separately. To verify feasibility and performance of this control strategy, results of fully autonomous and driver-in-the-loop simulations with step-steer and ramp inputs are presented.

4.1 Background

By far the deadliest risk facing SUV, minivan, and truck occupants is a rollover accident. According to NHTSA (National Highway Traffic Safety Administration), more than 280,000 rollover accidents are reported each year, claiming more than 10,000 lives annually. Research focus on active chassis control for rollover prevention has made remarkable progress in recent years. There are many factors that could cause the vehicles rollover, which can be divided into two categories, tripped rollover and un-tripped rollover [83][84][85]. The tripped rollover mainly refers to the generation of lateral side slip when the vehicle collides sideways with an obstacle on the road surface such as a curb or guardrail. The high tripping force applied to the tires in these situations can cause the vehicle to roll over. NHTSA data show that 95 percent of single-vehicle rollovers are tripped. And the un-tripped rollover mainly refers to the rollover caused by the vertical load transfer when the vertical tire force of inside wheels are reaching to zero because the lateral acceleration of vehicle body has exceeded a certain limit(including a lateral ramp). As discussed in Chapter 3, research focus on active chassis control for understeer mitigation has made remarkable progress in recent years. Understeer mitigation through direct yaw moment control is now a standard function of ESC. More recently, paper [37] formulated the problem of combined speed and directional control to minimize off-tracking when the curve entry speed is too high, or equivalently the tire-road friction is too low. The presented parabolic path reference (PPR) strategy showed a fundamental result to solve this problem. The moderated particle reference (MPR) control method has been introduced in last chapter. Demands from driver interpreter are fed into the moderator.

However, untripped rollover accidents for high CoG vehicle [86][87], caused by high speeds and road curvature [88], have not been considered in PPR or MPR control so far. Considerable research has focused on active anti-roll systems for high CoG vehicles [89][90][91][92]. For example, paper [93] used a Time-to-Rollover (TTR) metric to design a warning and control system for SUVs; paper [94] presented a nonlinear control strategy which guarantees asymptotic tracking of a yaw rate reference, while bounding the roll angle for rollover prevention. In paper [95], the authors proposed a differential braking control method and [96] proposed an active front steering (AFS) system for rollover prevention. A common theme for these methods of rollover prevention is a discrete, switched, intervention from the system, largely overriding the driver. Therefore there is a limitation in terms of keeping the driver in-the-loop.

As a short summary, the un-tripped rollover is not the only factor of rollover accidents. The generation of lateral side slip when the vehicle collides sideways with the obstacle

on the road surface such as a curb or guardrail and collides with the coming vehicle in the sideward lane as shown in Figure 4.1 have to be taken into consideration.

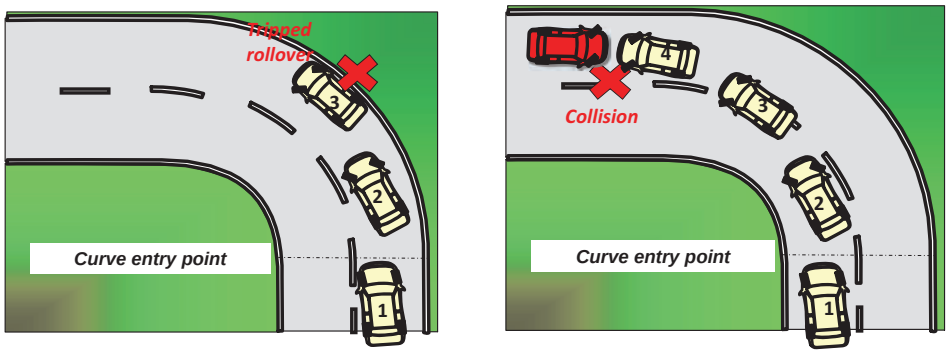

(a) Tripped rollover caused by road departure (b) Collision caused by road departure

FIGURE 4.1: Road departure accidents

4.2 Rollover prevention

The 'optimal inspired' control reference, based on an optimal particle taking both the understeer mitigation and rollover constraint into consideration is firstly presented in this chapter. This control method is designed for achieving a minimum road departure performance while preventing rollover. A control mediator is introduced to take account of both road (and potentially traffic) constraints, plus driver intentions. As shown in Figure 4.2, the mediator operates as a mapping in the vehicle G-G diagram. Inputs to the mediator are target accelerations obtained from the Rollover Prevention System a^{RPS} as well as from the driver interpreter a^{DI}. Hence, there exist a difference between the mediator in this chapter and the moderator in last chapter for the MPR, the mediator takes two inputs and includes the moderation part and the rollover prevention constraint for limiting the mapping process. The output reference a^{ref} is for braking control allocation, providing a continuously updating safety margin. Then through the control allocator, the feasible individual tire forces can be obtained as the actuator control reference for actuator regulation to track. This control method is designed for maintaining drivability in the critical vehicle over-speed curving situation and in the meantime taking safety (via understeer mitigation and rollover prevention) into consideration. The acceleration reference from the rollover prevention system a^{RPS} is taken as a constraint for control allocation in this chapter. The acceleration reference from driver a^{DI} can be calculated from the steering wheel angle and current vehicle velocity. The main theme of this chapter is to develop both a fully autonomous control method and systematic control mediation method from the a^{RPS} and a^{DI} to control reference.

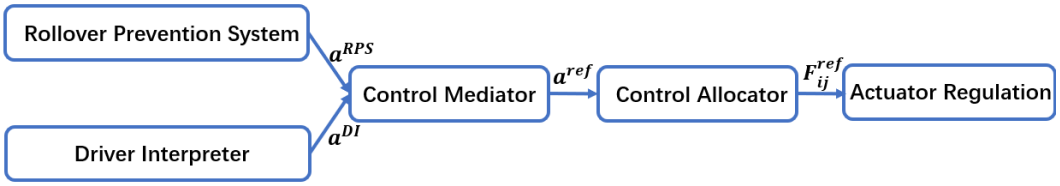

FIGURE 4.2: Summary of the control structure

4.2.1 4-DoF vehicle model

In this part, we define a 4-DoF vehicle model as a rollover reference when considering the high CoG vehicle 'untripped' rollover situation [97]. In this model, the main parameters should be matched with the real vehicle. In this we added a roll degree of freedom (with the vehicle roll dynamic model shown in Figure 4.4) into the normal 3-DoF vehicle model shown in Figure 4.3 which has been introduced in Chapter 2.

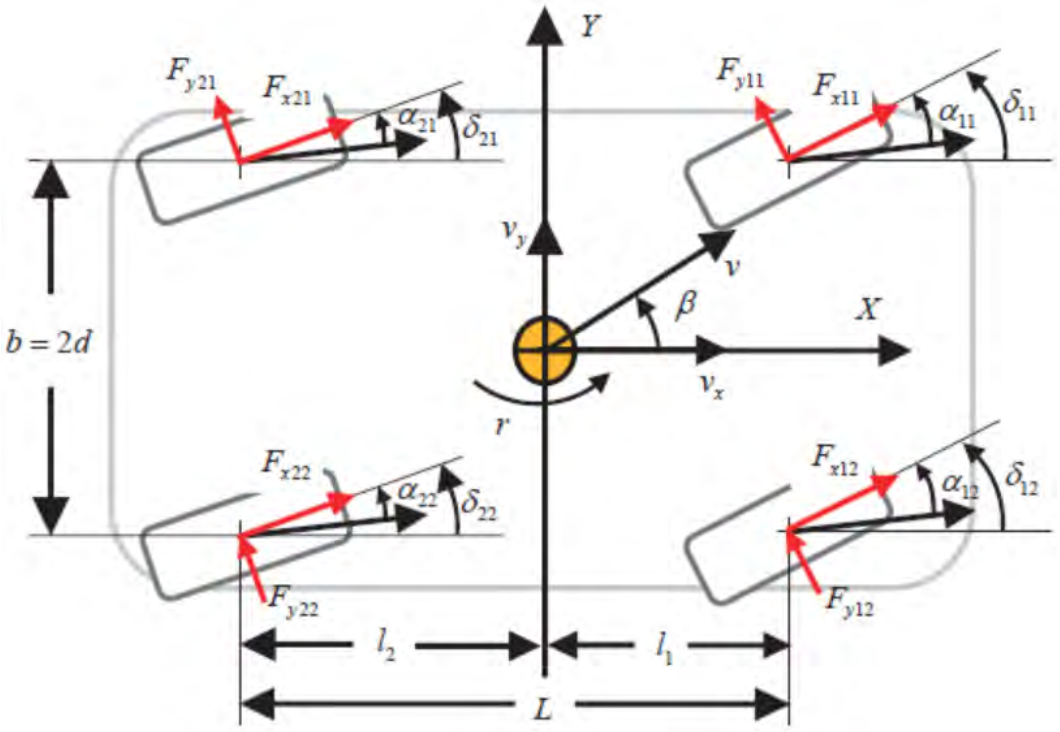

FIGURE 4.3: 3-DoF vehicle dynamic model

$$m(a_x - v_y r) + m_s e r\dot{\phi} = F_{xij}\cos\delta_{ij} - F_{yij}\sin\delta_{ij} \tag{4.1}$$

$$m(a_y + v_x r) - m_s e\ddot{\phi} = F_{xij}\sin\delta_{ij} + F_{yij}\cos\delta_{ij} \tag{4.2}$$

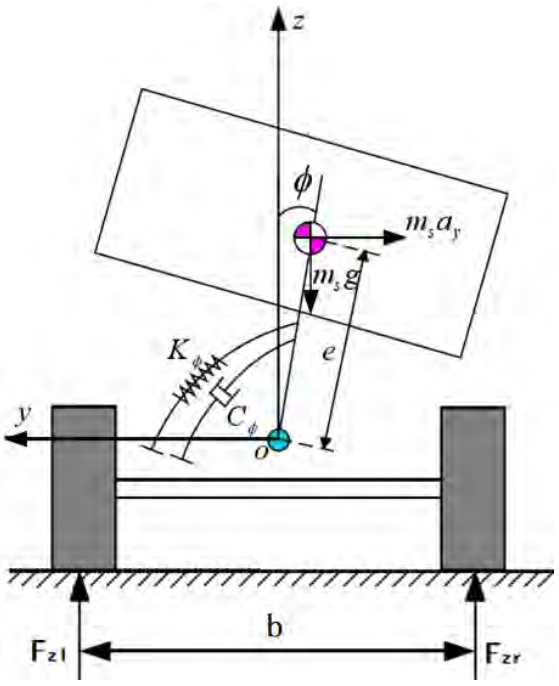

FIGURE 4.4: Vehicle roll dynamic model

$$I_z\dot{r} = \sum[(-1)^j dF_{xij} - (-1)^i l_i F_{yij}] \tag{4.3}$$

$$I_{xeq}\ddot{\phi} - m_s g e sin\phi = m_s a_y e cos\phi - C_\phi\dot{\phi} - K_\phi\phi \tag{4.4}$$

In Equation 4.4, the rotational inertia of sprung mass around X axis I_{xeq} is described as:

$$I_{xeq} = I_x + m_s e^2 \tag{4.5}$$

In Figure 1.4, $\dot{\psi} = r$. Then we can obtain:

$$\begin{aligned} \dot{x} &= v_x cos\psi - v_y sin\psi \\ \dot{y} &= v_x sin\psi + v_y cos\psi \end{aligned} \tag{4.6}$$

The accelerations can be described as:

$$\begin{aligned} a_x &= \dot{v_x} - v_y r \\ a_y &= \dot{v_y} + v_x r \end{aligned} \tag{4.7}$$

where m_s denotes vehicle sprung mass, a_x and a_y denote the longitudinal and lateral acceleration, e denotes the distance from vehicle roll center to mass center, ϕ denotes the roll angle, r denotes the vehicle yaw rate, l_1 and l_2 denote the distance from vehicle mass center to front axle and rear axle, C_ϕ denotes the roll damping coefficient and K_ϕ denotes

the effective roll stiffness. The vertical load on each tire F_{z**} is not a constant because of the vehicle's dynamics weight transfer caused by longitudinal and lateral acceleration. Separately, the longitudinal acceleration affects the vertical loading between front F_{zf*} and rear tires F_{zr*}, and the lateral acceleration influences the vertical loading between left side F_{z*l} and right side tires F_{z*r}. Hence, the dynamic vertical load can be modeled as:

$$\begin{aligned} F_{zfl} &= \frac{l_2}{2L}mg - \frac{h_{cg}}{2L}m_s a_x - \frac{C_\phi\dot{\phi} + K_\phi\phi}{2b} \\ F_{zfr} &= \frac{l_2}{2L}mg - \frac{h_{cg}}{2L}m_s a_x + \frac{C_\phi\dot{\phi} + K_\phi\phi}{2b} \\ F_{zrl} &= \frac{l_1}{2L}mg + \frac{h_{cg}}{2L}m_s a_x - \frac{C_\phi\dot{\phi} + K_\phi\phi}{2b} \\ F_{zrl} &= \frac{l_1}{2L}mg + \frac{h_{cg}}{2L}m_s a_x + \frac{C_\phi\dot{\phi} + K_\phi\phi}{2b} \end{aligned} \tag{4.8}$$

4.2.2 Effective roll stiffness identification

Initial simulations indicated that the parameter identification based on fixed constant of effective roll stiffness K_ϕ is imprecise. This is most likely due to the nonlinear suspension properties. To further improve model accuracy, the parameter of effective roll stiffness for steady state vehicle cornering under different speed and steering angle inputs was identified via CarSim and Matlab/Simulink which was employed to control a set of test runs of the CarSim model.

In this part, we considered the vehicle speed between 30km/h-120km/h, the steering wheel angle between $\pm 240°$. And we take every 5km/h and $10°$ as the simulation interval. With the CarSim simulation results and vehicle state equation shown above, we can identify the vehicle parameter of effective roll stiffness based on model matching with the vehicle running data in these simulation conditions. Thus a look-up table based on parameter identification for K_ϕ has been obtained for the controller design as shown in Figure 4.5. The validation of the proposed vehicle model with fitting parameter can be seen in Figure 4.7 [97].

In order to verify the reliability of the 4-DoF vehicle model in Simulink, we made a comparison to the step-steer response between CarSim and the mathematical model. We considered the vehicle velocity as 55km/h and the ramp steering angle to $90°$ shown in Figure 4.6.

The comparison results shown in Figure 4.7 demonstrated that with the identification of effective roll stiffness, the built 4-DoF vehicle model can correctly reflect the lateral acceleration and roll angle of the vehicle during experiments.

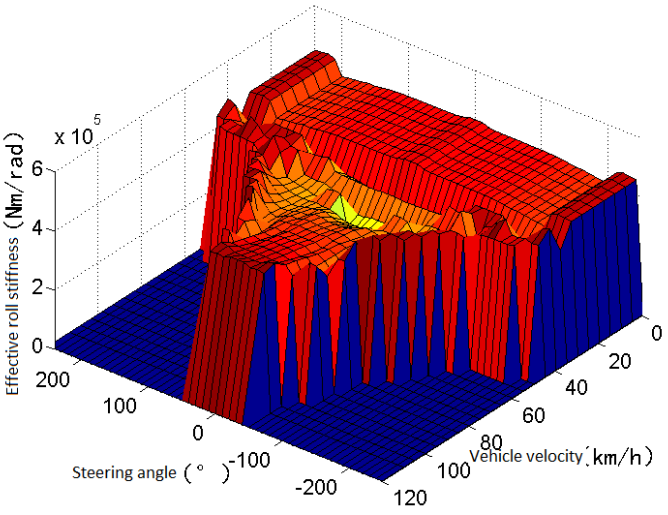

FIGURE 4.5: Effective roll stiffness identification

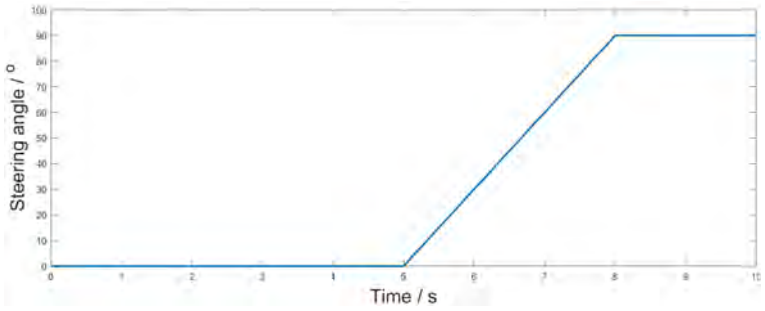

FIGURE 4.6: Steering angle input

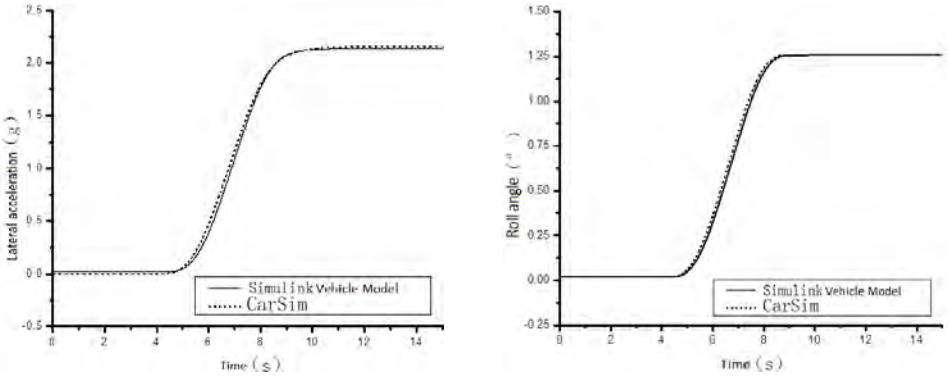

(a) Lateral acceleration comparison (b) Roll angle comparison

FIGURE 4.7: Comparison with the mathematical model

4.2.3 Lateral acceleration constraint

For this new control approach presented in this chapter, we require a lateral tire force constraint for the control allocation. This constraint puts a limitation on the vehicle

lateral acceleration in order to prevent untripped rollover. In the meantime, this constraint needs to satisfy the requirement for limit handling situation, in other words, it should maximally approach the actual value.

Lateral-load Transfer Ratio (LTR) [98] is a parameter to describe the change of vertical tire load which is widely used in the identification of vehicle rollover. LTR is defined as:

$$LTR = \frac{F_{zl} - F_{zr}}{F_{zl} + F_{zr}} \in [-1, 1] \tag{4.9}$$

where F_{zl} denotes the total left vertical tire forces and F_{zr} denotes the total right vertical tire forces. LTR ranges from -1 to 1, and when either right or left side of tires lifts off the ground, the LTR value can be -1 or 1. As the LTR of vehicle can not be determined directly from sensors, an equivalent transformation can be obtained from the vehicle roll dynamic equilibrium equation as shown in Figure 4.4: :

$$\Sigma M_{xi} = F_{zl}\frac{b}{2} + m_s a_y e cos\phi + m_s g e sin\phi - F_{zr}\frac{b}{2} = 0 \tag{4.10}$$

Then from equation 4.9 and 4.10, the expression of LTR can be obtained as:

$$LTR = \frac{-2m_s(a_y e cos\phi + g e sin\phi)}{mgb} \tag{4.11}$$

The analysis can be proceeded based on Equation 4.4,

$$I_{xeq}\ddot{\phi} + C_\phi\dot{\phi} + [K_\phi - m_s g e]\phi = m_s a_y e \tag{4.12}$$

By taking the Laplace transformation of Equation 4.12 and assuming zero initial conditions, a transfer function for the lateral acceleration and roll angle can be obtained as:

$$G_{roll}(s) = \frac{\phi(s)}{a_y(s)} = \frac{m_s e}{s^2 I_{xeq} + sC_\phi + (K_\phi - m_s g e)} \tag{4.13}$$

Then the corresponding impulse response $g_{roll}(t)$ can be obtained via the Inverse Laplace transform of $G_{roll}(s)$ as:

$$g_{roll}(t) = L^{-1}(G_{roll}(s)) \tag{4.14}$$

Then the roll angle of $\phi(t)$ is given by:

$$\begin{aligned} \phi(t) &= \int_0^\infty a_y(t-\tau) g_{roll}(\tau) d\tau \\ &\leq \| a_y \| \int_0^\infty | g_{roll}(\tau) | d\tau \end{aligned} \tag{4.15}$$

If the maximum allowable roll angle is given by ϕ_{max}, and $\int_0^\infty \mid g_{roll}(\tau) \mid d\tau = \parallel G_{roll} \parallel_L$, then the following inequality can be obtained as:

$$\parallel a_y \parallel \leq \frac{\phi_{max}}{\parallel G_{roll} \parallel_L} \tag{4.16}$$

Depending on the choice of ϕ_{max} , this method will provide a lower lateral acceleration limit than the static limits provided in other publications [94].

The other way to find the lateral acceleration limit is based on the assumption of small roll angle: from Equation 4.11, we assume the roll angle is small, so $ecos\phi = e$ and $esin\phi = e\phi \approx 0$; then the simplified LTR can be described as:

$$LTR = \frac{-2m_s a_y e}{mgb} \tag{4.17}$$

With this simplifying assumption we can just consider lateral acceleration as the only effect variable. If the maximum allowable LTR is given by R_t, then we can obtain that:

$$\parallel a_y \parallel \leq \frac{R_t mgb}{2m_s e} \tag{4.18}$$

Then the lateral acceleration limit a_y^* can be obtained as:

$$a_y^* = \frac{R_t mgb}{2m_s e} \tag{4.19}$$

It has been widely known that the LTR threshold R_t relates to steady-state handling and it depends on vehicle speed and steering angle. Hence, the identification of LTR threshold R_t is required based on the known vehicle parameters. After extensive CarSim simulation experiments (the vehicle parameters can be found in Appendix A), we obtained a 3-D look-up table shown in Figure 4.8.

Based on the identification results of Figure 4.8, to guarantee the safety in this critical situation, we set a minimum value of LTR threshold R_t which is $R_t = 0.87$ for this test SUV. So far, the lateral force limitation as control constraint for un-tripped rollover prevention can be theoretically obtained by equation 4.19.

Note that vehicles in real world often experiences rollover even with lateral acceleration much lower than the value computed by equation 4.19. The above equation is based on the simplification of small roll angle assumption, and the value is a result of steady-state analysis and does not take dynamics of factors (transient dynamics is the main point here) such as suspension compliance or tire deformation into account. However, it

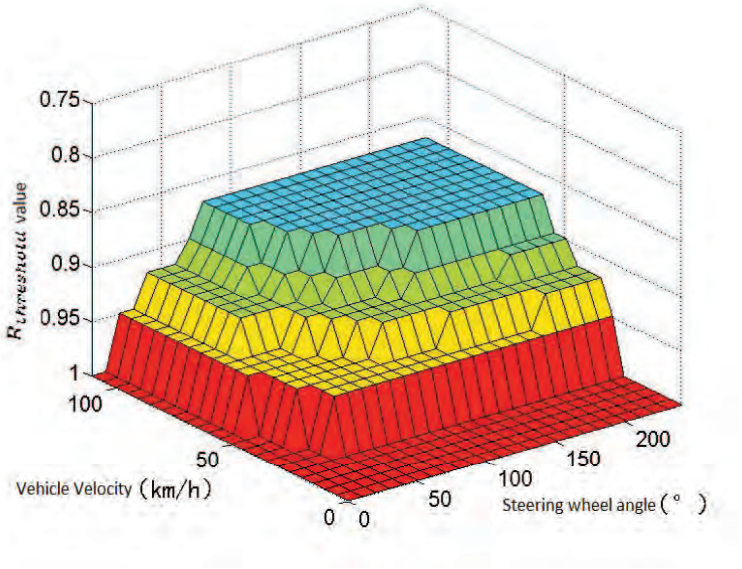

FIGURE 4.8: LTR threshold identification

should serve as a reasonable index of the lateral acceleration upper limit and in practice can include a safety factor at which a catastrophic situation could occur [99].

To further explore the lateral acceleration limit for this test SUV, the simulation test with different lateral accelerations was complemented using CarSim and Matlab/Simulink which was employed to control a set of test runs of the CarSim model. In this simulation, the test is conducted with a steady-state cornering scenario, with a constant vehicle speed as 120km/h, and a constant steering wheel angle between $\pm 240°$, the road friction coefficient is $\mu = 0.5$. We take every $0.005g$ as the simulation interval. As the example CarSim simulation results shown in Figure 4.9, when the lateral acceleration stays below $0.4g$, the vehicle can run safely, and if the lateral acceleration increase to $0.405g$, the vehicle rollover occurs.

Hence, for this particular SUV, we set the lateral acceleration limit as $0.4g$ for the following simulation tests.

4.3 Modified mapping of synthetic acceleration in G-G diagram

Based on aforementioned driving scenario in chapter 3, it was assumed that the road geometry consists of a straight-line segment joined to a circular arc of constant curvature, and that a PPR intervention takes place at the curve entry point. The optimal control problem for minimizing the maximum off-tracking from the circular reference trajectory

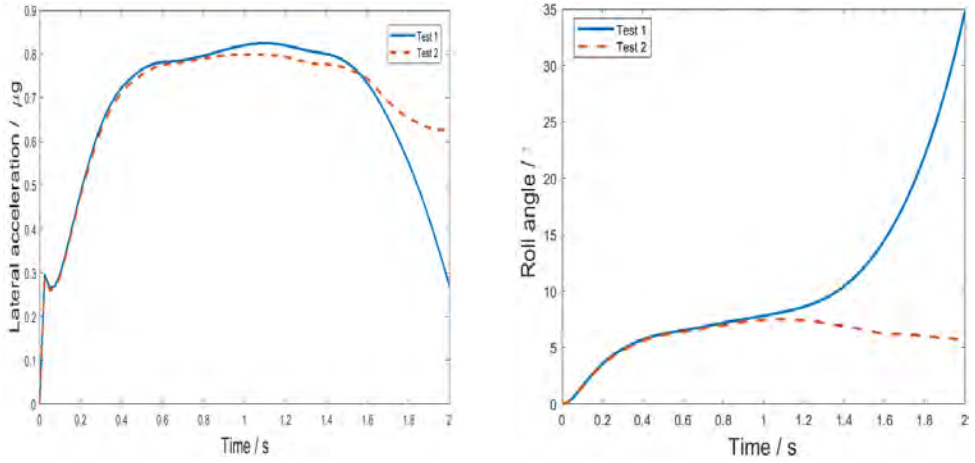

(a) lateral acceleration performance (b) Roll angle performance

FIGURE 4.9: Simulation validation of lateral acceleration constraint

was thereby established. The moderated particle reference (MPR) strategy is a simplification and generalization of PPR which is designed to minimize the maximum distance of off-tracking while preserving the driver maneuverability. Different from a step-steer input (PPR), MPR is intended to operate across a wide range of driving conditions. Derived from the basic idea of PPR and MPR, considering the lateral acceleration limits obtained from last chapter, we redesign the particle reference model based on the modified limitations.

4.3.1 PPR including rollover limits

The motivation for the particle representation is to be able to analytically derive an optimal strategy for recovery from terminal understeer while considering the rollover limitation.

In PPR, it is considered as the problem of a vehicle overshooting a reference trajectory (as shown in Figure 4.10) owing to friction limits, a situation referred to as terminal understeer. In order to minimize the effects of a deviation from the desired trajectory, the recovery task was formulated as an optimal control problem. In the global coordinate, the vehicle particle motion can be obtained by the acceleration vector $a^d = -\mu g(cos\theta i + cos\theta j)$ and initial vehicle velocity v_0 as [38]:

$$\begin{aligned} x &= R + v_0 sin\alpha t - \frac{1}{2}\mu g cos\theta t^2 \\ y &= v_0 cos\alpha t - \frac{1}{2}\mu g sin\theta t^2 \end{aligned} \tag{4.20}$$

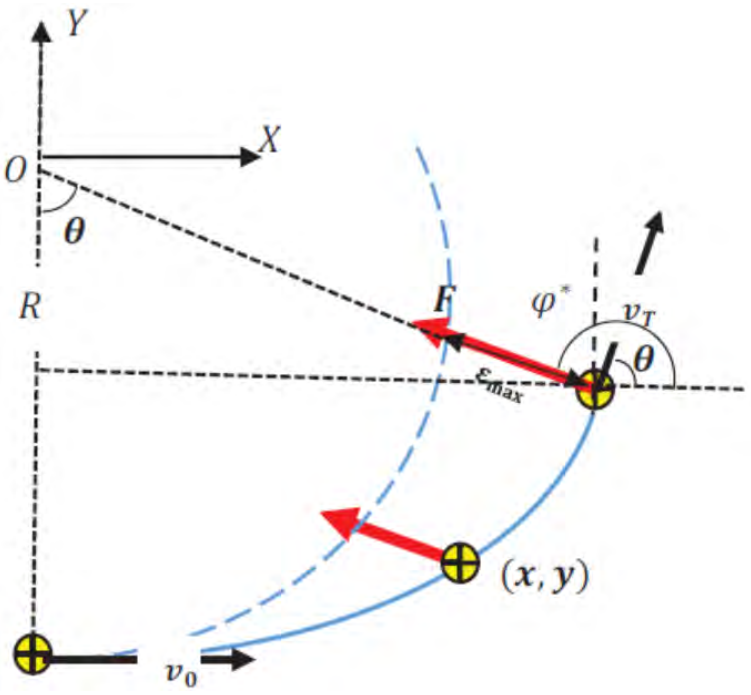

FIGURE 4.10: PPR/R-PPR calculation diagram. The maximum off-tracking ε_{max} occurs when the velocity vector v_T is parallel to the reference path direction

From the curvature shown in Figure 4.10, and the lateral acceleration limit a_y^* (in vehicle coordinate), the corresponding maximum achievable speed can be determined as:

$$v_{lim} = \sqrt{\frac{a_y^*}{R}} \tag{4.21}$$

In the case of excessive initial speed, $v_0 > v_{lim}$, the actual vehicle trajectory will deviate from the reference trajectory. Thus with initial conditions:

$$x_c(0) = R; y_c(0) = 0; \dot{x_c}(0) = 0; \dot{y_c}(0) = v_0 \tag{4.22}$$

the optimal control problem is to minimize:

$$J = x_c^2(T) + y_c^2(T) \tag{4.23}$$

subject to the following condition at $t = T$:

$$x_c(T)\dot{x_c}(T) + y_c(T)\dot{y_c}(T) = 0 \tag{4.24}$$

i.e. the velocity vector is perpendicular to the radial vector from the center of the circle at the final time.

Taking consideration of rollover constraint a_y^* in vehicle coordinate, we solve this problem via optimization tool, it is found that the optimal control input $(F_x^v(t), F_Y^v(t))$ minimizing

the road departure J is proved to be constant as (this optimization is based on the previous paper [100] and the off-line optimization tool JModelica with the optimization target of minimizing the road departure):

$$\begin{aligned} F_X^v(t) &\equiv \sqrt{(\mu F_Z)^2 - (ma_y^*)^2} \\ F_Y^v(t) &\equiv ma_y^* \end{aligned} \tag{4.25}$$

Hence the representation of extended PPR with rollover constraint, named as R-PPR, in the $G-G$ diagram can be shown as Figure 4.11, the point C' represent the optimal inputs as equation 4.25; and the point P' represent the optimal inputs obtained from PPR, according to the road conditions μ, R and vehicle initial velocity v_0, from the previously published PPR theory [50][37][38], we can obtain that: $a_y^{ref} = \frac{(\mu g)^2 R}{v_0^2}$. Hence, if the $a_y^* \geq a_y^{ref}$, then the ideal inputs are as before:

$$\begin{aligned} a_y^{ref} &= \frac{(\mu g)^2 R}{v_0^2} \\ a_x^{ref} &= \sqrt{(\mu g)^2 - (a_y^{ref})^2} \end{aligned} \tag{4.26}$$

if the $a_y^* \leq a_y^{ref}$, then the constraint is imposed to give:

$$\begin{aligned} a_y^{ref} &= a_y^* \\ a_x^{ref} &= \sqrt{(\mu g)^2 - (a_y^{ref})^2} \end{aligned} \tag{4.27}$$

4.3.2 MPR including rollover limits

The problem with equation 4.27 is that it does not respond to driver action. Taking the driver interaction into consideration, as an extension of R-PPR, a new concept is generated derived from the idea of MPR: Rollover limits based-Moderated Particle Reference (R-MPR).

As the driver interpreter (DI) including both longitudinal and lateral control described in section 2.2.2, input variables for R-MPR are also the current vehicle longitudinal acceleration demand and steering wheel angle, together with vehicle speed and a current estimate of tire/road friction. As an extension of R-PPR, considering rollover prevention as R-MPR, the reference acceleration is mapped to a new G-G diagram in a way that also respects the rollover prevention constraint. Based on the above lateral acceleration constraint, we can redesign the G-G diagram and mapping method from DI to control reference as a control mediation approach.

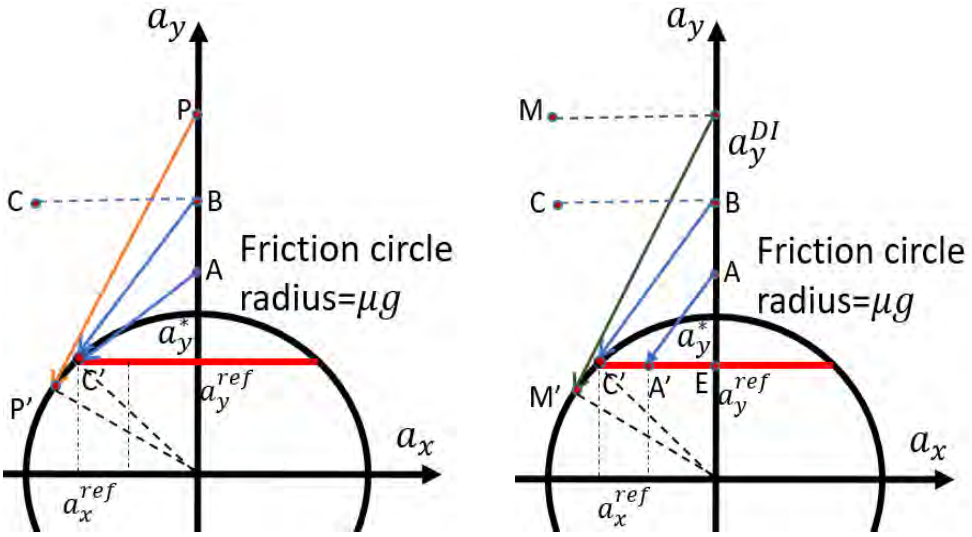

(a) R-PPR (b) R-MPR

FIGURE 4.11: Friction circle interpretation of particle reference with rollover constraint

In Figure 4.11, the red line shows the lateral acceleration constraint a_y^*, the arrows showing the proposed mapping method from driver interpreter to control reference. Based on the MPR mapping method mentioned in last chapter, the mapping from point M to M' is the most typical mapping method of MPR which is firstly horizontal mapping to the Y-axis, and then tangential mapping to the circle at point M'. But when the lateral demand from DI is lower than point B, we propose to retain angle θ obtained from equation 4.28 for the mapping to the limitary friction circle, as AA'. That is to say, the mapping lines are parallel to the mapping line from point B to C' if the lateral accelerations from driver interpreter are less than point B. The mapping angle θ from the DI to lateral acceleration limit line can be obtained by:

$$sin\theta = \frac{a_y^*}{\mu g} \tag{4.28}$$

Taking point A as an example, at this point the lateral acceleration demand is a_y^{DIa}. Then we can obtain:

$$a_x^{ref} = \frac{a_y^{DIa} - a_y^*}{tan\theta} \tag{4.29}$$

Using the θ from equation 4.28, we can obtain the a_x^{ref} for longitudinal control reference. Besides, if the lateral demand from DI is larger than point B, then we still use the previous MPR mapping method, as the mapping results will not exceed the lateral acceleration limit line. The value of point B can be obtained via:

$$a_y^B = \frac{(\mu g)^2}{a_y^*} \tag{4.30}$$

As a short summary, there comes out two mapping methods: i) the arrow from B to C' represents a fully autonomous way which the vehicle reference acceleration always fall to the point C'; ii) the arrow from A to A' represents the proposed driver-in-the-loop approach, the point will fall to the lateral acceleration limit line. Then the two mapping method establish the theoretical basis for the design of whole control strategy in following section. In this chapter, aforementioned different moderation approaches are compared and analyzed in detailed. For the particle model, the motion performances of i) can be obtained directly since the lateral and longitudinal acceleration are constant. For the motion performance of ii), the unpredicted changing of lateral acceleration demands bring great effects on the final performance.

4.4 Control strategies design

Here two specific scenarios are considered: (a) with sufficient lateral maneuvering room, un-tripped rollover has minimal risk, and driver-adaptive control moderation is introduced to keep driver fully in the control loop; (b) with limited lateral maneuvering room, the risk of tripped rollover (or lane/road departure) is higher and an automated intervention is required. Depending on road conditions and on driver actions, it is of course possible that scenario (a) will transition into scenario (b).

As mentioned, the past several years has witnessed a great progress in Advanced Driver Assistance System (ADAS) especially in the sensor technology such as radar, lidar, camera and GPS. Based on this, in this chapter, we assume that the road geometry, real-time vehicle position and traffic and road conditions are known for this control method. Hence, based on the known information (road width and traffic) from outside environment and initial vehicle velocity, we divide the control strategy into two sections for scenario (a) and (b), one is a fully autonomous controller minimizing the maximum road departure distance for scenario (b); another is a driving assistance controller preserving driver maneuverability for scenario (a). In addition, both the two control strategies are taking the un-tripped rollover prevention into consideration.

The design concept of R-PPR is to develop a fully autonomous controller which will achieve the optimal road departure mitigation in an 'optimal-inspired' conditions; and the R-MPR is to develop an ADAS controller to maintain driver operation into the control process. Then based on the known available road conditions and subject vehicle running parameters, the control strategy is presented as Figure 4.12:

As shown in Figure 4.12, the road departure particle model will select the control strategy (fully autonomous or ADAS) based on the current vehicle running data and

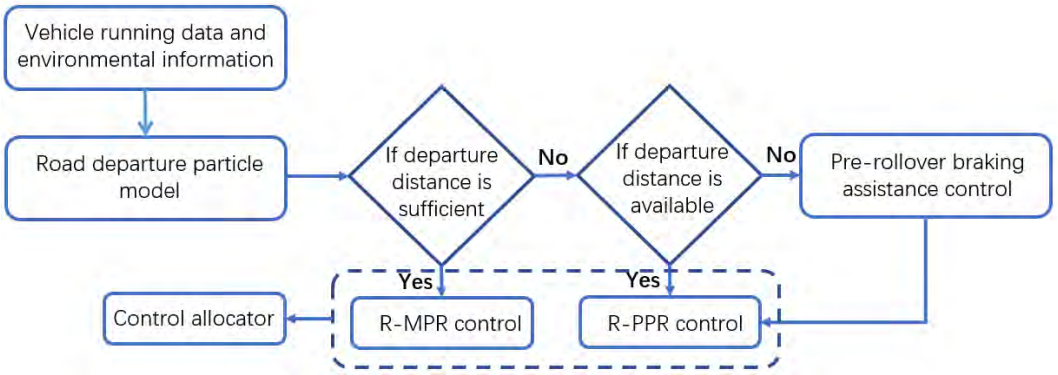

FIGURE 4.12: Control strategy

road information. That is, if there is sufficient distance for the road departure, then we select the R-MPR control method as an ADAS to preserve driver maneuverability in this critical situation, and if the allowed road departure distance is not sufficient enough but can still satisfy the optimal control, then we select R-PPR as a fully autonomous control method, furthermore, if the allowed road departure distance is even less, the initial velocity is the only parameter which can be controlled, then we have to implement braking assistance control in advance before entering into the curve, which derived from the Emergency Braking Assistance (EBA) System named as "Pre-rollover braking assistance control" in this chapter, to guarantee the vehicle speed reducing to a safety limitation. The conditional criterion of 'sufficient distance' and 'available distance' are depending on the vehicle parameter and road conditions which can be estimated based on the particle reference model and corresponding mapping method from Figure 4.11.

4.5 Simulation results and analysis

4.5.1 Step-steer inputs validation

Using vehicle dynamic simulation software CarSim, combined with the above proposed hierarchical control structure (introduced in chapter 2) which implemented in Matlab/Simulink, close-loop test (overspeed cornering condition) are simulated for the validation of the proposed control method. Particularly, the CA method based on pseudo-inverse matrix which will be described in next chapter is employed in this simulation. The vehicle parameters used in CarSim are listed in Appendix B.

As above, the driving scenario consist of a straight-line tangent connected to a constant-radius curved road, and the overspeed cornering test with step-steer steering wheel angle inputs are carried out at the initial speed of 120km/h under road condition of $\mu = 0.5$ and $R = 100m$. The lateral acceleration limit is set to be the same as $0.4g$ (validated

in section 4.2.3). As a comparison, we introduce a standard electronic stability control (ESC) model, as most of the current rollover prevention systems are generally integrated with the yaw stability control. The parametric ESC model comes from the CarSim (version 2018a) with exactly the same steering inputs and driving conditions of the particle reference based controller.

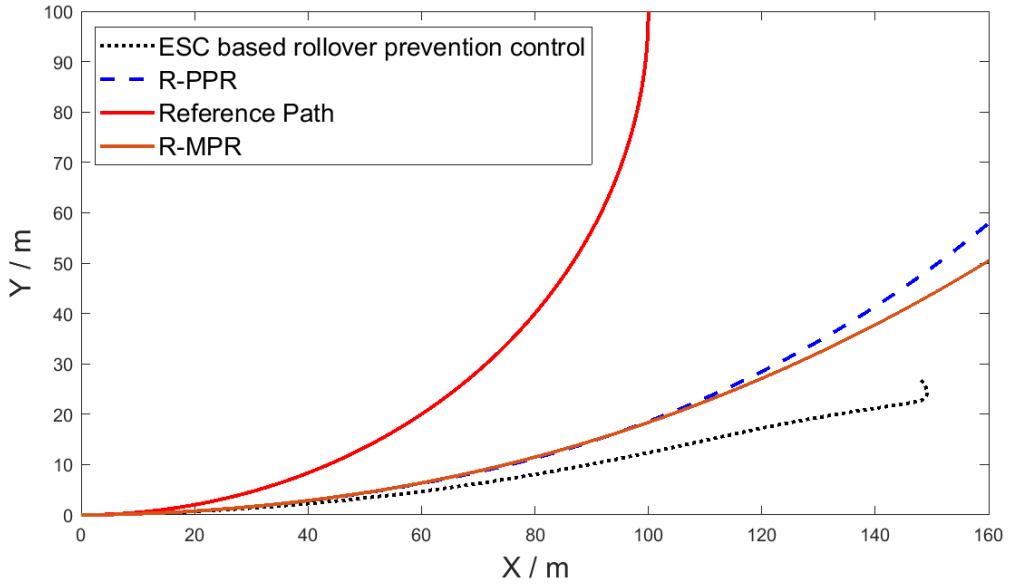

FIGURE 4.13: Vehicle motion performance comparison

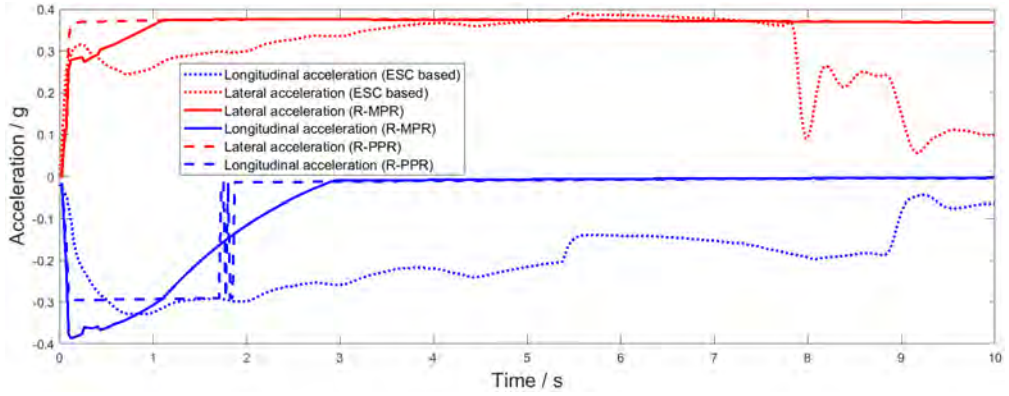

FIGURE 4.14: Vehicle acceleration performance comparison

The simulation results demonstrate the vehicle performance with different controllers. The motion performance comparison as shown in Figure 4.13 show that the vehicle can perform much better in road departure mitigation with R-PPR and R-MPR than with an ESC-based controller. The latter make more use of the tire forces to slow down as shown in Figure 4.15, rather than utilizing lateral and longitudinal tire forces for yaw moment control. Although it appears lower possibility for the rollover problem, with smaller roll angle shown in the Figure 4.16, which also means it's not taking full use of the lateral acceleration limitation as shown in Figure 4.14. On the other hand, the motion performance of proposed R-PPR and R-MPR are quite close in this situation, as

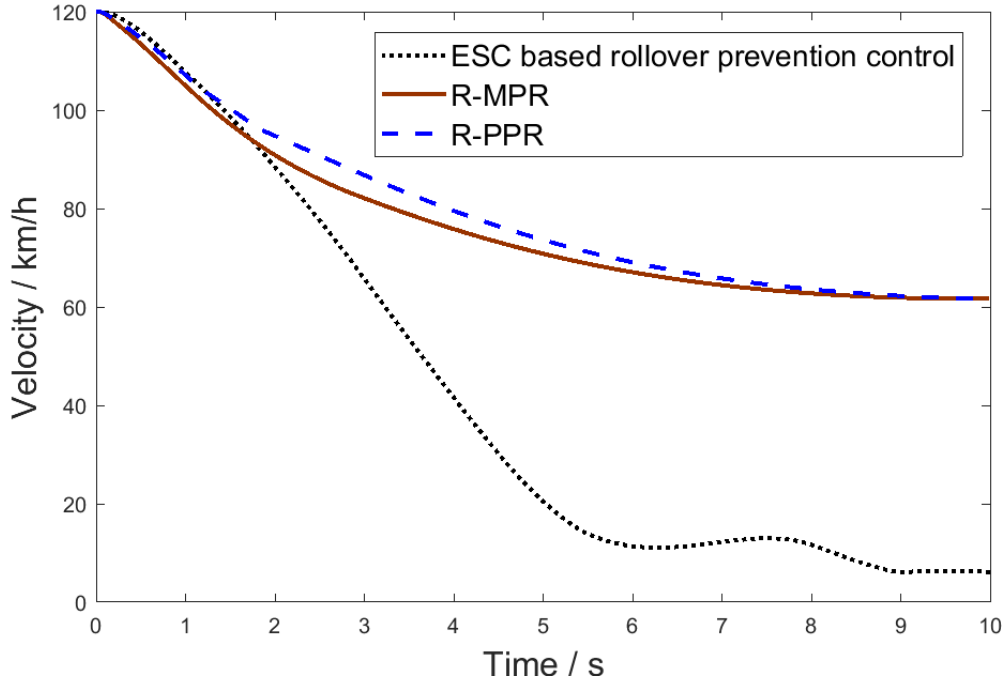

FIGURE 4.15: Vehicle velocity performance comparison

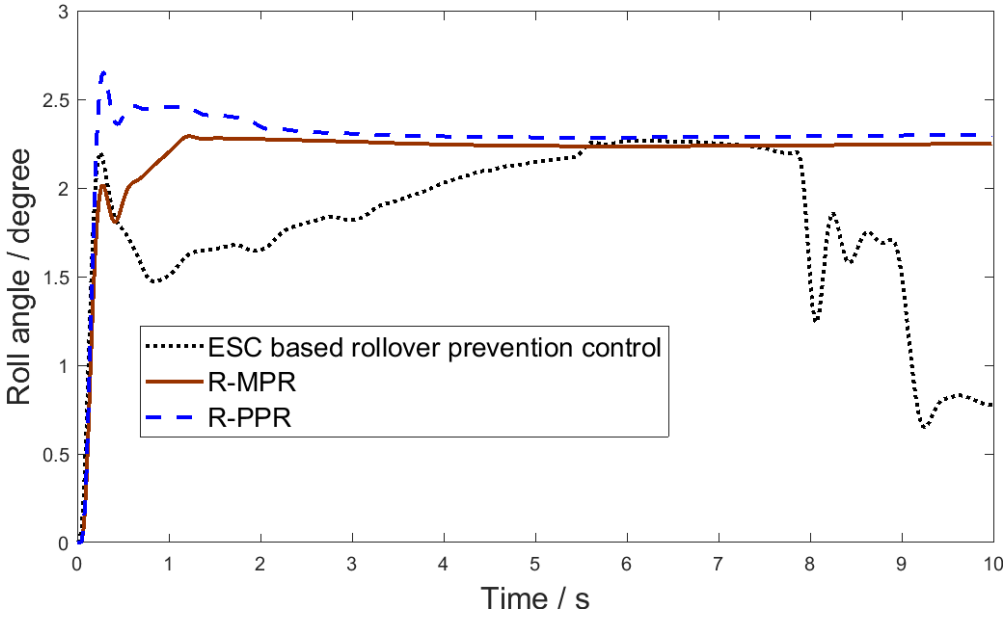

FIGURE 4.16: Vehicle roll performance comparison

the dashed line representing the R-PPR and the solid line representing the R-MPR in the Figure 4.13. From the velocity comparison (as shown in Figure 4.15), R-PPR and R-MPR strategy reduces the longitudinal velocity in a systematic way while making full use of the lateral acceleration limits. Further, the acceleration performances (as shown in Figure 4.14) basically verified our control strategies: R-PPR will immediately keep the vehicle in the stable state, and R-MPR will follow the driver intention and gradually control the vehicle to a stable condition.

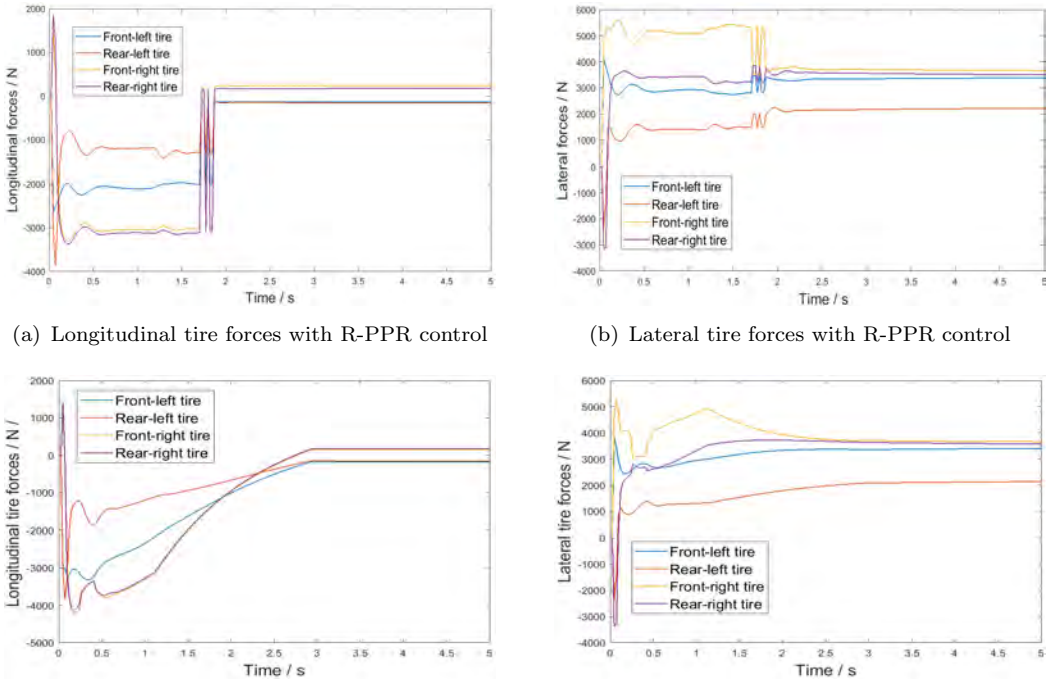

(a) Longitudinal tire forces with R-PPR control

(b) Lateral tire forces with R-PPR control

(c) Longitudinal tire forces with R-MPR control

(d) Lateral tire forces with R-MPR control

FIGURE 4.17: Control allocation results with particle reference model

The longitudinal and lateral tire forces results obtained from the CA process shown in Figure 4.17 demonstrate the effectiveness of CA process, the distribution of tire force are reasonable and achievable for the low-level controller to track. In addition, the individual tire forces shown in Figure 4.17 can well reflect and track the changes of vehicle longitudinal and lateral accelerations shown in Figure 4.14. Note that, during both the R-PPR and R-MPR simulation tests, the CA process performance operated with nearly zero allocation error $\| Bu-V \|_2$ as the case with MPR, shown in Figure 3.12 in last chapter, which further verify that the proposed CA method can well implemented in this control situation (tire force limiting condition).

4.5.2 Ramp inputs validation

To further validate the R-MPR control strategy can maintain driveability in these conditions, we select two ramp steering angle inputs with different changing rates as the control inputs for the simulation. The ramp inputs start exactly from the beginning, the steering hand wheel changing rate is $40 degree/s$ and $60 degree/s$ separately and the duration time of ramp inputs are 3 second.

As shown in the Figure 4.18, the vehicle performances are obviously influenced by the control inputs. Specifically, more steering angle inputs, means more lateral acceleration demands, reflect more braking efforts and less cornering efforts, which is in consistent

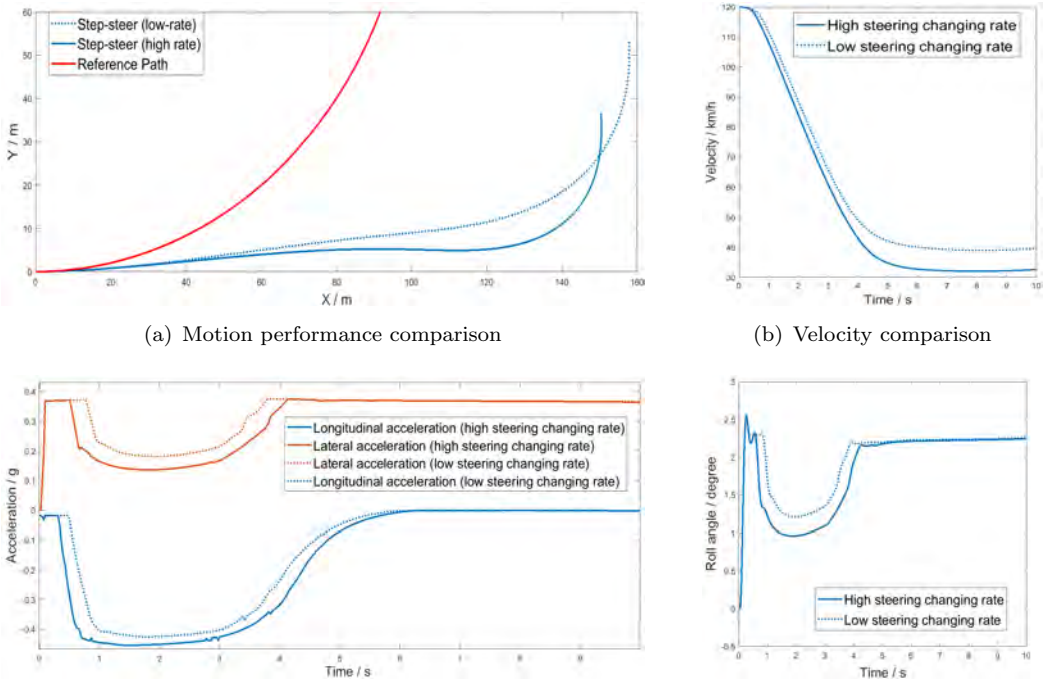

(a) Motion performance comparison

(b) Velocity comparison

(c) Acceleration comparison

(d) Roll performance comparison

FIGURE 4.18: R-MPR simulation results with ramp steering inputs

with the control design concept. Besides, when the DI demands go below the lateral acceleration limits, the vehicle can fully satisfy the driver's demand, hence the vehicle with more steering inputs can achieve a better cornering performance in latter phase of simulation as shown in the motion performance comparison in Figure 4.18. As a short summary, R-MPR strategy reduce the longitudinal velocity in a systematic way maintaining driver in the control loop, and the velocity and acceleration comparison with different steering changing rates demonstrate that the driver steering inputs indeed effect the mass-center longitudinal and lateral forces. Hence, although with R-PPR strategy the vehicle can always achieve a minimum path off-tracking performance considering rollover prevention ignoring the driver inputs, with R-MPR the vehicle can maintain maneuverability and flexibility from the driver. Note that these simulations have triggered R-PPR using driver input (same as R-MPR) but ideally it should be triggered autonomously based on the road geometry etc. This still fits in with the controller design methology.

4.6 Summary

The problem is formulated as one of minimizing lateral deviation from the intended path subject to friction and rollover limits. The presented control allocation and moderation method are developed to apply to the rollover problem in such a way that speed is

optimally reduced. Mediation provides a general approach to designing a cooperative system, coordinating between the human driver and the onboard autonomous safety system to reduce the sensitivity of vehicle response to any sudden or emergency driver actions. Control actuator presents a novel solution for the vehicle center forces distributing into individual tire forces while considering the friction limits. Finally, the proposed particle model with rollover constraint is integrated into a combined control strategy, including a fully autonomous controller and ADAS controller.

This chapter presents a novel technique for transforming driver commands into chassis control signals in the context of rollover prevention when a vehicle with a high mass center is driven at high speed on a curved road. The problem is complicated by the need to address issues such as un-tripped and tripped rollover, the trade-off between path following and rollover prevention, and also need for a seamless transition between keeping the driver in the control loop and allowing an electronic safety system to make a fully autonomous intervention. One approach is to override the driver and deploy fully autonomous braking based on the vehicle states and the road geometry. A second approach uses a driver interpreter (DI) and control moderation to avoid excessive lateral acceleration while keeping the driver fully in the control loop. The aim is to establish best-case methods for autonomous and driver-adaptive interventions based on different road conditions. After extended simulation testing, it demonstrate that the proposed two approaches can be used synergetically and efficiently to solve this problem.

Chapter 5

Pseudo-inverse based control allocation

CA determines how to distribute the required vehicle-level acceleration to the vehicle actuators, and is adopted as a suitably flexible and powerful control technique to address the challenges presented above, since it fits neatly into a general hierarchical control architecture (see section 2.3). In addition, the braking/driving force control allocation method can be integrated with the CA efficiency control, meaning that taking both the optimization of J_2 and J_3 (see equation 2.33 in section 2.3.1) into consideration. As discussed in Chapter 2, a common technique is the constrained quadratic programming (CQP) [101][102], which is viable but may be less reliable near the friction limits because of the inaccuracy of inverse tyre model. These issues are to be considered in detail in this chapter.

Due to the high computational load, the CQP may not be able to provide satisfactory control allocation solution in real-time [70]. However, the CQP approach can be considered as a benchmark here. Hence, a Pseudo Inverse Matrix approach was employed to implement the CA problem, which is proved to be having reduced computational cost. The Pseudo-inverse based CA approach is to be modified by applying a control reallocation (CRA) algorithm in this chapter, which can efficiently solve the CA problem near and even on the friction limits. Besides, the CRA can also be improved to solve the CA efficiency problem while minimizing the control allocation errors. Based on that, we propose a novel solution based on the Pseudo Inverse method for control allocation problem.

With the increasing capability of realtime onboard controller, there has been increasing interests in automotive applications that the control allocation (CA) is widely used to deal with the actuator control constraints. This chapter proposes a new approach for the

constrained CA method based on pseudo-inverse operator, which is named as Pseudo Inverse Control Allocation (PICA). There are two aspects of constraints discussed in this chapter: one is mechanical constraints which are considered as a hard constraint for the CA; another is actuator operational constraints including the tire force magnitude and changing rate limits. Taking the most traditional CA method-CQP as a benchmark (refer to section 2.3.1), this chapter compares the two methods with exactly the same upper-level controller and low-level controller which is included in a hierarchical control structure to close the control loop. In the high-level controller, the model predictive control (MPC) is used (refer to section 2.2.1) for the path tracking; the low-level controller is to achieve and track the desired tire forces obtained from the CA process. The simulations are conducted via a double-lane change (DLC) manoeuver for both low speed and high speed. The results demonstrate that the proposed PICA can deal with multiple constraints effectively and satisfy the hard constraints better than CQP, and with less usage of tire forces. Besides, it can always find a feasible solution for the actuators to track under variable situations. Hence, it can be widely applied for solving the vehicle constrained CA problem in variable driving situations.

5.1 Control re-allocation method

5.1.1 Tire friction constraint

Control allocation is commonly formulated as an optimization problem in which the allocation error $\parallel Bu - V \parallel_2$ is minimized, with V being the virtual control inputs and u being the actual control vector (refer to section 2.3). Generally, the control input constraints derive from tire force saturation, which follows an approximate friction circle:

$$\sqrt{F_{xij}^2 + F_{yij}^2} \leq \mu_{ij} F_{zij} \tag{5.1}$$

As discussed above, a Pseudo Inverse Matrix approach was employed to implement the CA problem, this having reduced computational cost.

$$u = B^{\sharp} V \tag{5.2}$$

where the $\sharp$ denotes the pseudo inverse operator and is mathematically well defined, without any issues over convergence or local minima.

For the constrained control allocation problem, where the friction constraint is to be satisfied, the solution of u may be infeasible. Generally there are feasible solution methods to solve this problem: (i) finding a feasible solution on a subset of the attainable

command set, which is called the feasible region for pseudo-inverse [103]; (ii) apply a re-allocation control algorithm, taken from the literature of aircraft flight control allocation [104][105],or redistributed pseudo-inverse method [106][73].

In this chapter, we develop the control reallocation algorithm (CRA). The method is checking out all the coupled results (longitudinal and lateral forces of each tire) satisfying with the constraint, if not, approximate the results within the constraint and the pseudo-inverse solution of Equation 5.2 were saturated and replaced by the approximate value. Then the control allocation problem was resolved with only the remaining control inputs as free variables.

Specific steps are described as follows:

Step 1: Use pseudo-inverse method (Equation 5.2) to distribute the desired control target V and get the distribution result u;

Step 2: According to whether the control variables u exceed the friction limits, if no control input exceeds, the final value of u can be directly obtained from Equation 5.2. However, if one or more control inputs exceed their operation limits, the optimization process continues: dividing the control variables into two groups, the first group u_1 is beyond friction constraint, the second group u_2 does not exceed the limits for the control variables. Correspondingly, the control effectiveness matrix B is also divided into two parts: B_1 and B_2.

Step 3: Set the control variables of u_1 at the corresponding maximum value according to the friction limits (as Equation 5.1) as $\tilde{u_1}$:

$$\begin{aligned} \widetilde{F}_{xij} &= \frac{F_{xij}\mu F_{zij}}{\sqrt{F_{xij}^2 + F_{yij}^2}} \\ \widetilde{F}_{yij} &= \frac{F_{yij}\mu F_{zij}}{\sqrt{F_{xij}^2 + F_{yij}^2}} \end{aligned} \tag{5.3}$$

then the $\tilde{u_1}$ can be obtained: $\tilde{u} = [\widetilde{F}_{xij}, \widetilde{F}_{yij}]^T$, assuming that $\tilde{u_1}$ can afford $V_1 = B_1\tilde{u_1}$. Then the remaining undistributed control target is $V_2 = V - V_1$.

Step 4: Solve the problem with the remaining control inputs as free variables through the pseudo inverse operator:

$$\tilde{u_2} = B_2^{\sharp}V_2 \tag{5.4}$$

Finally, the results can be obtained as $u = [\tilde{u_1}, \tilde{u_2}]$. If there is more than one coupled control input going beyond the limits, the modification process of the matrix and vector

should continue according to the steps described above till all control inputs satisfy the requirement.

To illustrate and verify the proposed CRA process, we sample a short time period (1 second) from the simulation (test conditions are described below in section 5.2.3) to demonstrate how the CRA affects the tire force control re-allocation. It is found from Figure 5.1 that during this interval, the distributed tire forces from outside the current friction circle will be mapped just on the friction circle or close to the friction circle while minimizing the CRA error ε to achieve the vehicle-level control efforts V in an executable way (to be demonstrated in Figure 5.13). Note that, only the locations of tire forces are shown in this Figure 5.1 during this time period, while not presenting the exact state of each tire force in every simulation step time. Hence, it has been verified that the proposed CRA method can effectively solve this constrained optimization problem. In addition, this CRA method is fully employed in Chapter 3 and 4 as the CA method for the simulation validations of the control strategies of PPR/MPR and R-PPR/R-MPR.

5.1.2 Actuator operational constraints

The vehicle actuators of braking/acceleration and steering mechanism and electronic actuators will be subject to a physical limitation, mainly amplitude saturations and rate limits, in a relatively short time. Generally, the control input constraints derive from tire force saturation and actuators constraints. The tire force saturation has been discussed above, then the realistic actuators are subject to amplitude saturations and rate limits, which may be expressed as:

$$\underline{u}(t) \leq u(t) \leq \overline{u}(t) \tag{5.5}$$

where,

$$\begin{aligned} \underline{u}(t) &= max[u_{min}, u(c) - T_0 \varrho_{min}] \\ \overline{u}(t) &= min[u_{max}, u(c) + T_0 \varrho_{max}] \end{aligned} \tag{5.6}$$

where u_c denotes the tire forces in current time, and T_0 denotes the sampling time of the controller.

For the CQP, these limitations can be taken into consideration by adding linear inequality constraints. However, it can only increase its computational consumption and lower the computation efficiency of CA process. In this chapter, derived from the idea of CRA, we propose a new CA method based on the Pseudo-Inverse matrix to deal with this constraint problem.

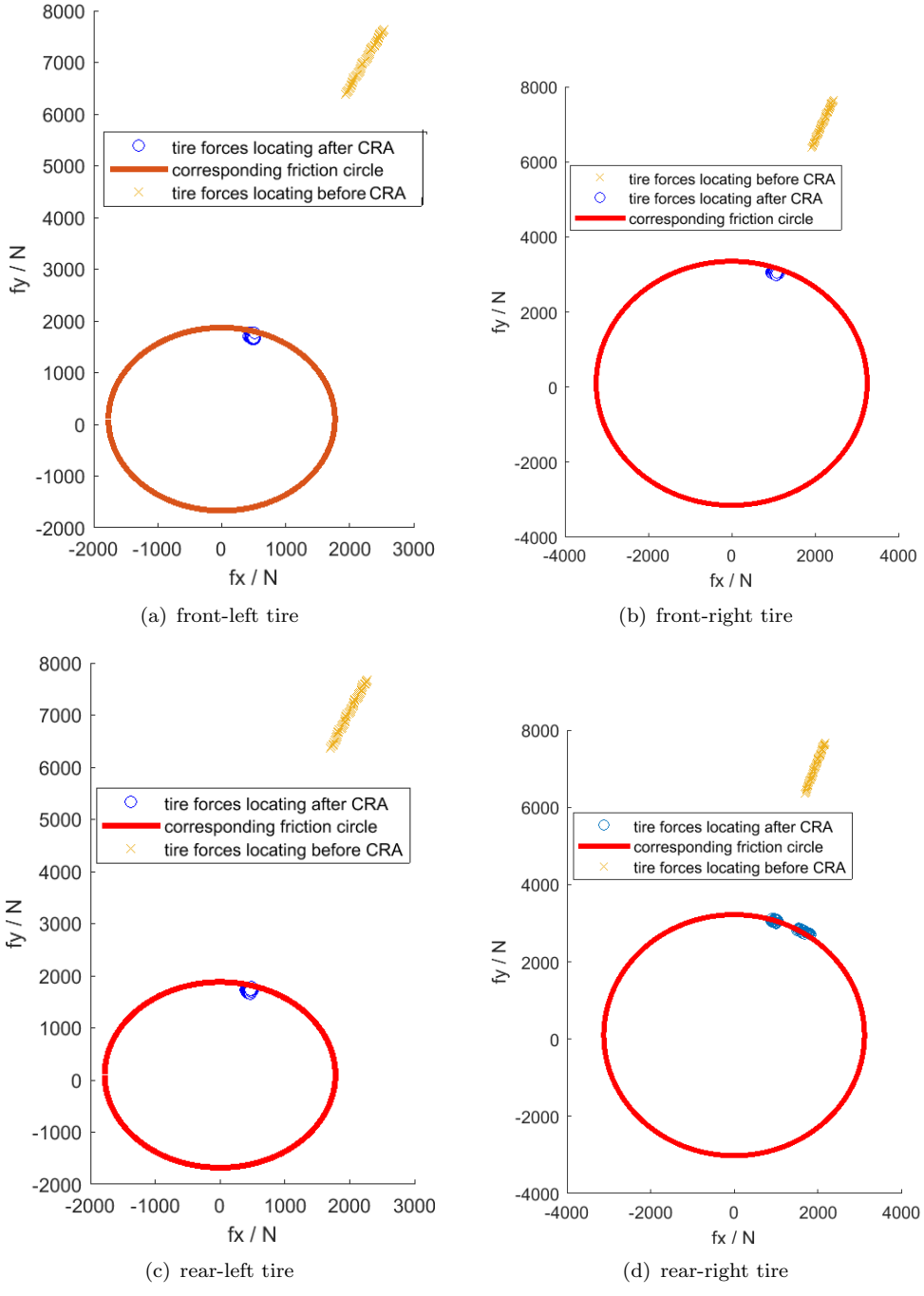

(a) front-left tire

(b) front-right tire

(c) rear-left tire

(d) rear-right tire

FIGURE 5.1: Comparison of tire forces locating between before and after CRA

Assuming the current value of each tire force u_c and the actuator rate limits ϱ are known. In the control time scale of T_0, the new constraints of the tire forces u can be described as a rectangle, where the boundary value can be expressed as:

$$\begin{aligned} F_{xij}^{min} &= F_{xij}^{c} - T_0\varrho; F_{xij}^{max} = F_{xij}^{c} + T_0\varrho \\ F_{yij}^{min} &= F_{yij}^{c} - T_0\varrho; F_{yij}^{max} = F_{yij}^{c} + T_0\varrho \end{aligned} \tag{5.7}$$

assuming this actuator operational constraint as $u \in \Omega_1$, and the tire friction constraint as $u \in \Omega_2$, then the new constraint can be obtained as $u \in \Omega$ where $\Omega = \Omega_1 \cap \Omega_2$.

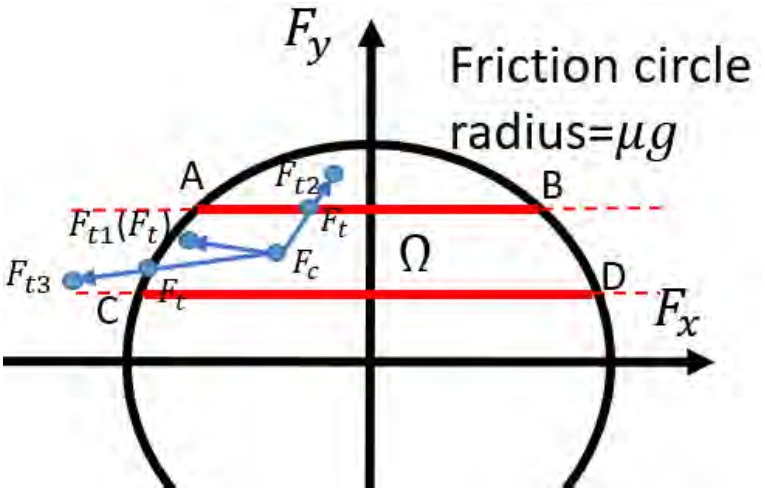

FIGURE 5.2: CRA of tire forces with combined actuator constraints

In addition, actuator rate limits can be used to narrow the search range, so rate limits can help with optimization (no point finding the absolute optimum if it cannot be reached during the next T_0 seconds).

Hence, the whole control process can be described as:

Step 1: if u satisfies the new combined constraint of Ω, then the solution can be directly achieved by equation 5.2;

Step 2: if u can not satisfy the new combined constraint of Ω, over-saturated elements of the control vector will be approximated to the feasible area of Ω, as shown in Figure 5.2. Note that, in real vehicle actuator control systems, the changing rate limits of longitudinal tire forces may be ignored due to the fast response of wheel speed controller, but normally the changing rate limits of lateral tire forces can not be ignored due to the relatively slow response of tyre steering actuators and yaw-sideslip dynamics (slip angle at unsteered wheels). Hence, we set the actuator operational constraints Ω_1 as a rectangle with unlimited length (corresponding to the longitudinal tire forces) ;

Step 3: making u be decomposed into the approximated control vector u_a and un-approximated control vector u_s, with the associated sub-matrix be B_a and B_s, then the global generalized control effort with the approximated control vector can be expressed as: $V_a = B_a u_a$, finally the un-approximated control vector u_s can be obtained by:

$$u_s = B_s^{\sharp}(V - V_a) \tag{5.8}$$

If there is more than one coupled results going beyond the limits, the CRA process of the matrix and vector should continue till all control inputs satisfy the requirement.

In this case, the method is checking out all the coupled results (longitudinal and lateral forces of each tire) satisfying with the new combined constraint. There are mainly two situations for approximating the control vector, as shown in figure 5.2: if the control target is located inside the combined constraint Ω, as point F_{t1}, then it can be directly achieved; and if the control target locate outside the combined constraint Ω, then based on where the connect line between current value and control target interset at, different cases as point F_{t2} and F_{t3}, the approximating results will locate to different boundaries. According to different cases, the results can be directly calculated by the known value of current states, control targets and specific boundary via the proportional relation.

5.2 Efficient control allocation

5.2.1 CQP

In the case where multiple solutions are possible, even after actuator constraints have been applied, then the optimal choice will be to make the control variable u as small as possible and the changing rate as low as possible for the CA efficiency. This is because achieving a same control target with less use of control actuators (in corresponding with small control variable and low changing rate of control inputs) will help to achieve reduced energy dissipation at the tyres.

The control allocation method of CQP can achieve the CA efficiency via minimizing the terms $\| (u - u_c) \|_2$ and $\| u \|_2$ in the same objective function. In the normal driving conditions, the equation $Bu = V$ can be assumed to be relatively easy to achieve, hence we set the equation $Bu = V$ as the control subject, then the object function become:

$$J = \min \frac{1}{2} \tilde{u}^T R \tilde{u} \tag{5.9}$$

where $\tilde{u} = \begin{bmatrix} u \\ \Delta u \end{bmatrix}$, and subject to:

$$\tilde{\mathbf{B}} \tilde{u} = \tilde{\mathbf{V}} \tag{5.10}$$

where $\tilde{\mathbf{B}} = \begin{bmatrix} \mathbf{B} & \mathbf{0} \\ \mathbf{I} & -\mathbf{I} \end{bmatrix}$, $\tilde{\mathbf{V}} = \begin{bmatrix} \mathbf{V} \\ \bar{\mathbf{V}} \end{bmatrix}$, and $\bar{\mathbf{V}} = \mathbf{B} u_c$

In the normal driving situation, the CA efficiency can be achieved by this method, however, during the critical situation, the target of $Bu = V$ can not be achieved under the friction limitation, then minimizing the CA error ε become the main control object. Referring back to section 2.3.1, in Equation 2.34, in this case the CA efficiency control can be achieved by solving the WLS problem, while the weighing parameter of W_1 are needed to be relatively large in order to emphasize the importance of minimizing the allocation error. Although the CA efficiency can be achieved via CQP in critical situations, the high computation cost and optimal fitting of weighting parameters W_2 and W_3 make it hard to be implemented into the real-time vehicle controller. In the latter simulation tests, for the normal driving condition (low speed), the W_1, W_2 and W_3 are set the same as unit matrix I; for the limit driving condition (high speed), to emphasize the importance of minimizing the allocation error (motion control become priority in this critical condition), the W_1 are set to be relatively large as $1000 \times I$, the W_2 and W_3 are still set to be I. Although the control targets (minimizing the allocation error and CA efficiency) can be separately emphasized by tuning the weighting parameter, the other control performance will become worse with a lower value of weighting parameter and the computation cost will become higher.

5.2.2 Pseudo Inverse Control Allocation (PICA)

For the pseudo-inverse based CA method, we can also achieve the CA efficiency via minimizing the control efforts $\| \Delta u \|_2$ and $\| u \|_2$. Referring to section 2.3.2, the pseudo-inverse based CA method can also be achieved by building a Hamiltonian function as Equation 2.38, where the expression can be reduced to the Moore-Penrose pseudo-inverse as Equation 2.40. Derived from this idea, the changing rate $\| \Delta u \|_2$ can also be considered via building a new Hamiltonian function where the objective function is shown as:

$$J = \min \frac{1}{2} \Delta u^T W \Delta u + \frac{1}{2} (u_c + \Delta u)^T R (u_c + \Delta u) \tag{5.11}$$

where the W and R is the weight coefficient matrix. Then the constraint can be described as:

$$\begin{aligned} B(u_c + \Delta u) &= V \\ \underline{u}(t) \leq u(t) &\leq \overline{u}(t) \end{aligned} \tag{5.12}$$

For solving this optimization problem, a Hamiltonian function is introduced as:

$$\begin{aligned} H = &\frac{1}{2} \Delta u^T W \Delta u + \frac{1}{2} (u_c + \Delta u)^T R (u_c + \Delta u) \\ &+ \lambda (B(u_c + \Delta u) - V) \end{aligned} \tag{5.13}$$

where λ denotes the Lagrange multiplier. Calculating the partial derivatives for Δu and λ for the Hamilton function and setting to 0 as:

$$\begin{aligned} \frac{\partial H}{\partial \Delta u} &= W\Delta u + R(u_c + \Delta u) + B^T\lambda^T = 0 \\ \frac{\partial H}{\partial \lambda} &= B(u_c + \Delta u) - V = 0 \end{aligned} \tag{5.14}$$

Then we can obtain:

$$\begin{aligned} &(W + R)\Delta u = -Ru_c - B^T\lambda^T \\ &B(W + R)^{-1}B^T\lambda^T = Bu_c - V - B(W + R)^{-1}Ru_c \end{aligned} \tag{5.15}$$

making $S_f = B(W + R)^{-1}B^T$, then we can obtain

$$\lambda^T = S_f^{-1}(Bu_c - V - B(W + R)^{-1}Ru_c) \tag{5.16}$$

Finally, we can obtain:

$$\begin{aligned} \Delta u &= (W + R)^{-1}(-Ru_c - B^T\lambda^T) \\ &= (W + R)^{-1}B^T S_f^{-1}V - u_c \\ &= B^\sharp V - u_c \end{aligned} \tag{5.17}$$

with

$$B^\sharp = (W + R)^{-1}B^T S_f^{-1} \tag{5.18}$$

where $B^\sharp$ denotes the pseudo-inverse matrix with the optimized objective. It can be further verified by assuming the weight coefficient matrix W as a null matrix, and the weight coefficient matrix R as a unit matrix, then the results of Equation 5.18 will be exactly the same as Equation 2.40 introduced in section 2.3.2.

Hence, it is found that the control efforts $\| \Delta u \|_2$ and $\| u \|_2$ can both be minimized via building a Hamiltonian function which reduces to the Moore-Penrose pseudo-inverse operator finally. Note that, in the latter comparison simulation tests with CQP, the weight coefficient matrix W and R are both set to be unit matrix I in corresponding to the parameter setting of CQP method. Based on the theoretical derivation in this chapter, it can be predicted that the CA efficiency can be effectively achieved via the proposed method in this section.

5.3 Simulation comparison of control allocation efficiency

Based on the proposed two efficient CA methods (CQP-based and PICA), it can be expected that the controller demand (desired tire forces) will become smooth. In addition, based on the mathematical characteristic of PICA, it can be expected that the PICA method can achieve a better results with less tire force utilization than CQP based CA method.

5.3.1 Normal driving condition

The simulating experiments in normal conditions are constructed with the high-level controller of MPC (refer to section 2.2.1). The target trajectory is selected as a double lane change (DLC) driving condition as shown in Figure 5.3 ,which is normally applied to test the vehicle's handling stability [107]. Comparing to ISO lane change maneuver, the reference lateral position y_{ref} and yaw angle ψ_{ref} of this DLC condition can be explicitly expressed by equation:

$$\begin{aligned} y_{ref}(x) &= \frac{d_{y1}}{2}(1+\tan(z_1)) - \frac{d_{y1}(1+\tan(z_1))}{2} \\ \psi_{ref}(x) &= \arctan(d_{y1}(\frac{1}{\cosh(z_1)})^2(\frac{1.2}{d_{x1}}) \\ &\quad - d_{y2}(\frac{1}{\cosh(z_2)})^2(\frac{1.2}{d_{x2}})) \end{aligned} \tag{5.19}$$

where $z_1 = \frac{2.4}{25}(x-27.19) - 1.2$, $z_2 = \frac{2.4}{21.95}(x-56.46) - 1.2$, $d_{y1} = 4.05$, $d_{y2} = 5.7$

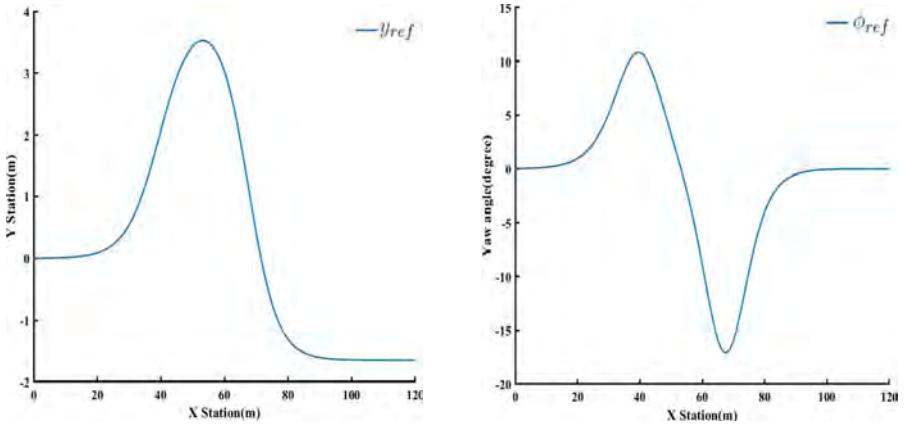

(a) Reference lateral position (b) Reference yaw angle

FIGURE 5.3: Desired tracking targets

When comparing the different control allocation methods (CQP and CRA), the MPC is employed as the upper-level controller. To make valid comparisons, the main control parameters of MPC (introduced in section 2.2.1) are set to be the same, thus avoiding the extra impact from feedback into the upper controller. DLC operation will be simulated separately with the CQP and CRA. Since the purpose of this section is to compare the two proposed CA approaches in normal condition, the target velocity is chosen as $72km/h$.

(a) Lateral view of steering actuator system

(b) Rear view of steering actuator system

FIGURE 5.4: steering actuator system

Particulary, a real vehicle steering actuator system as shown in Figure 5.4, with the operating voltage is 24V, and rated power is 360W with a upper limits of 720W, can achieve a maximum road wheel steering speeding of $30°/s$. This value obtained from a real vehicle will be set as the aforementioned rate limits of ϱ in the following CarSim simulation tests, and the rate limit of longitudinal tyre force control actuator is assumed to be limitless.

As the pseudo-inverse method can guarantee the obtained u to be minimum [75], we set the object function of CQP is to minimize the u. As shown in Figure 5.5 and 5.6, the vehicle path performance are highly coincident with both the CQP and PICA method, which demonstrate that the effect of control allocation are quite close. Note that, based on the mathematic characteristics, the solution obtained from pseudo-inverse operator can always guarantee the minimum control effort $\parallel u \parallel$, it is found that from the comparison of the tire forces utilization which is set to be $\sqrt{F_{xij}^2 + F_{yij}^2}$, the PICA method can still achieve a lower tire force utilization in comparison with the CQP, even though the object function of CQP in this simulation is only set to minimize the control effort of u. In the subsequent simulation tests in this chapter, it can also be found that the vehicle can achieve a lower tire force utilization with the pseudo-inverse based CA method in comparison with CQP.

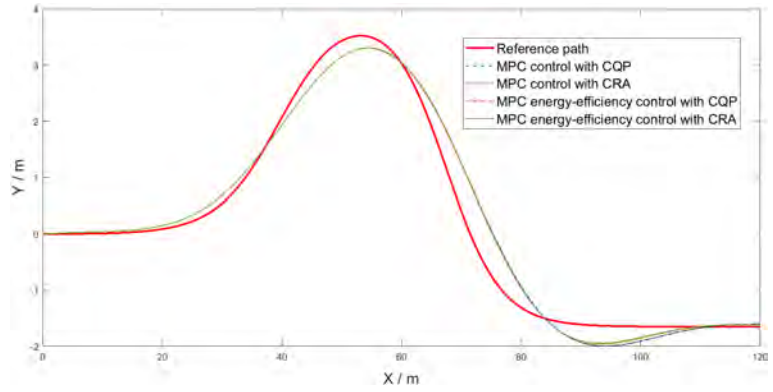

(a) Path performance

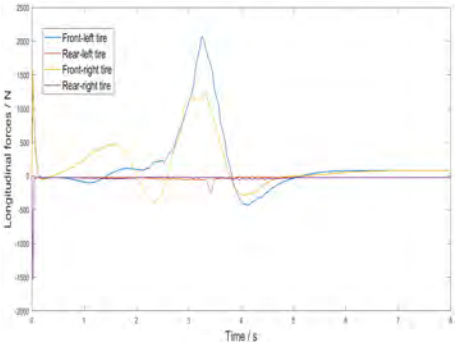

(b) Longitudinal tire forces with CQP

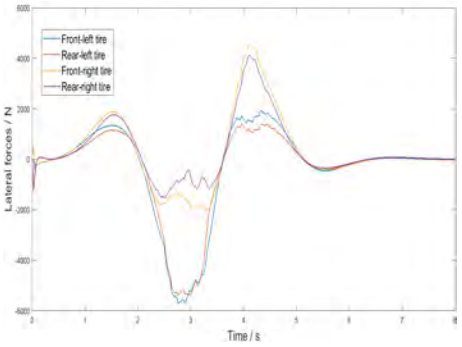

(c) Lateral tire forces with CQP

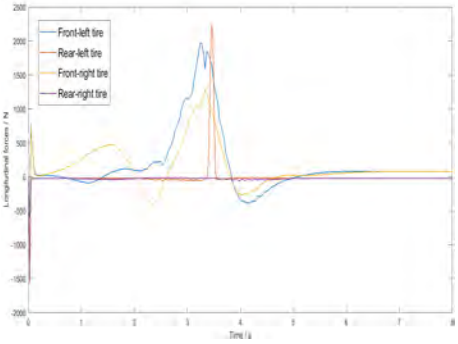

(d) Longitudinal tire forces with CRA

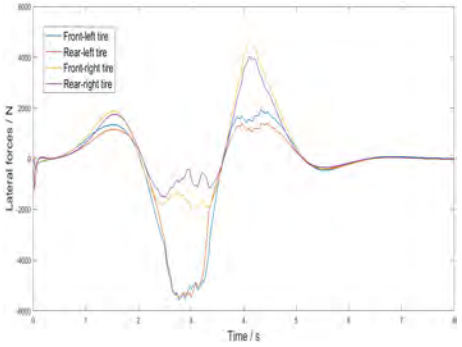

(e) Lateral tire forces with CRA

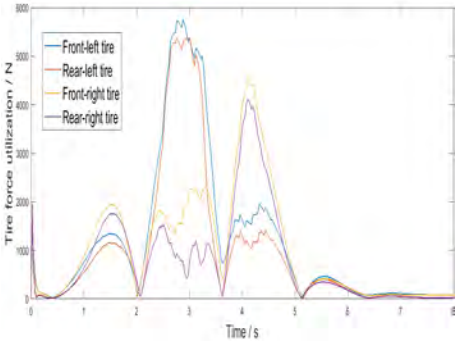

(f) Tire force utilization with CQP

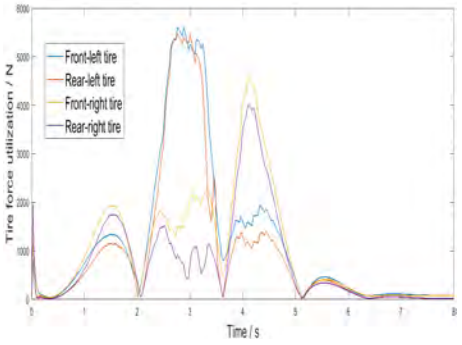

(g) Tire force utilization with CRA

FIGURE 5.5: Control allocation results for path tracking(normal condition)

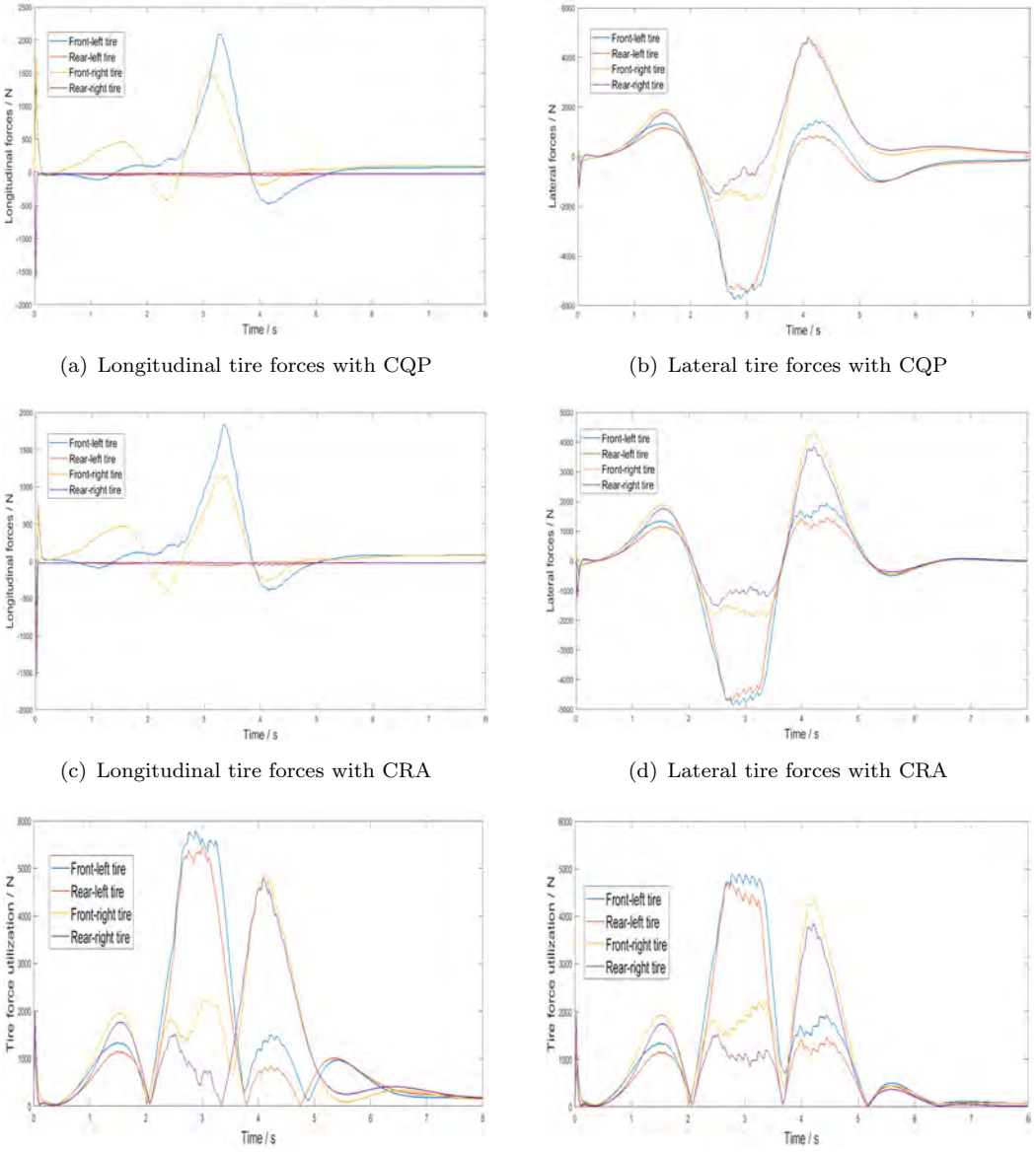

(a) Longitudinal tire forces with CQP

(b) Lateral tire forces with CQP

(c) Longitudinal tire forces with CRA

(d) Lateral tire forces with CRA

(e) Tire force utilization with CQP

(f) Tire force utilization with CRA

FIGURE 5.6: Control allocation results for path tracking and CA efficiency (normal condition)

5.3.2 Limit driving condition

As introduced in section 2.2.2, PPR is based on the optimal control of a friction-limited particle, the target being to minimize the maximum off-tracking from the commanded trajectory. It combines braking and turning accelerations of the vehicle mass center in such a way that a reduction in speed is coordinated with increasing path curvature. It emerges that the acceleration vector is fixed in the inertial reference frame C see Figure 2.5. Hence, for the comparison under limit driving conditions, the PPR control strategy (introduced in section 2.2.2) is employed in this experiment. In the following, this type of control will be further implemented via both the CQP and proposed CRA control

allocation approach for limit handling control. In the simulation, the steering wheel angle (from Driver Interpreter) is set to a constant value at $1.335rad$ corresponding with the intended path curvature (radius=100m), the initial velocity entering the curve is set to be $140km/h$ under the road surface condition $\mu = 1$.

During this critical situation, the vehicle control reference (longitudinal and lateral vehicle center forces) is obtained from PPR and the reference yaw moment is obtained from the SMC. The control allocation results are shown in Figure 5.7.

The results of path performance demonstrate that in this critical situation, the CRA method can perform slightly better than CQP. That is due to the linearization of tire friction circle within CQP which can not take full use of the tire forces in the limit condition. It is found that the results of CQP are noisier, which can also be due to the linearization of friction circle and the operating principle of CQP. Hence, to make the CA results smoother, the optimization target of Δu is added into the cost function for the CQP method. For the CRA method, the PICA method (for efficient control allocation) introduced in section 5.2.2 as Equation 5.18 is implemented in this simulation test to compare with the normal CRA method as Equation 2.39 introduced in section 2.3.2. It is found from Figure 5.7 that with both the CQP and CRA, the path performance results are exactly the same as without CA efficiency control, which demonstrate the effectiveness of PICA introduced in section 5.2.2; and for the CQP method, the result is reasonable because we set the minimizing control allocation error $\| (Bu - V) \|_2$ as the main control target in this critical situation. The CA results are shown in the Figure 5.8. It is found that with the CA efficiency control both the CQP and CRA results become smoother. However, the results of CRA are seen to be better than CQP both in the minimization of u and Δu.

As a short summary, the CRA method can achieve a quite close effect in normal situation but a better performance in limit situation in comparison with the CQP. Besides, PICA method can also achieve multiple optimization targets (such as CA efficiency) as the CQP, and even with better vehicle performance.

5.4 Constrained control allocation with mechanical constraints

Up to now, the CRA method of solving the constraint problem with tire force friction limits has been introduced in section 5.1. However, for the real vehicle control application, there may be additional hard constraints to be considered. For example, for the

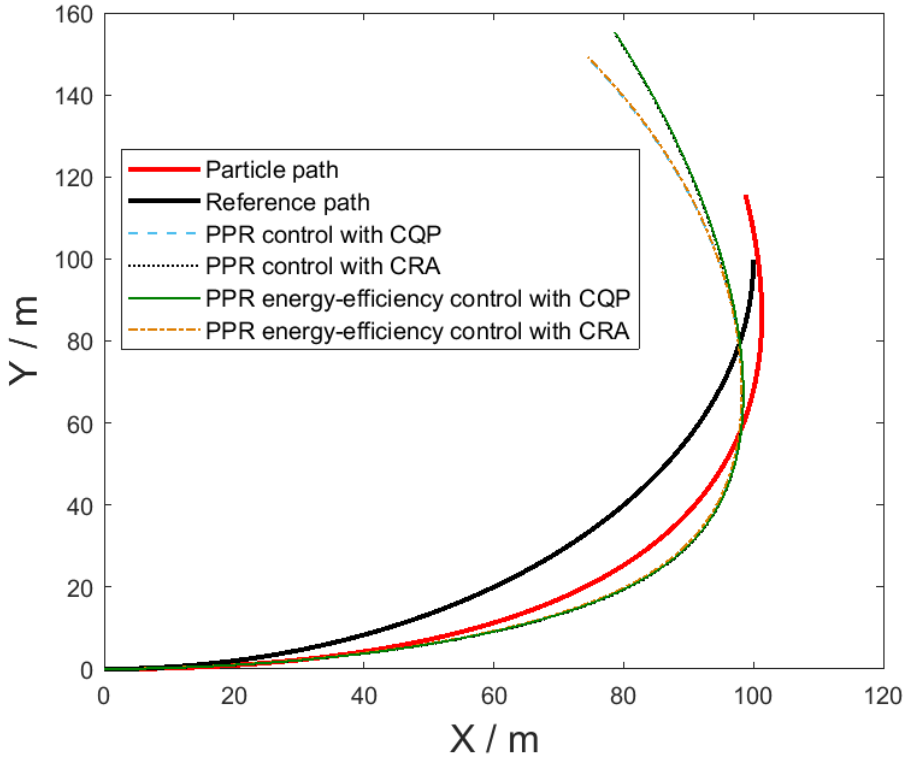

(a) Path performance

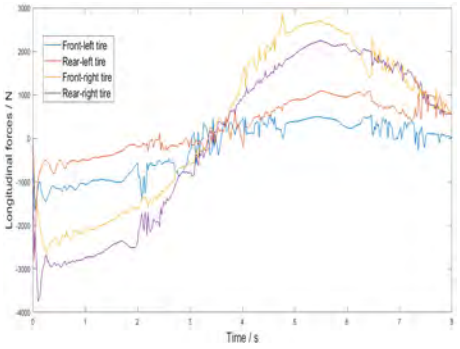

(b) Longitudinal tire forces with CQP

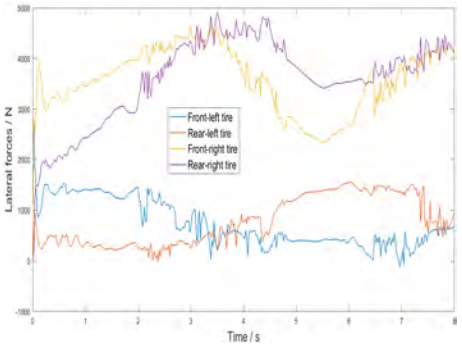

(c) Lateral tire forces with CQP

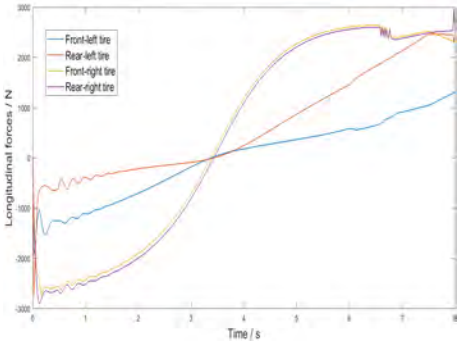

(d) Longitudinal tire forces with CRA

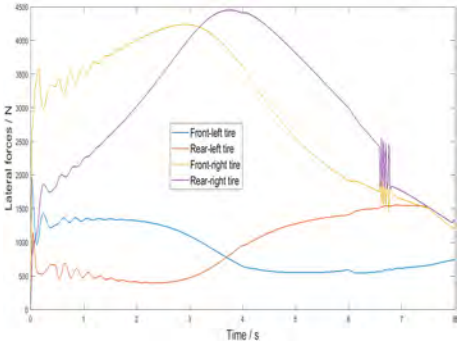

(e) Lateral tire forces with CRA

FIGURE 5.7: Control allocation results for road departure mitigation(limit condition)

traditional chassis (front axle steering, independent wheel torque) other than the individual steering vehicle which is the control object up to now, the mechanical connection

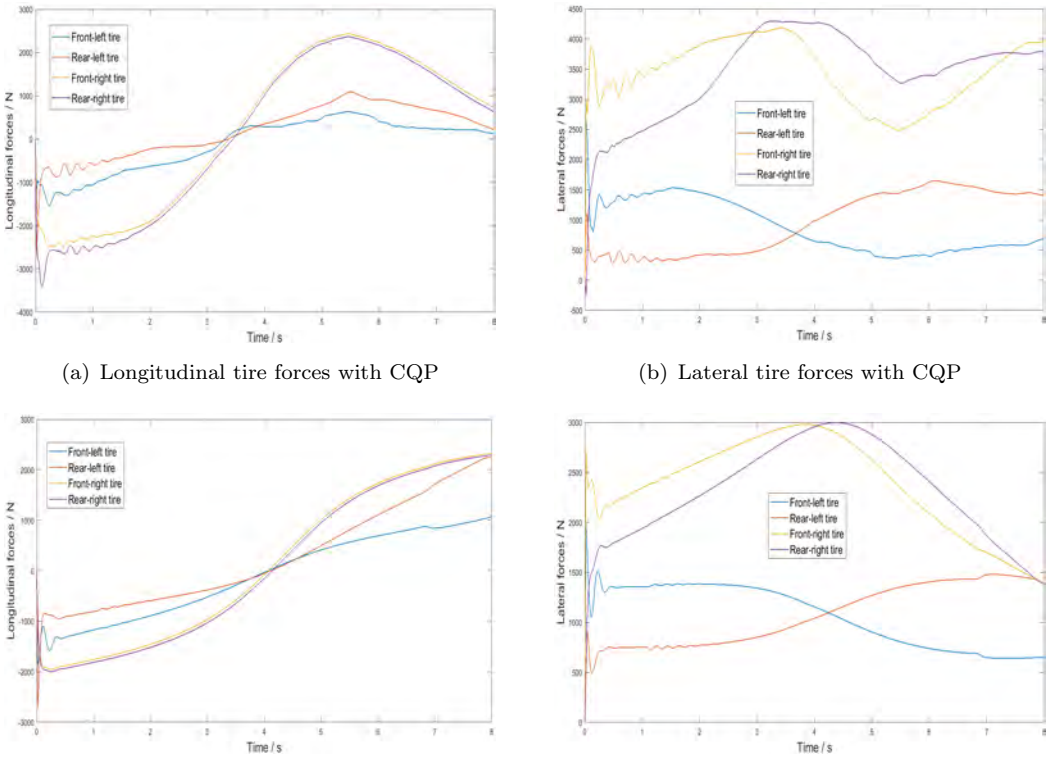

(a) Longitudinal tire forces with CQP

(b) Lateral tire forces with CQP

(c) Longitudinal tire forces with CRA

(d) Lateral tire forces with CRA

FIGURE 5.8: Control allocation results for road departure mitigation and CA efficiency(limit condition)

of tyres in a same axle will need to be considered as hard constraints for the tyre steering manoeuvre. This is the same to the chassis with rear-axle steering functions (which is called two-axle steering vehicle in this chapter as shown in Figure 5.9). However, considering the vehicle mechanical constraint as hard constraint is not trivial for implementation with pseudo-inverse matrix. Researchers would rather select CQP to solve this multi-constrained CA problems. Because a linear constraint can be directly added as hard constraint via CQP method. However, the same reason as adding actuator operational constraints into CQP, it can only increase its computational consumption and lower the computation efficiency of CA process.

FIGURE 5.9: Two-axle steering vehicle

5.4.1 Application of two-axle steering vehicle

In this section, we firstly employ the pseudo-inverse matrix as the basic CA tool to deal with multiple hard constraints. Taking the two-axle steering vehicle as an example. The additional constraints for two-axle steering vehicle, in comparison with fully actuated vehicle, is the mechanical connection of the right and left tires in the same axle, which will led to the equality of the change of steering angles in the same axle. This constraint can be described as:

$$\begin{aligned} \Delta\delta_{11} &= \Delta\delta_{12} \\ \Delta\delta_{21} &= \Delta\delta_{22} \end{aligned} \tag{5.20}$$

then we can obtain that:

$$\begin{aligned} F_{y11} &= F_{y11}^c + \frac{\partial F_{y11}}{\partial \alpha_{11}}(\alpha_{11} - \alpha_{11}^c) \\ F_{y12} &= F_{y12}^c + \frac{\partial F_{y12}}{\partial \alpha_{12}}(\alpha_{12} - \alpha_{12}^c) \end{aligned} \tag{5.21}$$

where $C_{\alpha ij} = \frac{\partial F_{yij}}{\partial \alpha_{ij}}$ can be considered as the local tire cornering stiffness.

In a very short time interval, from equation (5.20), we can assume that: $\Delta\alpha_{11} = \Delta\alpha_{12}$, then it can be obtained that:

$$\begin{aligned} C_{\alpha 12}F_{y11} - C_{\alpha 11}F_{y12} &= F_{y11}^c C_{\alpha 12} - F_{y12}^c C_{\alpha 11} \\ C_{\alpha 22}F_{y21} - C_{\alpha 21}F_{y22} &= F_{y21}^c C_{\alpha 22} - F_{y22}^c C_{\alpha 21} \end{aligned} \tag{5.22}$$

where F_{yij}^c is the current value of lateral tire forces.

For the two-axle steering vehicle, the constraint of rear axle is similar to that of the front. Then, we can obtain two additional linear constraints for the CA of two-axle steering vehicle. Assuming that the hard constraints can be separately satisfied. Then this constrained CA problem with hard constraints can also be solved via pseudo-inverse matrix:

Step 1: firstly we add the hard constraints of Equation (5.20) into the original equations:

$$\widetilde{B} = \begin{bmatrix} B \\ B_c \end{bmatrix}, \widetilde{V} = \begin{bmatrix} V \\ V_c \end{bmatrix}, \tag{5.23}$$

where $B_c = \begin{bmatrix} 0 & 0 & 0 & 0 & C_{\alpha 12} & -C_{\alpha 11} & 0 & 0 \\ 0 & 0 & 0 & 0 & 0 & 0 & C_{\alpha 22} & -C_{\alpha 21} \end{bmatrix}$, and $V_c = \begin{bmatrix} F_{y11}^c C_{\alpha 12} - F_{y12}^c C_{\alpha 11} \\ F_{y21}^c C_{\alpha 22} - F_{y22}^c C_{\alpha 21} \end{bmatrix}$, denotes the hard constraints which is required to be satisfied firstly.

Step 2: with the pseudo-inverse operator, it can be obtained that $u_c = B_c^{\sharp} V_c$. To satisfy this CA problem with hard constraints, the Singular value decomposition (SVD) is introduced, which is an eigenvalue-like decomposition for rectangular matrices [71][72]. The Singular Value Decomposition (SVD) of B_c can be expressed as:

$$\mathbf{B}_c = \mathbf{USW}^T \tag{5.24}$$

where U and W denote orthogonal matrices of dimensions 2×2, 8×8 respectively.

Step 3: Define the projection matrix $\mathbf{P} = \mathbf{I} - \mathbf{WW}^T$ and $u = B^{\sharp} V$, finally we can obtain the candidate control vector:

$$\widetilde{u} = u_c + \mathbf{PM} \tag{5.25}$$

where

$$\mathbf{M} = (B\mathbf{P})^{\sharp}(V - Bu_c) \tag{5.26}$$

where the $\widetilde{u}$ will be the final results that satisfy the hard constraints absolutely and in the meantime minimizing the CA error of $\parallel Bu - V \parallel$. The theoretical formulation of this result can be found in Appendix B, and it will be further validated in the following simulation tests. The results of CA error shown in Figure 5.13 and Figure 5.14 illuminate its effectiveness.

This proposed pseudo-inverse based CA method can therefore be used to solve the constrained CA problems even with hard constraints. For a wider application scenarios, with other hard constraints which can be expressed as a linear equality relationship, this method can still be employed via modifying the aforementioned B_c and V_c.

5.4.2 Application of traditional vehicle

Taking the traditional vehicle (front axle steering, independent wheel torque control) as another application target, the mechanical constraint are exactly the same with two-axle steering vehicle for the front axle. However, the rear tires of traditional vehicle can not actively steer, which makes the lateral forces of rear tires not directly controllable. Note that, for the traditional vehicle, the rear tire forces actually can be changed by controlling the rear axle side slip, but it is more slowly than one CA time step, hence we assume that the lateral force of rear tire will stay the same during the short period of simulation step time.

Hence, two more additional constraints can be expressed as $F_{y21} = F_{y21}^c$ and $F_{y22} = F_{y22}^c$. Based on that, modifying the B_c and V_c as:

$$B_c = \begin{bmatrix} 0 & 0 & 0 & 0 & C_{\alpha 12} & -C_{\alpha 11} & 0 & 0 \\ 0 & 0 & 0 & 0 & 0 & 0 & 1 & 0 \\ 0 & 0 & 0 & 0 & 0 & 0 & 0 & 1 \end{bmatrix} \text{ and } V_c = \begin{bmatrix} F^c_{y11} C_{\alpha 12} - F^c_{y12} C_{\alpha 11} \\ F^c_{y21} \\ F^c_{y22} \end{bmatrix},$$

Then this constrained CA problem can also be solved by the method introduced in last subsection.

To be mentioned, researchers commonly introduce the bicycle vehicle model to deal with the mechanical constrained CA problem for the control applications of two-axle steering vehicle or traditional vehicle. However, during the real vehicle running process, especially for steering situations, the vertical load transfer will have a great influence on the tyre limits. Ignoring the vertical load transfer as the assumption of bicycle vehicle model is expected to make the control allocation process unreliable where the CA requires precise information of four individual tyre friction limits. In addition, the bicycle model is not appropriate in this case due to lack of considering the four individual tyre braking control. Researchers would commonly select to equally divide the obtained front axle braking force to the two front tires which is imprecise and will make the control performance worse.. Hence, the four-wheel vehicle model considering the vertical load transfer as introduced in section 3 is more convincing for the real-vehicle control applications.

5.4.3 Simulation comparison-Case A: Two-axle steering vehicle application

With a constant target vehicle speed of either 36km/h or 72km/h, and coefficient of road adhesion of $\mu = 0.8$, the test is employed to compare the different performance of CQP (introduced above with hard constraints) and PICA for the two-axle steering vehicle application. The simulating experiments for both applications are constructed with the high-level controller of MPC (refer to section 2.2.1). The target trajectory is again the DLC condition introduced in section 5.2.3. Note that, the simulations use a four-wheel steering vehicle but with preset hard mechanical constraints as Equation (5.22).

The vehicle path performance is shown in figure 5.10 which show that both in low-speed and high-speed situation, the two proposed CA methods perform in a very similar way. When analysing the vehicle running performance as shown in figure 5.11, it can be found that with the two CA methods, the vehicle motion states are seen to be different. In detail, although the CA errors are equal to zero for both method during the whole control process, the longitudinal and lateral forces obtained from the two CA processes are different. Without consideration of longitudinal and lateral forces changing rate, the PICA method makes the tire forces change very sharply, which might be a result of the optimization target (smoothness of control outputs is not taken into consideration) and

process of PICA (this is to be modified via considering the changing rate limits in the following simulation). However, the lateral forces obtained from the PICA are much smaller than from the CQP (both are without any further efficiency/smoothness terms), and leading to less effort of wheel steering actuators. Besides, from figure 5.11 , it can be found that the PICA method can satisfy the hard constraint of same wheel steering angles (and changing rate) on one axle properly, while the CQP does not always succeed on the front axle (the front axle wheels' angles did not meet the constraint). From figure 5.11, it is found that the vehicle motion performances are also very close. The vehicle with CQP method is however running a little bit smoother than PICA, which is due to the noise of tire forces calculated via PICA.

As a short summary, the CA methods of CQP and PICA can achieve a quite close effect in this DLC low-speed driving situation, however, without considering the lateral tire force changing rate, the PICA will suffer from noisy results.

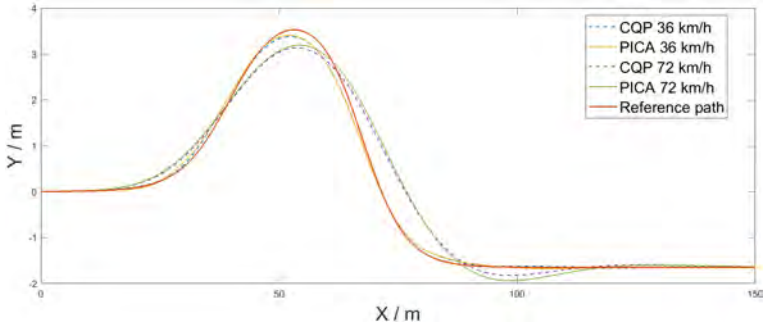

FIGURE 5.10: Path tracking performances

Then, the second test is to increase the target vehicle speed to 72km/h, which might make the vehicle suffer some limit driving situation, and the more important is that the CA process will not fully meet the control target, in other word, the $Bu = V$ can not be fully satisfied. Hence, as shown in the path performance in figure 5.10, the vehicle's tracking ability is decreasing with a high speed. As the PICA method appears noisy in the low-speed condition, then we take the tire force changing rate limits into consideration (the method is described in section 5.4.1) in this high-speed test, and also we add the same inequality constraint as shown in equation 5.5 into the CQP method.

From the tire forces obtained via different CA method shown in figure 5.12, it is found that the PICA can obtain a much smaller value of tire forces, which demonstrate that the PICA can find a best solution of minimizing the CA error $Bu - V$ with a minimum control inputs $u(t)$. Although there is still some noise in lateral tire forces with PICA, it has been verified that the changing rates are within design limits. The comparison results of wheel steering angles also demonstrate that the PICA can meet the mechanical constraint much better than CQP which can not provide satisfying results. Note that,

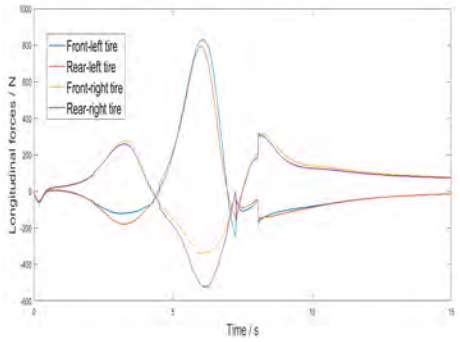

(a) Longitudinal tire forces with CQP

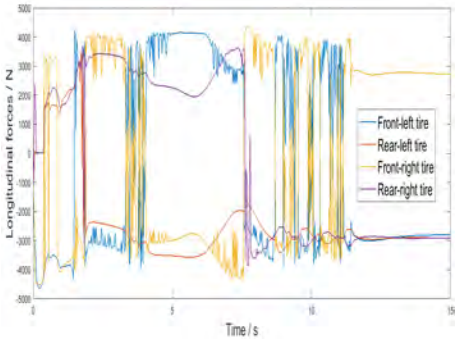

(b) Longitudinal tire forces with PICA

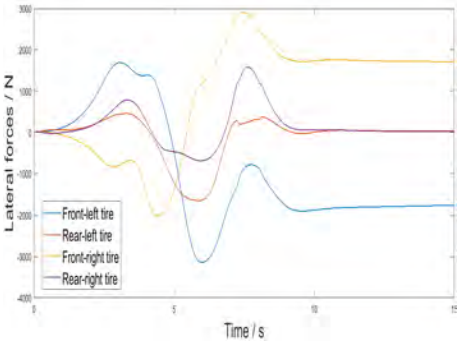

(c) Lateral tire forces with CQP

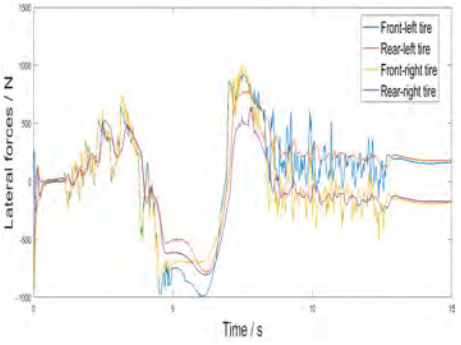

(d) Lateral tire forces with PICA

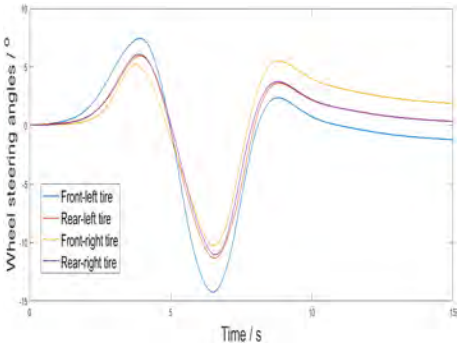

(e) Wheel steering angles with CQP

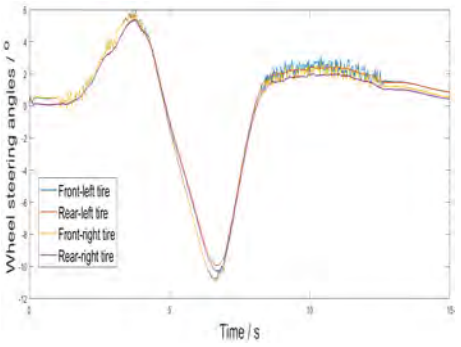

(f) Wheel steering angles with PICA

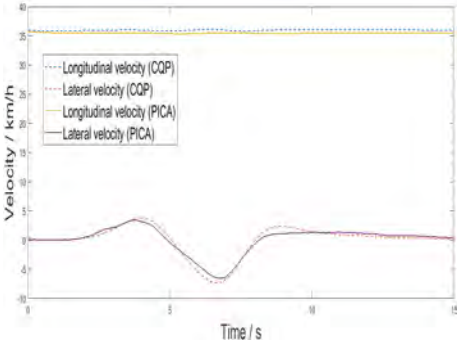

(g) Vehicle velocity

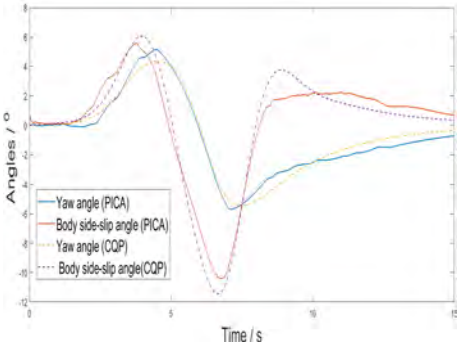

(h) Vehicle stability performance

FIGURE 5.11: Vehicle performances with CA method of CQP and PICA (low-speed driving condition with two-axle steering vehicle)

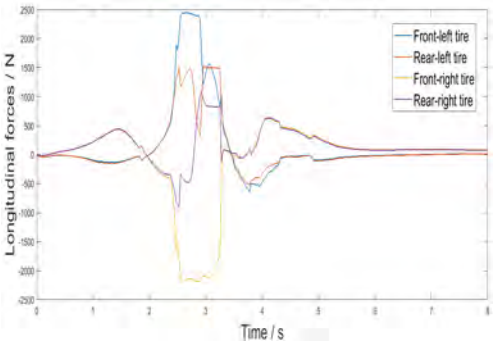

(a) Longitudinal tire forces with CQP

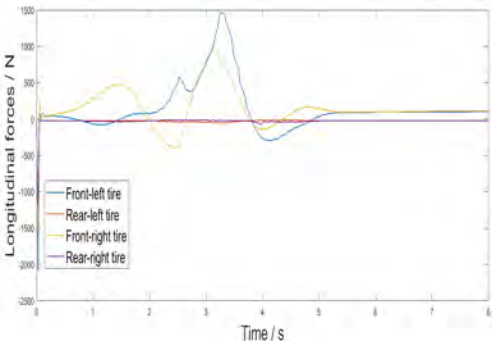

(b) Longitudinal tire forces with PICA

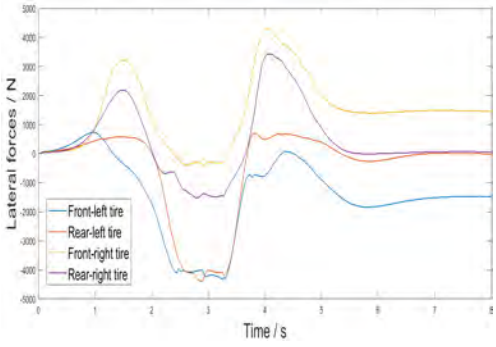

(c) Lateral tire forces with CQP

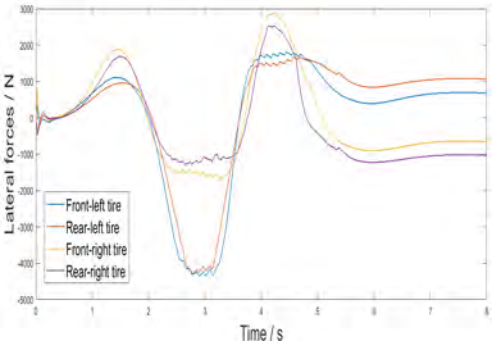

(d) Lateral tire forces with PICA

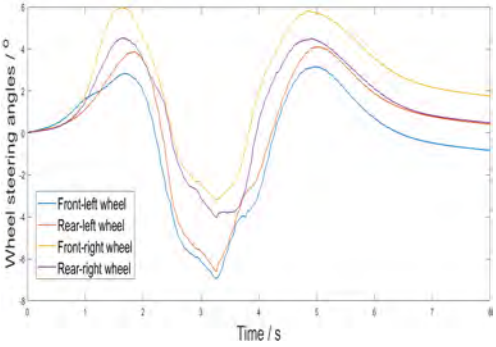

(e) Wheel steering angles with CQP

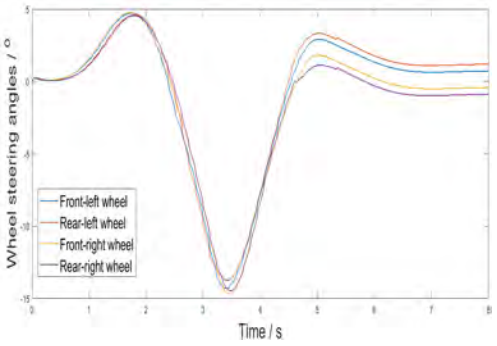

(f) Wheel steering angles with PICA

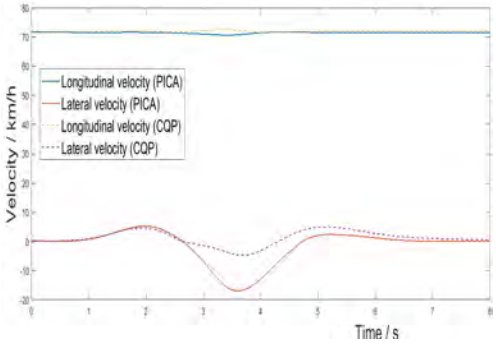

(g) Vehicle velocity

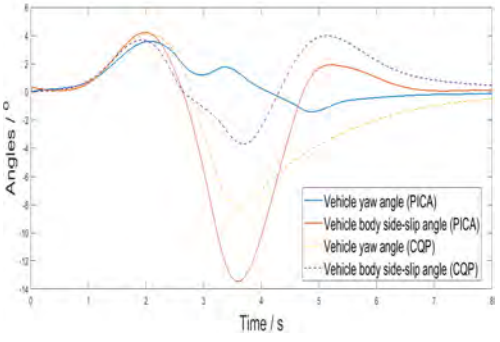

(h) Vehicle stability performance

FIGURE 5.12: Vehicle performances between CA with method CQP and PICA (high-speed driving condition with two-axle steering vehicle)

there exist differences between the wheel steering angles in same axle, which is due to that during the calculation of wheel steering angles, the sideslip angles are obtained by the tire force look-up table via lateral and vertical tire forces (a 3-D look-up table). There exist errors when employing the look-up table obtained from CarSim. In addition, the hard constraint made as equation 5.21 is based on the assumption of constant cornering stiffness in a sampling control time, the accuracy of the online estimation of tire cornering stiffness will also influence the calculation of lateral tire forces, furthermore, it will influence the calculation of wheel steering angles. The vehicle with CQP will show a higher lateral velocity during the driving process, which is due to a larger solution of lateral tire forces, and then lead to a different yaw stability performance, where the yaw angle are bigger with CQP and the body side-slip angle are larger with PICA. This is due to that the PICA will make more use of the steering angle during the running process to complete the DLC, which lead to a larger body side-slip angle.

Note that, from the longitudinal tire force performance in figure 5.12, it is found that during the whole control process, the vehicle use more longitudinal tire forces in front axle than rear axle, which are obtained from the CA process. This might be a result of the control re-allocation (CRA) process when the front axle tire forces firstly exceed the friction limits, then the front axle tire forces might retain a relatively large value (on the friction circle) for the calculation of the remaining tire forces (next calculation loop in CRA).

As shown in figure 5.14, the path performance on traditional vehicle are very close to the two-axle steering vehicle. The results of wheel steering angles also satisfy the mechanical constraint. Although the CA error always exist, it can be limited inside an acceptable range, and the hard constraint CA error for traditional vehicle are also ignorable.

5.5 Summary

This chapter proposes a new approach for the constrained CA based on the pseudo-inverse matrix. Firstly, the hierarchical integrated vehicle control structure is developed to achieve maximum stability margins, CA efficiency and optimal motion control, which is including a high-level controller for the path tracking in normal driving conditions and road departure mitigation under critical situations. Primarily, a novel CA approach based on the pseudo-inverse method is proposed for the force distribution where the relevant path planning and tracking controls are integrated with the optimal CA efficiency control. Taking the traditional CQP method as a benchmark, the simulation results demonstrate that: 1) the vehicle with PICA method can achieve a close performance in normal conditions for path tracking and CA efficiency, in comparison with the CQP

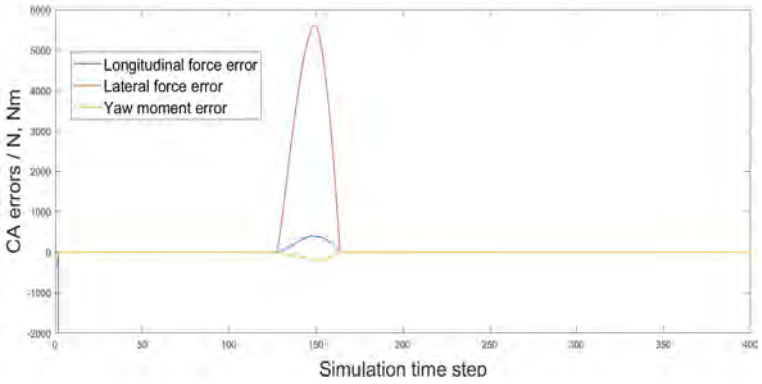

(a) CA error with CQP

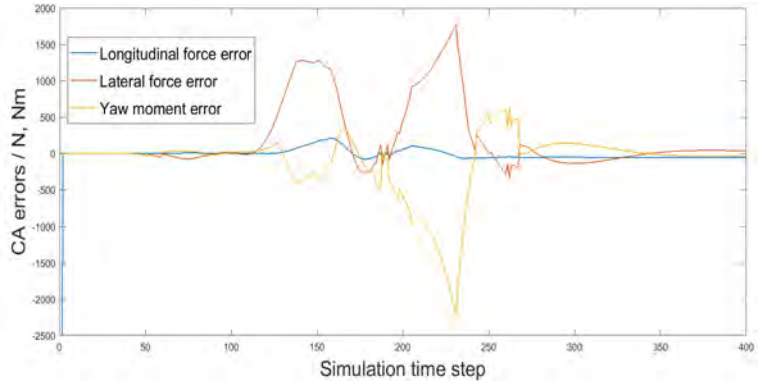

(b) CA error with PICA

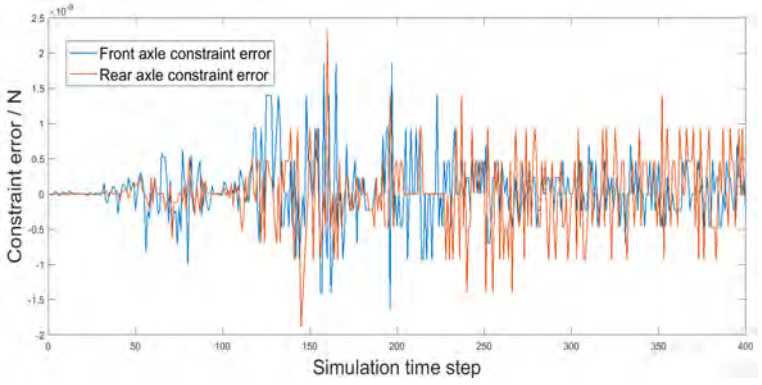

(c) Hard constraint CA error with PICA

FIGURE 5.13: Control allocation errors (high-speed driving condition with two-axle steering vehicle)

method. 2) the vehicle can achieve a better performance in limit conditions for road departure mitigation and CA efficiency, in comparison with the CQP method.

There are two aspects of constraints discussed in this chapter: one is the mechanical constraint which comes from the mechanical connection of tires on one same axle, which is considered as a hard constraint for the CA; another is actuator operational constraints including the tire force magnitude and changing rate limits. Both constraints are crucial in the real vehicle controller but commonly ignored by the simulation assumption or

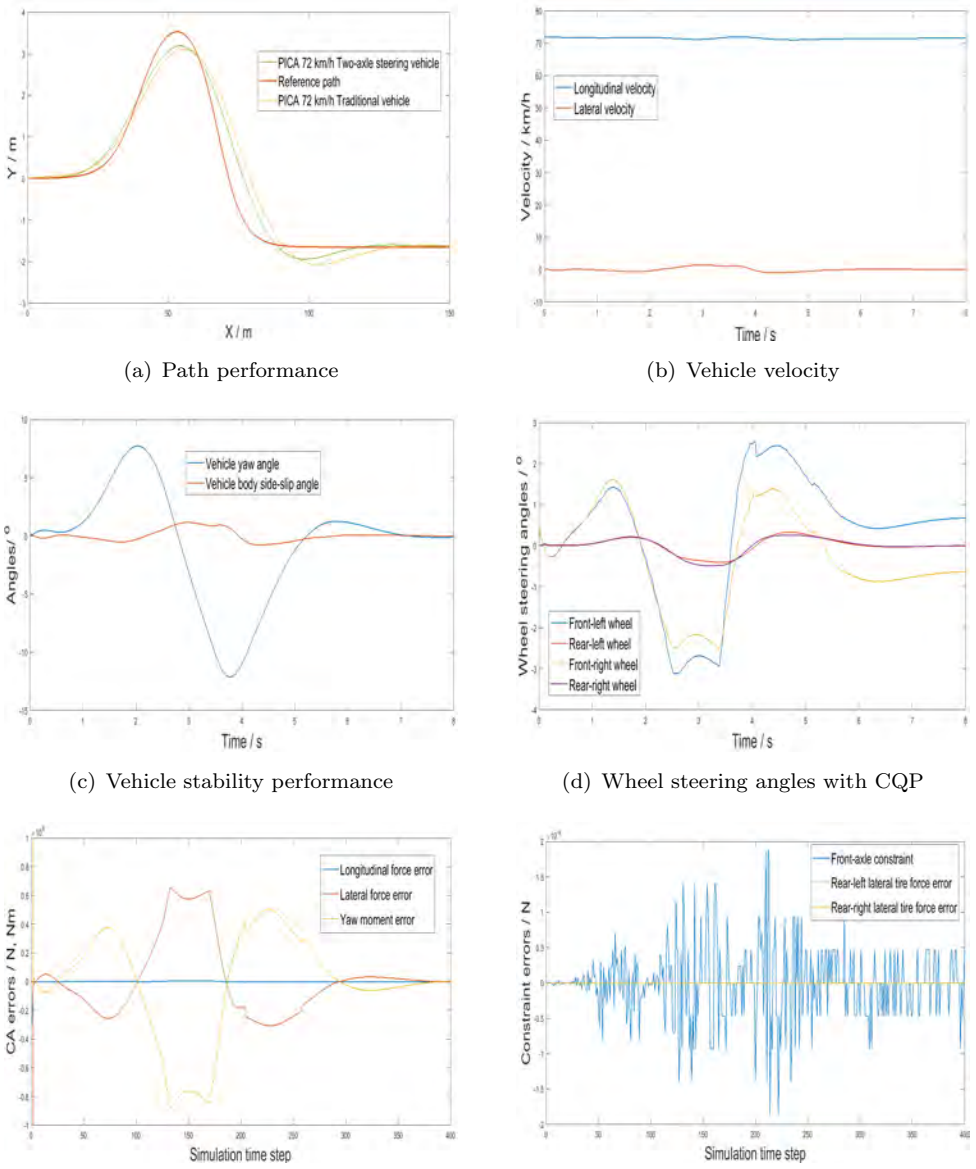

(a) Path performance (b) Vehicle velocity

(c) Vehicle stability performance (d) Wheel steering angles with CQP

(e) CA error (f) CA hard constraint error

FIGURE 5.14: Traditional vehicle performances with PICA (high-speed)

solved by the Quadratic programming method. The pseudo-inverse based CA method has been proved to be efficient for low computation cost, which makes it realistic to be implemented into the real-time controller. Based on pseudo-inverse, this chapter proposes a new method of PICA to deal with this constrained CA problem. Taking CQP method as a benchmark, this chapter compares the two methods with exactly the same upper-level controller and low-level controller. A hierarchical control structure is introduced to close the control loop, which is including the upper-level controller for the path tracking via MPC and low-level controller for the actuator to track the target tire forces. This comparison simulation is conducted via a DLC manoeuver with low-speed and high-speed respectively for the application objects of two-axle steering vehicle and

traditional vehicle.

The simulation results demonstrate that: for the application of two-axle steering vehicle, vehicles with both two CA methods perform similarly; however, the PICA can make less use of tire force efforts and satisfy the hard constraints better. The CQP can also highlight the optimization of minimizing the tire force usage or hard constraints, but the tradeoff between them and the online fitting of weight coefficient are complex; for the application of traditional vehicle, due to the computation characteristics and operating principle of CQP, with additional hard constraints, the vehicle with CA method of CQP can not complete the driving task, because there is no solution of tire forces can be obtained via CQP and delivered to the low-level controller. However, the vehicle with PICA can finish the driving task smoothly and perform very close in comparison with two-axle steering vehicle, which demonstrates that the additional hard constraints have little influence for the CA process with PICA. Besides, the PICA can also account for the actuator operational constraints problem during the whole control process.

As a summary, the proposed PICA mainly shows three advantages in comparison with the CQP method:

1) It can achieve all the aforementioned performance with much less computational cost, which makes it realistic to be implemented into the real-time controller.

2) It can deal with multiple constraints, including mechanical and actuator operational constraints effectively and satisfy the hard constraints better with even less usage of tire forces.

3) With the characteristics of the pseudo-inverse, it can always find a feasible solution for the actuators to track, on the contrary, the CQP method might get stuck and fail to converge, leading to possible system failure.

Chapter 6

Hardware and driver in the loop experimental validation

This chapter provides experimental validation for the proposed MPR and R-MPR control strategy with hardware and driver in the control loop tests. The target of these tests is to validate the proposed control strategy of MPR and R-MPR with the proposed hierarchical control structure, showing that it can be well implemented in the realtime controller and can realize the desired function with hardware and human driver in the control loop.

6.1 Full-scale driving simulator

To introduce driver interactions using a controlled environment, the full-scale driving simulator shown in Figure 6.1 is employed for this experiment. The simulator is located in *Liaoning University of Technology, Jinzhou, China,* where the experiments were carried out with support from the graduated students and research academics in the *School of Automotive and Transportation Engineering.* The simulator has a fixed base and therefore does not represent the vibration environment of the vehicle. However, it otherwise provides a full driving experience with large field of view and high resolution graphics. The driving simulator provides vital information about driver interaction with the proposed control strategy with a large curved screen with 3 individual projectors for road scene visualization, integrated in soft-real-time via CarsimRT. To provide high fidelity steering torque feedback derived from the road friction, the Micro-Autobox from dSPACE is employed to control the force feedback motor via the data obtained from

software CarsimRT. The control algorithm is embedded into the real-time controller-dSPACE MicroAutobox-in Simulink for experiments of closed-loop control, the diagram of the experimental data flow is shown in Figure 6.2.

(a) Side view of driving simulator (b) Rear view of driving simulator

FIGURE 6.1: Full-scale driving simulator

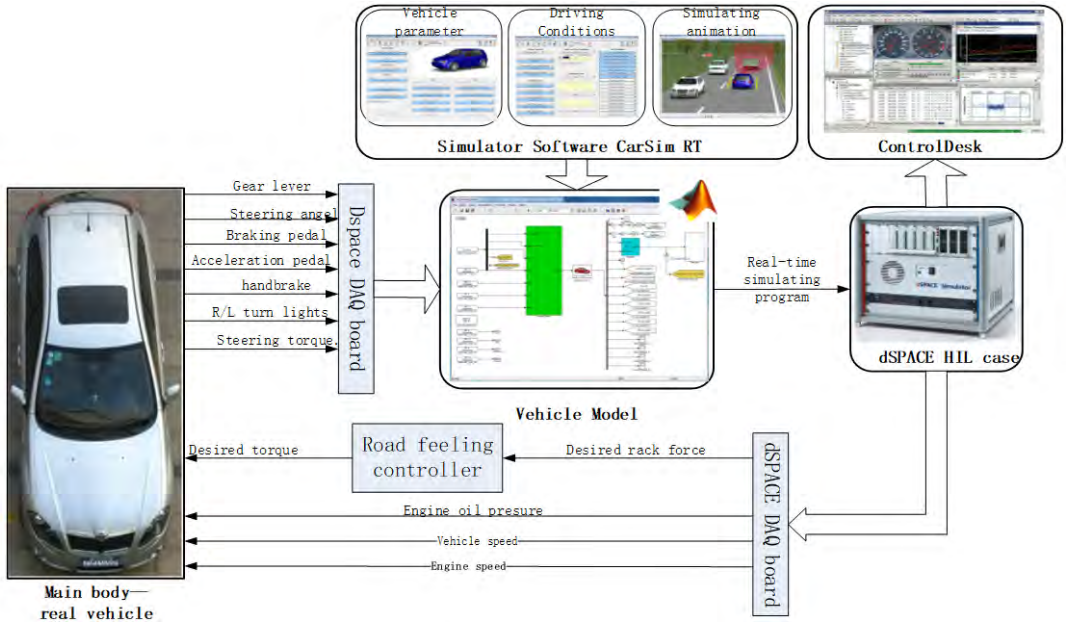

FIGURE 6.2: Diagram of experimental data flow

6.2 Experiments and result analysis

The target of these experiments is to validate that the proposed control strategy of MPR and R-MPR with the proposed hierarchical control structure can be well implemented in the realtime controller and can realize the desired function.

6.2.1 MPR experiment

The experiment is conducted with a designed over-speed cornering driving scenario, with the the initial speed of 140km/h under road condition of $\mu = 1.0$ and $R = 100m$. The proposed hierarchical control system is compiled into the real-time controller-dSPACE Control Autobox. For the control allocation from vehicle level reference accelerations to individual tire forces, the PICA methods introduced in chapter 5 are implemented into the real-time controller. For the experiments, we selected 20 drivers having different driving ages, driving frequency, and driving experiences. Some of the test drivers obtained their driving license within three years and seldom drive, and some of them obtained their driving license for more than 3 years, and even some test drivers drive for a living, such as professional test drivers or full-time drivers. We need to be aware of the fact that all the drivers are generally less likely to encounter extreme limit driving conditions, especially for this over-speed cornering situation. Hence, all the test drivers will have a chance to get used to the driving simulator and also the over-speed cornering driving scenario. The driving scenario was as previously, a straight-line tangent connected to a constant-radius curved road. The driver is initially driving in the straight line with a constant speed of 140km/h, and then the driver will steer the vehicle according to their own driving intention and skill. There exist differences in the drivers' steering timing, and the influence of the different timing has been discussed in previous work [108]. As a short summary, the reasons for the big differences are that human driver can not act as a steering robot, in other words, the driver can not perform the steering operation just at the time when the vehicle exactly reaches the cornering point and during the cornering process the drivers can not strictly steer just the theoretically optimal angle. It can be concluded from [108] that the steering operation start time has a very large influence on the vehicle cornering performance. Generally, the shorter the driver delay, the better cornering performance, though of course the steering action should not take place before the curve is reached.

Because the PPR/MPR intervention is designed to minimize the off-tracking distance, and to emphasize the path lateral deviation performance, all the test drivers were told to try to recover the vehicle back to the intended path as quick as possible, in the meantime minimizing the path lateral deviation. They were not asked to recover the reference curve shown in Figure 6.4 by a series of cones.

Before the experiment, each driver had 10 test drives to get familiar with the driving simulator and also the driving scenario with proposed MPR/R-MPR control system. We then record the vehicle motion data for the 11th driving test as the final results for each driver. Steering wheel angles (the steering ratio i is 18:1) shown in figure 6.3, there is quite a large differences between each driver's steering performance (Note that,

the driver is steering, and that MPR/R-MPR are controlling only braking). To be mentioned, the influence of driving experiences for the driving behavior in this extreme limit driving conditions is ignored in this chapter and will be discussed in the future work. For the MPR experiment, we select 3 typical drivers driving behavior (see figure 6.4) among the 20 drivers for further analysis of the experimental test.

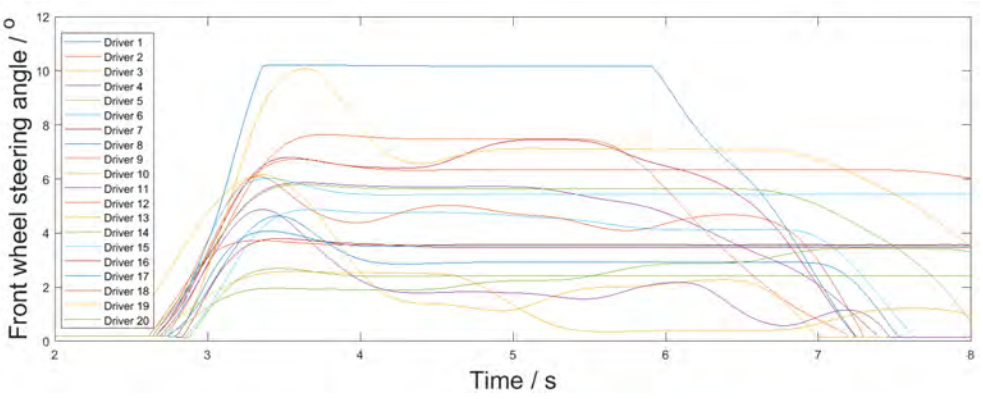

FIGURE 6.3: Test drivers' steering performance

6.2.2 MPR result analysis

Three typical drivers were selected having a range of driving skill and experience to drive with driving simulator in this safety-critical situation. The 3 different drivers' driving behavior and motion performance are shown in the Figure 6.4. It's found that with quicker and larger steering angle inputs, the vehicle will cut back to the intended path faster, which is consistent with the design concept of MPR: from the result of acceleration comparison, more steering angle means a larger demand of lateral acceleration, the larger demand of lateral acceleration will trigger larger vehicle deceleration, and the larger vehicle deceleration will cause less lateral acceleration, according to the MPR mapping concept. Subjectively for the operating driver, he/she will feel more braking and can cut back to the reference path faster if increase the steering wheel angle; inversely, less braking and later cutting in with decreasing steering wheel angle.

In addition, with the comparison between the step steer and driver model response (with MPR) introduced in section 3.3, it can be found that, because of the step-steer's near-instantaneous response, it can achieve a better overall performance than the driver model, which also demonstrates that the vehicle control performance is interacted with the steering behavior, in correspondence with the human drivers performance shown in Figure 6.4. However, for the driver-in-the-loop MPR controller, the system also performs well and can always keep the human drivers in the control loop in this challenging scenario. This maneuverability is remarkable, given the variability of the individual drivers with different driving styles, experience and skills.

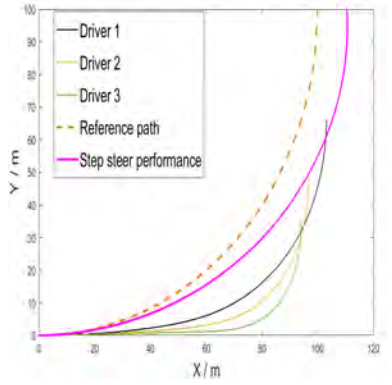

(a) Vehicle motion performance with driver in the loop

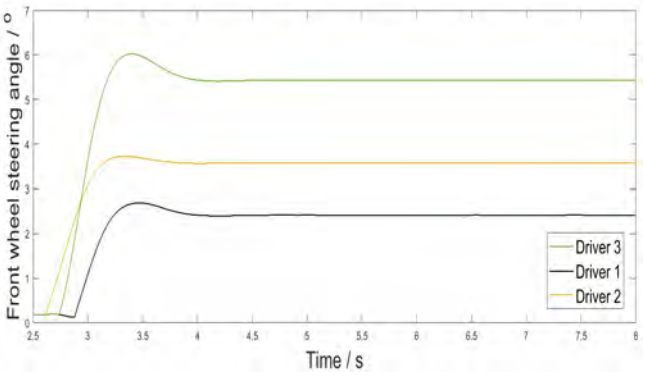

(b) Driver steering behaviors

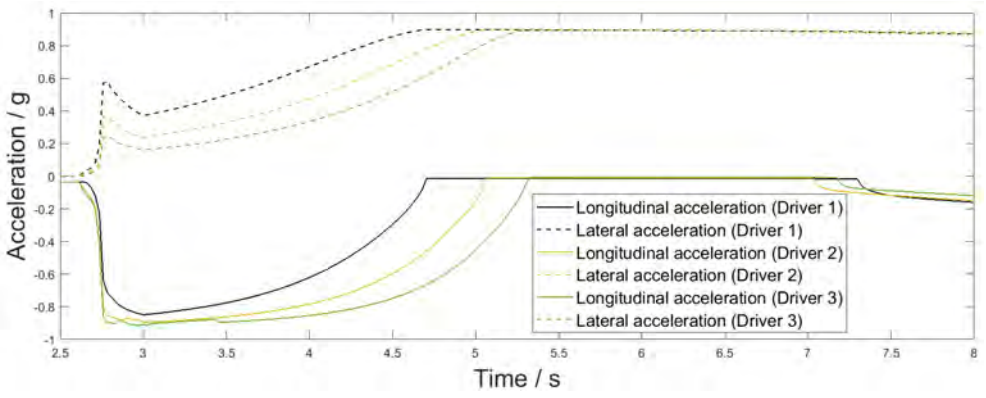

(c) Acceleration performance

FIGURE 6.4: MPR simulation with driving simulator

6.2.3 R-MPR experiment

The R-MPR experiments is also conducted with a designed over-speed cornering driving scenario, with the the initial speed of 140km/h under road condition of $\mu = 1.0$ and $R = 100m$. The proposed hierarchical control system is compiled into the real-time controller-dSPACE Control Autobox. For the control allocation from vehicle level reference accelerations to individual tire forces, the PICA methods introduced in chapter 5 are again implemented into the real-time controller. In the fixed based driving simulator, actually the human driver can not feel the roll angle inside the fixed cockpit. It is assumed that the roll feeling inside the vehicle has little influence on the driver steering behavior, accordingly, it is considered that there is little difference of driving behavior between with the MPR and R-MPR for one tester. Hence, we also select the same 3 test drivers as the MPR experiment, their steering performance is shown in Figure 6.5. The driving scenario again consists of a straight-line tangent connected to a constant-radius curved road. The 3 drivers are initially driving in the straight line with a constant speed of 140km/h, and then the driver will steer the vehicle according to their own driving intention and skill. Note that, the same as the MPR experiment, all the 3 test drivers

were told to try to recover the vehicle back to the intended path as quick as possible. From section 4.2.3, the lateral acceleration limit inside R-MPR control strategy is obtained based on the vehicle's constant lateral acceleration, hence, the 3 test drivers are instructed not to sharply reverse the steering wheel (in case of causing a large reverse lateral acceleration).

6.2.4 R-MPR result analysis

It's found that with quicker and larger steering angle inputs, the vehicle will again cut back to the intended path faster, which is in harmony with the design concept of R-MPR: from the result of acceleration comparison, more steering angle means a larger demand of lateral acceleration, the larger demand of lateral acceleration will trigger larger vehicle deceleration, and the larger vehicle deceleration will cause less lateral acceleration, according to the R-MPR mapping concept. To be mentioned that, the lateral acceleration limit of the test vehicle in this driving conditions are pre-calculated as $0.6g$. It is found from the acceleration performance that, the vehicle can be stable just at the limit lateral acceleration (the minor error comes from the air resistance), when the vehicle speed is constant (zero longitudinal acceleration). Subjectively for the operating driver, he/she will feel more braking and can cut back to the reference path faster if increase the steering wheel angle; inversely, less braking and later cutting in with decreasing steering wheel angle.

In addition, with the comparison between the step-steer and driver inputs, it can be found that, because of the step-steer's near-instantaneous response, it can achieves a better overall performance than the human driver. However, for the driver-in-the-loop R-MPR controller, the system also performs well and can always keep the human drivers in the control loop in this challenging scenario. Compared to driver model simulation, the inclusion of different human drivers has quite systematic effect on the results. Importantly, the different driver steering inputs are seen to give different vehicle responses and the trade-off between longitudinal and lateral accelerations is clear.

As a short summary, based on the proposed experimental simulations, it is found that the proposed hierarchical control structure with the PICA method can obtain desired performance and dominate near and even over the limits of friction. Hence it can be widely applied in the real-time vehicle control applications. The upper-level control strategies, MPR and R-MPR, which are both benefitted from the efficient hierarchical control structure, can well achieve their designed functions with the real-time controller, in consistency with the conclusion obtained via the simulation tests.

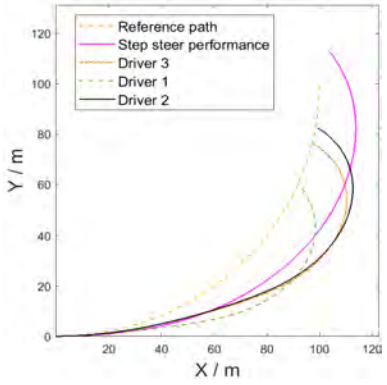

(a) Vehicle motion performance with driver in the loop

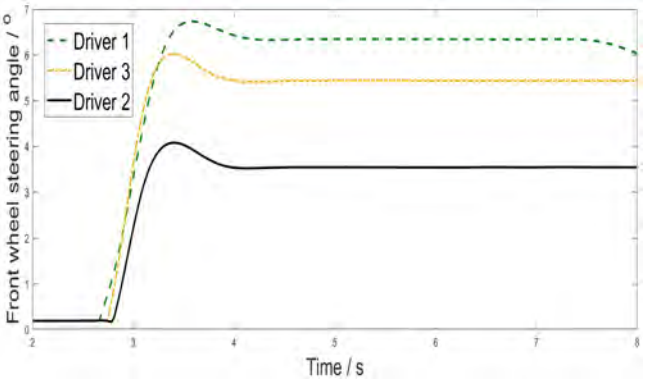

(b) Driver steering behaviors

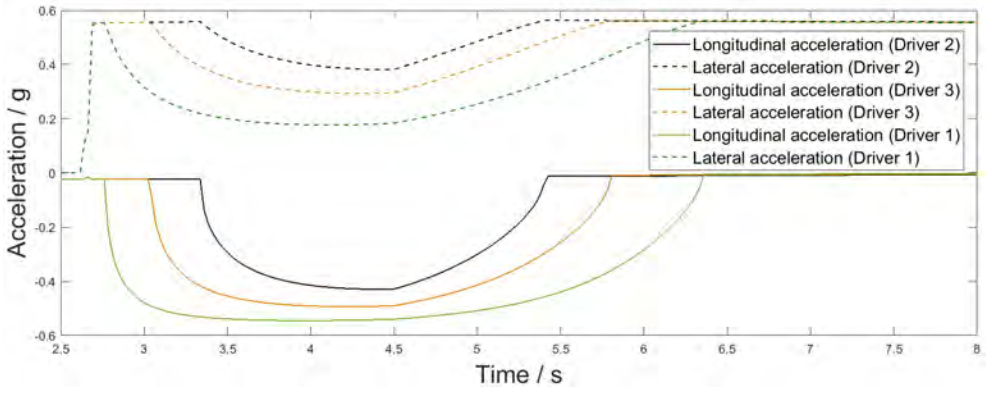

(c) Acceleration performance

FIGURE 6.5: R-MPR simulation with driving simulator

6.3 Summary

The driving simulator tests demonstrate the proposed MPR and R-MPR control strategies and PICA method can be effectively implemented in real-time control applications while preserving the control interaction of the driver. On a macro level, this proposed MPR and R-MPR methods maintain the driver's drivability in this critical situation as well as take full use of road friction. In this over-speed curving situation, with the MPR and R-MPR as the driver assistance system, the driver will experience increased braking in proportion to subsequent increases in steering wheel angle. Thus the proposed methods emphasize keeping the 'driver-in-the-loop' during the brake intervention, unlike more discrete methods which override the driver though full brake application for example. In particular, the proposed PICA can fully satisfy the real-time computing requirement, which provides reliable basis for this kind of onboard control applications.

Chapter 7

Conclusion and Future Work

This chapter summarizes the research presented in this dissertation and outlines potential future work based on the research presented.

7.1 Summary and Conclusion

A hierarchical vehicle dynamics control system, with three control layers, has been proposed. The control system is mostly applicable to vehicles with "over-actuated" chassis systems, where the number of independent actuator modes is more than three (the number of degrees of freedom under control: longitudinal, lateral and yaw). The upper-level controller is designed to cover both dynamic (linear region), limit and even beyond the limit (nonlinear region) tire control domains. Specifically, the MPC control strategy is employed as an optimal path tracking controller under normal driving conditions (dynamic control domains); a PPR based control strategy-MPR and R-MPR are proposed as fully autonomous and driver assistance understeer mitigation controller under limited and over-limited driving conditions (at and beyond tire control limit). Sliding mode control is also adopted for the upper-level vehicle motion controller, to provide the generalized forces/moment, then distributed to longitudinal and lateral forces of each wheel by control allocation. In the bottom layer of control allocation (CA), two particular CA methods, constrained quadratic programming and pseudo-inverse, are introduced in detail. Based on the current progress of the two CA methods, a novel CA method based on the pseudo-inverse matrix (PICA) is proposed. The results demonstrate that PICA can be a potential CA method for the real vehicle controller and show significant advantages in comparison with the current CA progress. Finally, tire slip ratio can be controlled by a lower-level controller to track the desired slip ratio, though for limit conditions, errors

in tyre model inversion seem to favour a simpler type of 'static' force-based actuator control.

In particular, this dissertation introduces a systematic method for moderating driver or system demands so that an integrated chassis and driveline control system can operate in a predictable manner within available friction constraints even when driver demands exceed the available friction limits. It is easy to saturate the driver demands, but not so easy to maintain a predictable dynamic. The methodology is applied to a highly actuated vehicle: individual four-wheel steering and independent driveline/braking torque, however, based on imposing actuator constraints and uncontrolled axle sets, the conclusions appear general, provided the over-actuated condition is met. Demands from a driver interpreter are fed into the new moderator, based on the dynamics of a friction-limited particle, the result being a moderated particle reference (MPR). MPR is derived from a previously published Parabolic Particle Reference (PPR), based on optimal control theory. The moderated particle reference (MPR) model has been validated to ensure predictable and stable operation near the friction limits, maintaining controllability for curvature and speed tracking. Evaluation of the overall system is accomplished by simulation testing with a driver model and driving simulator under vehicle over-speed cornering conditions. The MPR strategy effectively limits demands on the vehicle and achieve a similar performance to the fully autonomous control with PPR for road departure mitigation, while preserving the control interaction of the driver, which is in contrast to the simple yaw rate based controller, like ESC. The moderator also ensures that reference demands are feasible and hence tire model inversion and control allocation can be precisely implemented.

Based on the proposed MPR, taking the rollover prevention control into consideration, this dissertation introduce a novel technique, R-MPR, for transforming driver commands into chassis control signals in the context of rollover prevention when a vehicle with a high mass center is driven at high speed on a curved road. R-MPR is proposed to satisfy the need to address issues such as un-tripped and tripped rollover, the trade-off between path following and rollover prevention, and also need for a seamless transition between keeping the driver in the control loop and allowing an electronic safety system to make a fully autonomous intervention. The R-MPR concept, which is a natural extension from MPR but with more stringent limitations on path-lateral acceleration, includes two separate functions: overriding the driver and deploying fully autonomous braking based on the vehicle states and the road geometry; and applying a driver interpreter (DI) and control moderation to avoid excessive lateral acceleration while keeping the driver fully in the control loop. The aim is to establish best-case methods for autonomous and driver-adaptive interventions based on different road conditions. It was shown that the proposed two approaches can be used synergetically and efficiently to solve this problem.

To ensure the real-time computing requirement of the onboard vehicle controller, this dissertation proposes a new approach for the constrained CA based on the pseudo-inverse matrix. Taking the most traditional CA method-CQP as a benchmark, the new proposed PICA method shows clear advantages:

1) It can achieve all the vehicle CA performance including dealing with tire friction limits and achieving CA efficiency, with much less computational cost, which makes it realistic to be implemented into the real-time controller.

2) One of the more serious challenges for pseudo-inverse methods is the inclusion of hard constraints. In this dissertation, the proposed PICA method can deal with multiple constraints including mechanical and actuator constraints effectively and satisfy the hard constraints better with even less usage of tire forces than the benchmark CQP method.

3)With the characteristics of the pseudo-inverse, it can always find a feasible solution for the actuators to track, in contrast to the CQP which might get stuck in some specific conditions, which can lead to system failure. Based on these, it is validated that the proposed PICA method can obtain desired CA performance and perform both inside and near the limits of friction. Hence it can be widely applied in the real-time vehicle control applications.

As a summary, this dissertation proposes a systematic method for moderating driver or system demands so that an integrated chassis and driveline control system can operate in a predictable manner. The moderated particle reference (MPR) model has been validated via the simulation with the driver model and in driving simulator tests with human drivers in the control loop. The results demonstrate that it can ensure predictable and stable operation near the friction limits, maintaining controllability for curvature and speed tracking; and R-MPR is validated via the simulation test to well satisfy the need to address issues such as un-tripped and tripped rollover, the trade-off being between path following and rollover prevention, and also need for a seamless transition between keeping the driver in the control loop and allowing an electronic safety system to make a fully autonomous intervention. To ensure the proposed control method can be well implemented into the real-time controller, this dissertation also proposes a novel CA approach based on the pseudo-inverse matrix. This PICA method shows great advantages and it is proved to obtain desired CA performance and perform both inside and near the limits of friction. The hardware and driver in the loop driving simulator test results well confirm the approach.

7.2 Future Work

7.2.1 MPR/R-MPR improvement based on Driver identification

The work presented in this dissertation is directed towards increasing the functionality of ADAS systems. The current benchmark for ADAS is ESC, which is designed by setting up a stable risk standard: when the vehicle running state exceeds a preset standard, the active controller will be triggered to intervene into driver operation to secure the vehicle safety. Generally, the ESC system will monitor the vehicle side slip angle and yaw rate in real-time, and if these values exceed the preset limitation, the controller will automatically be triggered to decrease the value to a safe range. There are also some other ADAS which will intervene into driver operation, like Lane Keeping Assistance System (LKAS) [109][110][111]and Rollover Prevention System (RPS)[93]. However, whether this kind of indiscriminate interference will be acceptable and necessary to all kinds of drivers is still unclear. This kind of ADAS is currently playing a positive role for the aspect of driving safety, but its intervention into driver operation might have a negative influence on the vehicle's drivability and maneuverability, especially for some 'skilled' drivers who might have the ability to handle some of the 'emergency' cases by themselves.

Based on the development idea of MPR/R-MPR, these provide a new developing concept for the ADAS engineer. The MPR strategy can effectively limit demands on the vehicle while preserving the control interaction of the driver, which is in contrast to the simple yaw rate based controller, like ESC. This design concept without indiscriminate interference into driver operation is potentially more acceptable for drivers. However, the indiscriminate 'assistance' from MPR/R-MPR still seems not sufficiently intelligent and 'driver-adaptive'.

Hence the further development of MPR/R-MPR system can include the online driving behavior identification. That is, the different individual's driving characteristics including driving skill, driving habit and driver state can be considered specifically from the initial stage of system development. Research on the driving behavior identification has been mainly focus on the driving characteristics, Zong et al. [33][112] built ideal characteristics reference model based on identification and classification of the driver characteristics, where different drivers were matched with different vehicle reference models for the vehicle to achieve an optimal performance. This kind of research is aimed at the optimal design on dynamic performance of the closed-loop system, which might reduce the vehicles drivability and driver's driving experiences. If the MPR and R-MPR system can be improved based on the online driver identification, then the intervention sensitivity for MPR/R-MPR triggering time can be separately designed based on the

results of driver identification. Then it may not only preserve the control interaction of the drivers, but also adapt the system to individual's driving characteristics. Hence, upgrading the current MPR/R-MPR system based on the online driving behavior identification shows the potential of making the ADAS more intelligent and adaptive to individuals.

7.2.2 MPR/R-MPR application with adaptive road friction moderator

The proposed systematic approach including MPR/R-MPR and PICA are all based on the exact estimation of current road friction level. However, errors in estimation of the friction coefficient will make a great influence on the control effect. In addition, the nonlinear vehicle system discussed in this dissertation is comprised of longitudinal, lateral and yaw motion. Longitudinal and lateral motions are taken into consideration in MPR strategy, which is proposed on the assumption that yaw motion can be ensured during the dynamic process. But under a very serious situation with a very large steering amplitude, yaw rate may not be capable of tracking the desired value very well due to the sharp changing of the front wheel steering angle and which may lead to vehicle sideslip angle being too large to secure the vehicle safety. Hence, an adaptive $\mu - moderator$ needs to be developed to guarantee the stable vehicle performance under conditions of unprecise estimation of road friction level and critical condition on the basis of MPR/R-MPR strategy.

The goal of the adaptive μ-moderator is to decrease the speed of the vehicle to tighten the radius of curvature and to offer the driver enough safety margins to face unpredictable situations. It consists in automatically initiating deceleration, as soon as the steering command exceeds a threshold (circle 1 on figure 7.1). If the steering command exceeds a second threshold (circle 2 on figure 7.1), yaw rate may be temporarily limited, braking being optimized to carry out the best compromise between turning and speed decreasing. The applied deceleration automatically tightens the turn up to the desired value.

In order to ensure the longitudinal, lateral and yaw motion, the adhesion between road and tire should theoretically include three parts, $\mu = \mu_{ax} + \mu_{ay} + \mu_r$, and three parts coordinately guarantee the longitudinal, lateral and yaw motion. In the adaptive μ-moderator, three zones are defined: the dotted zone, the "vertically lined" zone and the "horizontally lined" zone shown in figure 7.1.

Each part has their own responsibility, μ_1 for longitudinal and lateral acceleration (the dotted zone in figure 7.1), $\mu_r = \mu_2 - \mu_l$ for yaw motion and sideslip angle, and the safety margins $\Delta\mu$ for unpredictable emergency situation. The dotted zone appears when vehicle resultant acceleration is less than $\mu_l mg$. That means the magnitude of the

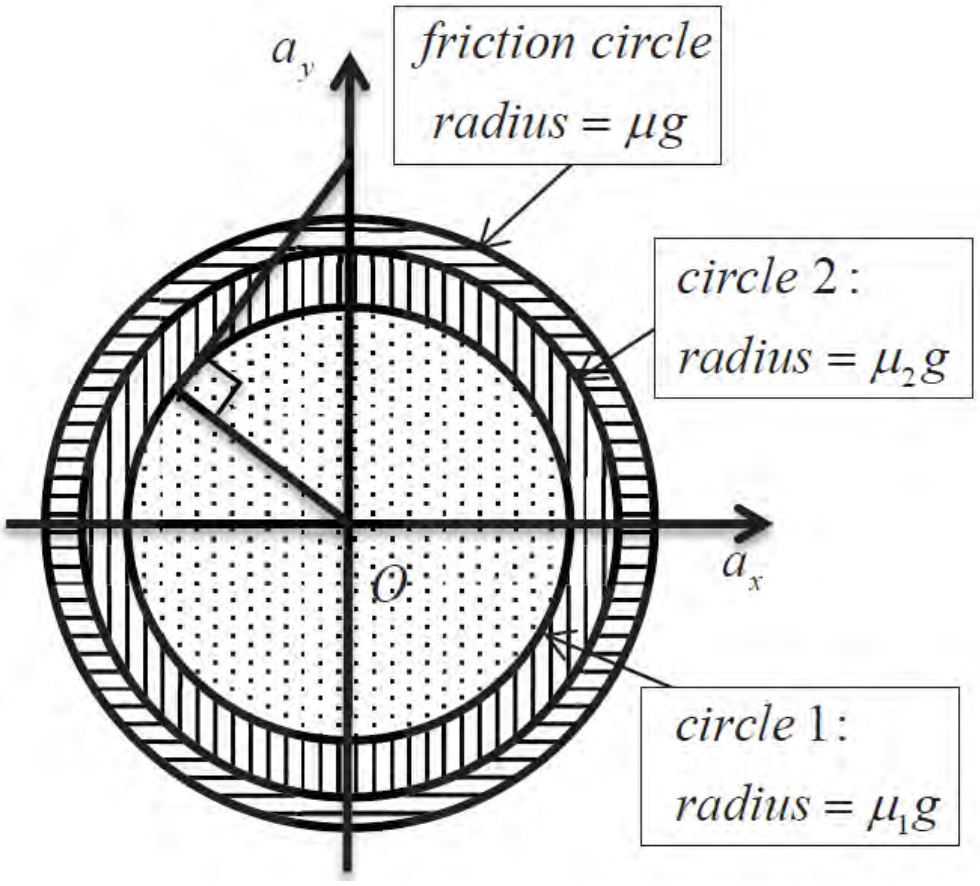

FIGURE 7.1: Adaptive μ-moderator

resultant force implemented in MPR strategy is $\mu_l mg$ instead of μmg. Theoretically, the larger the μ_r is, the smaller the error between the actual and desired yaw rate would be and the smaller vehicle sideslip angle would be. But if $\Delta\mu$ is fixed, the more friction in the "vertical line" zone, the less will be remain in dotted zone, then longitudinal and lateral motion will be more restricted. The adaptive μ-moderator is a tradeoff between vehicle resultant acceleration and yaw stability. The design and evaluation of the adaptive μ-moderator for the real vehicle application will be of much interest as a further topic.

7.2.3 Fault-tolerant control with PICA

While the focus of the dissertation has been on advanced ADAS systems, using control to assist the driver, future development can also apply to autonomous driving. Autonomous driving cars can realize advanced environment recognition, intelligent decision-making and coordinated control with its onboard sensors, controllers and actuators. However, failure of autonomous system would lead to performance reduction and dangerous accidents due to its complex system. A fault-tolerant control (FTC) approach is adopted

in the integrated chassis controller for autonomous driving vehicle to keep its safety and stability when the actuators failure occurs. The existing FTC utilizes a controlling principle that pre-sets a corresponding allocation control law for different fault forms[113][114][115][116]. Nevertheless, current research still has many weaknesses, such as the inability to apply to different types of actuator failures, including driving motor and steering motor failures. Furthermore, research on the combination of the actuators failure and tire blow out remains a blank field. Considering that the actuator failure has many kinds of characteristics, such as susceptibility, the FTC should handle various types of real-time actuator failure and has high-grade performance in path tracking and stability maintenance. When an actuator failure occurs, the tire force of the faulty actuator would be estimated via online state estimator, and then the PICA method can be employed to decouple the forces and moment according to the current states of the tires.

Appendix A

Vehicle Parameters for Simulation

A.1 List of Vehicle Parameters for Simulation (Passenger car)

TABLE A.1: Vehicle (B-class passenger car) simulation parameters in CarSim

vehicle body mass	m	1843 kg
Sprung mass	m_s	1723 kg
Unsprung mass	m_u	120 kg
mass center height	h_s	0.54m
vehicle body roll inertia	I_{xx}	$440.6kgm^2$
vehicle body pitch inertia	I_{yy}	$1343.1kgm^2$
vehicle body yaw inertia	I_{zz}	$4175kgm^2$
distance (CoG to front axle)	l_1	1.232m
distance (CoG to rear axle)	l_2	1.468m
track width	b	1.85m
Gravitational constant	g	$9.8m/sec^2$

A.2 List of Vehicle Parameters for Simulation (SUV with High CoG)

TABLE A.2: Vehicle (SUV) simulation parameters in CarSim

vehicle body mass	m	3507 kg
vehicle sprung mass	m_s	3257 kg
Unsprung mass	m_u	250 kg
vehicle body yaw inertia	I_{zz}	$3524.9kgm^2$
vehicle body roll inertia	I_{xx}	$846.6kgm^2$
distance (CoG to front axle)	l_1	1.33m
distance (CoG to rear axle)	l_2	1.81m
track width	b	2.029m
Height of sprung mass	h_s	0.781m
Effective roll stiffness	K_ϕ	Figure 4.4
Gravitational constant	g	$9.8m/sec^2$

Appendix B

Theoretical Formulation of PICA

The target is to find a pseudo-inverse based control allocation (PICA) solution that fully satisfies any hard constraints and meanwhile satisfies the control target (which is described as $Bu = V$ in chapter 5) as much as possible. Assuming that:

$$\widetilde{B} = \begin{bmatrix} B_1 \\ B_2 \end{bmatrix}, \widetilde{V} = \begin{bmatrix} V_1 \\ V_2 \end{bmatrix}, \tag{B.1}$$

where the $B_1 u_1 = V_1$ is set to be the control target, and the $B_2 u_2 = V_2$ is set to be the hard constraint. Even though the hard constraints can be satisfied, the conventional use of pseudo-inverse does not properly address the problem.

Here, a combined method is proposed to solve this problem.

First apply the the Singular Value Decomposition (SVD) to B_1 and B_2:

$$\mathbf{B}_i = \mathbf{U_i S_i W_i}^T \tag{B.2}$$

where $\mathbf{B}_i \in \mathbb{R}^{q_i \times n}$, $\mathbf{U}_i \in \mathbb{R}^{q_i \times q_i}$, $\mathbf{S}_i \in \mathbb{R}^{q_i \times n}$ and $\mathbf{W}_i \in \mathbb{R}^{n \times n}$, with $q = q_1 + q_2$ and $q < n$. The U_i and W_i denote orthogonal matrices, i.e. $\mathbf{W_i}^T \mathbf{W_i} = \mathbf{I}$ and $\mathbf{U_i}^T \mathbf{U_i} = \mathbf{I}$ [117], and $\mathbf{S}_i$ can be expressed as:

$$\mathbf{S}_i = \begin{bmatrix} S_1 & 0 & 0 & ... & 0 \\ 0 & S_2 & 0 & ... & 0 \\ 0 & 0 & S_3 & ... & 0 \\ ... & ... & ... & ... & ... \\ 0 & 0 & ... & S_{q_i} & 0 \end{bmatrix} \tag{B.3}$$

then we can obtain that:

$$\mathbf{B}_i^{\sharp} = \mathbf{W_i S_i}^{-T} \mathbf{U_i}^T \tag{B.4}$$

where $\mathbf{S_i}^{-T} = \begin{bmatrix} S_1^{-1} & 0 & 0 & ... & 0 \\ 0 & S_2^{-1} & 0 & ... & 0 \\ 0 & 0 & S_3^{-1} & ... & 0 \\ 0 & 0 & 0 & ... & S_{q_i}^{-1} \\ 0 & 0 & 0 & 0 & 0 \end{bmatrix}$

and $\mathbf{S_i S_i}^{-T} = \mathbf{I}$

Define the projection operator:

$$\mathbf{P} = \mathbf{I} - \mathbf{W_2 W_2}^T \tag{B.5}$$

where the $\mathbf{I}$ is an unit matrix, the $\mathbf{W_2}$ is obtained from Equation B.2 and $\mathbf{P}$ projects onto the null space of $\mathbf{B_2}$, which means for any $n \times 1$ vector $\mathbf{u}$, the projection $\mathbf{V} = \mathbf{Pu}$ will satisfy $\mathbf{B_2 V} = \mathbf{0}$.

Now we propose a solution:

$$\widetilde{u} = \tilde{u_2} + \mathbf{PM} \tag{B.6}$$

where

$$\mathbf{M} = (B_1 \mathbf{P})^\sharp (V_1 - B_1 \tilde{u_2}) \tag{B.7}$$

where $\tilde{u_2} = B_2^\sharp V_2$. To verify the hard constraint:

$$\begin{aligned} B_2 \widetilde{u} &= B_2 \tilde{u_2} + B_2 \mathbf{PM} \\ &= B_2 B_2^\sharp V_2 + \mathbf{0} \\ &= \mathbf{U_2 S_2 W_2}^T \mathbf{W_2 S_2}^{-T} \mathbf{U_2}^T V_2 \\ &= \mathbf{I} V_2 \\ &= V_2 \end{aligned} \tag{B.8}$$

Hence, this solution $\widetilde{u}$ can absolutely satisfy the hard constraint of $B_2 \widetilde{u} = V_2$, and in the meantime it take the control target of $B_1 \widetilde{u} = V_1$ into consideration and minimize the CA error of control target $B_1 \widetilde{u} - V_1$ as much as possible.

Taking a random numerical example:

$$B = \begin{bmatrix} 0.1869 & 0.7094 & 0.6551 & 0.9597 & 0.7513 \\ 0.4898 & 0.7547 & 0.1626 & 0.3404 & 0.2551 \\ 0.4456 & 0.2760 & 0.1190 & 0.5853 & 0.5060 \\ 0.1869 & 0.7094 & 0.6551 & 0.9597 & 0.7513 \\ 0.4898 & 0.7547 & 0.1626 & 0.3404 & 0.2551 \end{bmatrix} \text{ and } V = [1, 2, 3, 4, 5]^T.$$

Assuming

$$B = \begin{bmatrix} B_1 \\ B_2 \end{bmatrix}, V = \begin{bmatrix} V_1 \\ V_2 \end{bmatrix}, \tag{B.9}$$

where the B_1 is the first three rows of B and the $B_1 u_1 = V_1$ is set to be the control target, the B_2 is the last two rows of B and $B_2 u_2 = V_2$ is set to be the hard constraint.

Firstly, we try to emphasize the hard constraint $B_2 u_2 = V_2$ via a weighting coefficient of 10^4, then the new matrix is:

$$\tilde{B} = \begin{bmatrix} 0.1869 & 0.7094 & 0.6551 & 0.9597 & 0.7513 \\ 0.4898 & 0.7547 & 0.1626 & 0.3404 & 0.2551 \\ 0.4456 & 0.2760 & 0.1190 & 0.5853 & 0.5060 \\ 1869 & 7094 & 6551 & 9597 & 7513 \\ 4898 & 7547 & 1626 & 3404 & 2551 \end{bmatrix} \text{ and } \tilde{V} = [1, 2, 3, 40000, 50000]^T.$$

Then we compare the CA errors $e = Bu - V$ with different methods.

Firstly, we solve this problem directly via the pseudo-inverse operator $u = B^{\sharp} V$, then the error of e_1 can be obtained as:

$e_1 = [1.5, 1.5, 0, -1.5, -1.5]^T$.

Then, we solve this problem via the weighted pseudo-inverse operator $\tilde{u} = \tilde{B}^{\sharp} \tilde{V}$, and then the error of e_2 can be obtained as:

$e_2 = [3, 3, 0, -0.0003, -0.0003]^T$.

We employ the same matrix and apply the proposed PICA method, then the result of error e_3 can be obtained as:

$e_3 = [3, 3, 0, 0, 0]^T$.

which completely satisfy the hard constraint $B_2 u_2 = V_2$.

Bibliography

[1] ParkIT. Self driving cars: Will they improve parking solutions? *Industry News*, 2017.

[2] Miltos Kyriakidis, Carlo van de Weijer, Bart van Arem, and Riender Happee. The deployment of advanced driver assistance systems in europe. *Available at SSRN 2559034*, 2015.

[3] Pan Song, Masayoshi Tomizuka, and Changfu Zong. A novel integrated chassis controller for full drive-by-wire vehicles. *Vehicle System Dynamics*, 53(2):215–236, 2015.

[4] Kristin Houser. Many self-driving car accidents have been caused by humans. *Business Insider*, 2018.

[5] Adnan Shaout, Dominic Colella, and S.s Awad. Advanced driver assistance systems - past, present and future. *Proc. 7th Int. Computer Engineering Conf*, 12 2011. doi: 10.1109/ICENCO.2011.6153935.

[6] Feng Gao, Shengbo Eben Li, Yang Zheng, and Dongsuk Kum. Robust control of heterogeneous vehicular platoon with uncertain dynamics and communication delay. *IET Intelligent Transport Systems*, 10(7):503–513, 2016.

[7] Steven E Shladover. Longitudinal control of automotive vehicles in close-formation platoons. *Journal of dynamic systems, measurement, and control*, 113(2):231–241, 1991.

[8] Roozbeh Kianfar, Bruno Augusto, Alireza Ebadighajari, Usman Hakeem, Josef Nilsson, Ali Raza, Reza S Tabar, Naga VishnuKanth Irukulapati, Cristofer Englund, Paolo Falcone, et al. Design and experimental validation of a cooperative driving system in the grand cooperative driving challenge. *IEEE transactions on intelligent transportation systems*, 13(3):994–1007, 2012.

[9] Tom Robinson, Eric Chan, and Erik Coelingh. Operating platoons on public motorways: An introduction to the sartre platooning programme. In *17th world congress on intelligent transport systems*, volume 1, page 12, 2010.

[10] Sadayuki Tsugawa, Shin Kato, and Keiji Aoki. An automated truck platoon for energy saving. In *2011 IEEE/RSJ International Conference on Intelligent Robots and Systems*, pages 4109–4114. IEEE, 2011.

[11] Riccardo Scattolini. Architectures for distributed and hierarchical model predictive control–a review. *Journal of process control*, 19(5):723–731, 2009.

[12] Mihajlo D Mesarovic, Donald Macko, and Yasuhiko Takahara. *Theory of hierarchical, multilevel, systems*, volume 68. Elsevier, 2000.

[13] Chang-Fu Zong, Gang Li, Hong-Yu Zheng, Lei He, and Ze-Xing Zhang. Study progress and outlook of chassis control technology for x-by-wire automobile. *Zhongguo Gonglu Xuebao(China Journal of Highway and Transport)*, 26(2):160–176, 2013.

[14] Walter Brenner and Andreas Herrmann. An overview of technology, benefits and impact of automated and autonomous driving on the automotive industry. In *Digital Marketplaces Unleashed*, pages 427–442. Springer, 2018.

[15] Nidhi Kalra and Susan M Paddock. Driving to safety: How many miles of driving would it take to demonstrate autonomous vehicle reliability? *Transportation Research Part A: Policy and Practice*, 94:182–193, 2016.

[16] Jack Creasey. On the road to autonomous driving - are we there yet? In *www.2025ad.com*. January 31, 2019.

[17] Daniel J Fagnant and Kara Kockelman. Preparing a nation for autonomous vehicles: opportunities, barriers and policy recommendations. *Transportation Research Part A: Policy and Practice*, 77:167–181, 2015.

[18] Lulu Chang and Luke Dormehl. 6 self-driving car crashes that tapped the brakes on the autonomous revolution. *Emerging Tech*, 2018.

[19] National Highway Traffic Safety Administration et al. Traffic safety facts 2010 data: Bicyclists and other cyclists. *DOT HS*, 810:986, 2012.

[20] Airini Ab Rahman, Umar Zakir Abdul Hamid, and Thoo Ai Chin. Emerging technologies with disruptive effects: a review. *Perintis e-Journal*, 7(2):111–128, 2017.

[21] Farbod Fahimi. Full drive-by-wire dynamic control for four-wheel-steer all-wheel-drive vehicles. *Vehicle System Dynamics*, 51(3):360–376, 2013.

[22] Masato Abe, Naoto Ohkubo, and Yoshio Kano. A direct yaw moment control for improving limit performance of vehicle handling-comparison and cooperation with 4ws. *Vehicle System Dynamics*, 25(S1):3–23, 1996.

[23] Shinichiro Horiuchi, Naohiro Yuhara, and Akihiko Takei. Two degree of freedom/h controller synthesis for active four wheel steering vehicles. *Vehicle System Dynamics*, 25(S1):275–292, 1996.

[24] Masao Nagai. The perspectives of research for enhancing active safety based on advanced control technology. *Vehicle System Dynamics*, 45(5):413–431, 2007.

[25] Masao Nagai, Motoki Shino, and Feng Gao. Study on integrated control of active front steer angle and direct yaw moment. *JSAE review*, 23(3):309–315, 2002.

[26] Tim Gordon, Mark Howell, and Felipe Brandao. Integrated control methodologies for road vehicles. *Vehicle System Dynamics*, 40(1-3):157–190, 2003.

[27] G Mastinu, E Babbel, P Lugner, D Margolis, P Mittermayr, and B Richter. Integrated controls of lateral vehicle dynamics. *Vehicle System Dynamics*, 23(S1): 358–377, 1994.

[28] Ansgar Trachtler. Integrated vehicle dynamics control using active brake, steering and suspension systems. *International Journal of Vehicle Design*, 36(1):1–12, 2004.

[29] Fan Yu, Dao-Fei Li, and DA Crolla. Integrated vehicle dynamics controlstate-of-the art review. In *2008 IEEE Vehicle Power and Propulsion Conference*, pages 1–6. IEEE, 2008.

[30] Junjie He, David A Crolla, MC Levesley, and WJ Manning. Coordination of active steering, driveline, and braking for integrated vehicle dynamics control. *Proceedings of the Institution of Mechanical Engineers, Part D: Journal of Automobile Engineering*, 220(10):1401–1420, 2006.

[31] Howard Dugoff, PS Fancher, and Leonard Segel. An analysis of tire traction properties and their influence on vehicle dynamic performance. *SAE transactions*, pages 1219–1243, 1970.

[32] Shin-Ichiro Sakai, Hideo Sado, and Yoichi Hori. Dynamic driving/braking force distribution in electric vehicles with independently driven four wheels. *Electrical Engineering in Japan*, 138(1):79–89, 2002.

[33] Na Lin, Changfu Zong, Masayoshi Tomizuka, Pan Song, Zexing Zhang, and Gang Li. An overview on study of identification of driver behavior characteristics for automotive control. *Mathematical Problems in Engineering*, 2014, 2014.

[34] Baisravan HomChaudhuri, Runing Lin, and Pierluigi Pisu. Hierarchical control strategies for energy management of connected hybrid electric vehicles in urban roads. *Transportation Research Part C: Emerging Technologies*, 62:70–86, 2016.

[35] Guilherme V Raffo, Guilherme K Gomes, Julio E Normey-Rico, Christian R Kelber, and Leandro B Becker. A predictive controller for autonomous vehicle path tracking. *IEEE transactions on intelligent transportation systems*, 10(1):92–102, 2009.

[36] Jie Ji, Amir Khajepour, Wael William Melek, and Yanjun Huang. Path planning and tracking for vehicle collision avoidance based on model predictive control with multiconstraints. *IEEE Transactions on Vehicular Technology*, 66(2):952–964, 2017.

[37] Matthijs Klomp, Mathias Lidberg, and Timothy J Gordon. On optimal recovery from terminal understeer. *Proceedings of the Institution of Mechanical Engineers, Part D: Journal of Automobile Engineering*, 228(4):412–425, 2014.

[38] Timothy Gordon and Yangyan Gao. A flexible hierarchical control method for optimal collision avoidance. In *Proceedings of the 16th International Conference on Mechatronics-Mechatronika 2014*, pages 318–324. IEEE, 2014.

[39] TJ Gordon, Matt C Best, and PJ Dixon. An automated driver based on convergent vector fields. *Proceedings of the Institution of Mechanical Engineers, Part D: Journal of Automobile Engineering*, 216(4):329–347, 2002.

[40] Anugrah K Pamosoaji and Keum-Shik Hong. A path-planning algorithm using vector potential functions in triangular regions. *IEEE Transactions on Systems, Man, and Cybernetics: Systems*, 43(4):832–842, 2013.

[41] Alexey S Matveev, Michael C Hoy, and Andrey V Savkin. Extremum seeking navigation without derivative estimation of a mobile robot in a dynamic environmental field. *IEEE Transactions on Control Systems Technology*, 24(3):1084–1091, 2016.

[42] Michael Hoy, Alexey S Matveev, and Andrey V Savkin. Algorithms for collision-free navigation of mobile robots in complex cluttered environments: a survey. *Robotica*, 33(3):463–497, 2015.

[43] Mengxuan Song, Nan Wang, Timothy Gordon, and Jun Wang. Flow-field guided steering control for rigid autonomous ground vehicles in low-speed manoeuvring. *Vehicle System Dynamics*, pages 1–18, 2018.

[44] Paolo Falcone. *Nonlinear model predictive control for autonomous vehicles*. PhD thesis, Università del Sannio, 2007.

[45] Luigi Del Re, Frank Allgöwer, Luigi Glielmo, Carlos Guardiola, and Ilya Kolmanovsky. *Automotive model predictive control: models, methods and applications*, volume 402. Springer, 2010.

[46] Makoto Yamakado, Jyunya Takahashi, Shinjiro Saito, Atsushi Yokoyama, and Masato Abe. Improvement in vehicle agility and stability by g-vectoring control. *Vehicle System Dynamics*, 48(S1):231–254, 2010.

[47] Matthew Blank and Donald L Margolis. Minimizing the path radius of curvature for collision avoidance. *Vehicle System Dynamics*, 33(3):183–201, 2000.

[48] Roy S Rice. Measuring car-driver interaction with the gg diagram. Technical report, SAE Technical Paper, 1973.

[49] Efstathios Siampis, Matteo Massaro, and Efstathios Velenis. Electric rear axle torque vectoring for combined yaw stability and velocity control near the limit of handling. In *52nd IEEE Conference on Decision and Control*, pages 1552–1557. IEEE, 2013.

[50] Matthijs Klomp. *Longitudinal force distribution and road vehicle handling*. Chalmers University of Technology, 2010.

[51] Christopher Edwards and Sarah Spurgeon. *Sliding mode control: theory and applications*. Crc Press, 1998.

[52] JJE Slotine and W Li. Applied nonlinear control prentice hall englewood cliffs. *New Jersey*, 1991.

[53] Ola Härkegård. *Backstepping and control allocation with applications to flight control*. PhD thesis, Linköpings universitet, 2003.

[54] Wayne C Durham. Constrained control allocation. *Journal of Guidance, control, and Dynamics*, 16(4):717–725, 1993.

[55] Tankut Acarman. Nonlinear optimal integrated vehicle control using individual braking torque and steering angle with on-line control allocation by using state-dependent riccati equation technique. *Vehicle System Dynamics*, 47(2):155–177, 2009.

[56] P Tondel and TA Johansen. Control allocation for yaw stabilization in automotive vehicles using multiparametric nonlinear programming. In *Proceedings of the 2005, American Control Conference, 2005.*, pages 453–458. IEEE, 2005.

[57] Junmin Wang and Raul G Longoria. Coordinated vehicle dynamics control with control distribution. In *2006 American control conference*, pages 6–pp. IEEE, 2006.

[58] Lu Xiong and Zhuoping Yu. Control allocation of vehicle dynamics control for a 4 in-wheel-motored ev. In *2009 2nd International Conference on Power Electronics*

and Intelligent Transportation System (PEITS), volume 2, pages 307–311. IEEE, 2009.

[59] Juyong Kang, Hyundong Heo, et al. Control allocation based optimal torque vectoring for 4wd electric vehicle. Technical report, SAE Technical Paper, 2012.

[60] Yan Chen and Junmin Wang. Fast and global optimal energy-efficient control allocation with applications to over-actuated electric ground vehicles. *IEEE Transactions on Control Systems Technology*, 20(5):1202–1211, 2012.

[61] Gene H Golub and Charles F Van Loan. *Matrix computations*, volume 3. JHU press, 2012.

[62] Martin Kirchengast, Martin Steinberger, and Martin Horn. Input matrix factorizations for constrained control allocation. *IEEE Transactions on Automatic Control*, 63(4):1163–1170, 2018.

[63] Tor A Johansen and Thor I Fossen. Control allocationa survey. *Automatica*, 49 (5):1087–1103, 2013.

[64] Jinghua Guo, Yugong Luo, Keqiang Li, and Yifan Dai. Coordinated path-following and direct yaw-moment control of autonomous electric vehicles with sideslip angle estimation. *Mechanical Systems and Signal Processing*, 105:183–199, 2018.

[65] Junmin Wang and Raul G Longoria. Coordinated and reconfigurable vehicle dynamics control. *IEEE Transactions on Control Systems Technology*, 17(3):723–732, 2009.

[66] Jonas Fredriksson, Johan Andreasson, and Leo Laine. Wheel force distribution for improved handling in a hybrid electric vehicle using nonlinear control. In *2004 43rd IEEE Conference on Decision and Control (CDC)(IEEE Cat. No. 04CH37601)*, volume 4, pages 4081–4086. IEEE, 2004.

[67] Shuibo Zheng, Houjun Tang, Zhengzhi Han, and Yong Zhang. Controller design for vehicle stability enhancement. *Control Engineering Practice*, 14(12):1413–1421, 2006.

[68] Johannes Tjonnaas and Tor Arne Johansen. Adaptive optimizing dynamic control allocation algorithm for yaw stabilization of an automotive vehicle using brakes. In *2006 14th Mediterranean Conference on Control and Automation*, pages 1–6. IEEE, 2006.

[69] Ake Bjorck. *Numerical methods for least squares problems*, volume 51. Siam, 1996.

[70] Dong Zhang, Timothy Gordon, Rui Zhang, and Changfu Zong. Development and validation of the moderated particle reference strategy with driver in the loop. In *Advanced Vehicle Control: Proceedings of the 14th International Symposium on Advanced Vehicle Control (AVEC'18)*. CRC Press, 2018.

[71] Gene H Golub and Christian Reinsch. Singular value decomposition and least squares solutions. In *Linear Algebra*, pages 134–151. Springer, 1971.

[72] Lloyd N Trefethen and David Bau III. *Numerical linear algebra*, volume 50. Siam, 1997.

[73] JingPing Shi, WeiGuo Zhang, GuangWen Li, and XiaoXiong Liu. Research on allocation efficiency of the redistributed pseudo inverse algorithm. *Science China Information Sciences*, 53(2):271–277, 2010.

[74] Jinghua Guo, Yugong Luo, and Keqiang Li. Adaptive coordinated leader–follower control of autonomous over-actuated electric vehicles. *Transactions of the Institute of Measurement and Control*, 39(12):1798–1810, 2017.

[75] Nobuo Shinozaki, Masaaki Sibuya, and Kunio Tanabe. Numerical algorithms for the moore-penrose inverse of a matrix: direct methods. *Annals of the Institute of Statistical Mathematics*, 24(1):193–203, 1972.

[76] Yangyan Gao, Mathias Lidberg, Timothy Gordon, et al. Modified hamiltonian algorithm for optimal lane change with application to collision avoidance. *MM Science Journal*, pages 576–584, 2015.

[77] Yangyan Gao, Timothy Gordon, and Mathias Lidberg. Implementation of a modified hamiltonian algorithm for control allocation. In *Advanced Vehicle Control: Proceedings of the 13th International Symposium on Advanced Vehicle Control (AVEC'16), September 13-16, 2016, Munich, Germany*, page 157. CRC Press, 2016.

[78] Rui Zhang, Timothy Gordon, Mathias Lidberg, and Chengning Zhang. A moderated particle reference strategy for integrated chassis and driveline control. 2014.

[79] Manfred Plöchl and Johannes Edelmann. Driver models in automobile dynamics application. *Vehicle System Dynamics*, 45(7-8):699–741, 2007.

[80] Konghui Guo and Hsin Guan. Modelling of driver/vehicle directional control system. *Vehicle System Dynamics*, 22(3-4):141–184, 1993.

[81] Yuhang Chen, J Karl Hedrick, and Konghui Guo. A novel direct yaw moment controller for in-wheel motor electric vehicles. *Vehicle System Dynamics*, 51(6): 925–942, 2013.

[82] Timothy Gordon, Matthijs Klomp, and Mathias Lidberg. Experimental verification of understeer compensation by four wheel braking. In *FISITA 2014 World Automotive Congress-2-6 June 2014, Maastricht, The Netherlands.*, 2014.

[83] Gridsada Phanomchoeng and Rajesh Rajamani. New rollover index for the detection of tripped and untripped rollovers. *IEEE Transactions on Industrial Electronics*, 60(10):4726–4736, 2013.

[84] Zhilin Jin, Lei Zhang, Jiale Zhang, and Amir Khajepour. Stability and optimised h control of tripped and untripped vehicle rollover. *Vehicle System Dynamics*, 54 (10):1405–1427, 2016.

[85] Desmond N Penny. Rollover of sport utility vehicles. *The Physics Teacher*, 42(2): 86–91, 2004.

[86] Björn Johansson and Magnus Gafvert. Untripped suv rollover detection and prevention. In *2004 43rd IEEE Conference on Decision and Control (CDC)(IEEE Cat. No. 04CH37601)*, volume 5, pages 5461–5466. IEEE, 2004.

[87] Garrick J Forkenbrock, W Riley Garrott, Mark Heitz, and Bryan C O'Harra. An experimental examination of j-turn and fishhook maneuvers that may induce on-road, untripped, light vehicle rollover. *SAE transactions*, pages 1112–1127, 2003.

[88] Nong Zhang, Guang-Ming Dong, and Hai-Ping Du. Investigation into untripped rollover of light vehicles in the modified fishhook and the sine maneuvers. part i: Vehicle modelling, roll and yaw instability. *Vehicle System Dynamics*, 46(4): 271–293, 2008.

[89] John T Pearson, Roger M Goodall, and Ian Pratt. Control system studies of an active anti-roll bar tilt system for railway vehicles. *Proceedings of the Institution of Mechanical Engineers, Part F: Journal of Rail and Rapid Transit*, 212(1):43–60, 1998.

[90] Paul Hendrik Cronje and Pieter Schalk Els. Improving off-road vehicle handling using an active anti-roll bar. *Journal of Terramechanics*, 47(3):179–189, 2010.

[91] Seongjin Yim, Kwangki Jeon, and Kyongsu Yi. An investigation into vehicle rollover prevention by coordinated control of active anti-roll bar and electronic stability program. *International Journal of Control, Automation and Systems*, 10 (2):275–287, 2012.

[92] Noraishikin Zulkarnain, Fitrian Imaduddin, Hairi Zamzuri, and Saiful Amri Mazlan. Application of an active anti-roll bar system for enhancing vehicle ride and

handling. In *2012 IEEE Colloquium on Humanities, Science and Engineering (CHUSER)*, pages 260–265. IEEE, 2012.

[93] Bo-Chiuan Chen and Huei Peng. Differential-braking-based rollover prevention for sport utility vehicles with human-in-the-loop evaluations. *Vehicle System Dynamics*, 36(4-5):359–389, 2001.

[94] Brad Schofield, Tore Hagglund, and Anders Rantzer. Vehicle dynamics control and controller allocation for rollover prevention. In *2006 IEEE Conference on Computer Aided Control System Design, 2006 IEEE International Conference on Control Applications, 2006 IEEE International Symposium on Intelligent Control*, pages 149–154. IEEE, 2006.

[95] Thomas J Wielenga and Milton A Chace. A study in rollover prevention using anti-rollover braking. Technical report, SAE Technical Paper, 2000.

[96] Taehyun Shim and Daniel Toomey. Investigation of active steering/wheel torque control at the rollover limit maneuver. *SAE transactions*, pages 1133–1140, 2004.

[97] Dong Zhang, Timothy Gordon, Yangyan Gao, Changfu Zong, and Mathias Lidberg. A novel control mediation approach to active rollover prevention. In *Advanced Vehicle Control: Proceedings of the 13th International Symposium on Advanced Vehicle Control (AVEC'16), September 13-16, 2016, Munich, Germany*, page 203. CRC Press, 2016.

[98] Bo-Chiuan Chen and Huei Peng. A real-time rollover threat index for sports utility vehicles. In *Proceedings of the 1999 American Control Conference (Cat. No. 99CH36251)*, volume 2, pages 1233–1237. IEEE, 1999.

[99] Shuichi Takano and Masao Nagai. Dynamics control of large vehicles for rollover prevention. In *IVEC2001. Proceedings of the IEEE International Vehicle Electronics Conference 2001. IVEC 2001 (Cat. No. 01EX522)*, pages 85–89. IEEE, 2001.

[100] Dong Zhang, Timothy Gordon, Yangyan Gao, and Rui Zhang. A unified approach to rollover prevention based on control allocation. In *Dynamics of Vehicles on Roads and Tracks Vol 1: Proceedings of the 25th International Symposium on Dynamics of Vehicles on Roads and Tracks (IAVSD 2017), 14-18 August 2017, Rockhampton, Queensland, Australia*, page 87. CRC Press, 2017.

[101] John H Plumlee, David M Bevly, and A Scottedward Hodel. Control of a ground vehicle using quadratic programming based control allocation techniques. In *Proceedings of the 2004 American Control Conference*, volume 5, pages 4704–4709. IEEE, 2004.

[102] Tor Arne Johansen, Thor I Fossen, and Stig P Berge. Constrained nonlinear control allocation with singularity avoidance using sequential quadratic programming. *IEEE Transactions on Control Systems Technology*, 12(1):211–216, 2004.

[103] E Omerdic and GN Roberts. Extension of feasible region of control allocation for open-frame underwater vehicles. *IFAC Proceedings Volumes*, 37(10):315–320, 2004.

[104] Youmin Zhang, V Sivasubramaniam Suresh, Bin Jiang, and Didier Theilliol. Reconfigurable control allocation against aircraft control effector failures. In *2007 IEEE International Conference on Control Applications*, pages 1197–1202. IEEE, 2007.

[105] RR Huber and B McCulloch. Self-repairing flight control system. Technical report, SAE Technical Paper, 1984.

[106] John Virnig and David Bodden. Multivariable control allocation and control law conditioning when control effectors limit. In *Guidance, Navigation, and Control Conference*, page 3609, 1994.

[107] Paolo Falcone, H Eric Tseng, Francesco Borrelli, Jahan Asgari, and Davor Hrovat. Mpc-based yaw and lateral stabilisation via active front steering and braking. *Vehicle System Dynamics*, 46(S1):611–628, 2008.

[108] Dong Zhang, Tim Gordon, Yangyan Gao, and Changfu Zong. Intelligent electronic steering program based on road departure mitigation control. In *2016 IEEE International Conference on Systems, Man, and Cybernetics (SMC)*, pages 001567–001572. IEEE, 2016.

[109] Shinnosuke Ishida and Jens E Gayko. Development, evaluation and introduction of a lane keeping assistance system. In *IEEE Intelligent Vehicles Symposium, 2004*, pages 943–944. IEEE, 2004.

[110] Jochen Pohl, Wolfgang Birk, and Lena Westervall. A driver-distraction-based lane-keeping assistance system. *Proceedings of the Institution of Mechanical Engineers, Part I: Journal of Systems and Control Engineering*, 221(4):541–552, 2007.

[111] C Blaschke, F Breyer, B Färber, J Freyer, and R Limbacher. Driver distraction based lane-keeping assistance. *Transportation research part F: traffic psychology and behaviour*, 12(4):288–299, 2009.

[112] Zhong Changfu, Lin Na, Zhang Zexing, et al. A study on the identification algorithm of driver characteristics for x-by-wire vehicles. *Automotive Engineering*, 36 (9):1140–1144, 2014.

[113] Yu-seok Jeong, Seung-Ki Sul, Steven E Schulz, and Nitin R Patel. Fault detection and fault-tolerant control of interior permanent-magnet motor drive system for electric vehicle. *IEEE Transactions on Industry Applications*, 41(1):46–51, 2005.

[114] Rongrong Wang and Junmin Wang. Fault-tolerant control with active fault diagnosis for four-wheel independently driven electric ground vehicles. *IEEE Transactions on Vehicular Technology*, 60(9):4276–4287, 2011.

[115] Rongrong Wang and Junmin Wang. Fault-tolerant control for electric ground vehicles with independently-actuated in-wheel motors. *Journal of Dynamic Systems, Measurement, and Control*, 134(2):021014, 2012.

[116] Leila Parsa and Hamid A Toliyat. Fault-tolerant interior-permanent-magnet machines for hybrid electric vehicle applications. *IEEE transactions on vehicular technology*, 56(4):1546–1552, 2007.

[117] Gene Golub and William Kahan. Calculating the singular values and pseudo-inverse of a matrix. *Journal of the Society for Industrial and Applied Mathematics, Series B: Numerical Analysis*, 2(2):205–224, 1965.